THE USE OF SURFACTANTS TO AID AND IMPROVE THE LEACHING OF LOW GRADE COPPER ORES

by

Kush Shah

B.A.Sc., The University of British Columbia, 2014

A THESIS SUBMITTED IN PARTIAL FULFILLMENT OF

THE REQUIREMENTS FOR THE DEGREE OF

MASTER OF APPLIED SCIENCE

in

THE FACULTY OF GRADUATE AND POSTDOCTORAL STUDIES

(MATERIALS ENGINEERING)

THE UNIVERSITY OF BRITISH COLUMBIA

(Vancouver)

May 2017

Abstract

Copper heap leach operations often suffer from reduced efficiency due to long leach times and variable recoveries. Surfactants have been considered as an option in increasing the leachability of ores. Improvements in overall copper extraction have been noted with their use, though testing has only been conducted on a limited scale. The molecular function of surfactants in heap leaching has not been extensively studied and is not well explored. The work in this thesis was aimed at better understanding and characterizing the function of the surfactants. Work was performed with surfactants developed by BASF specifically for heap leaching.

Initial experimentation consisted of using flooded vats to compare copper extraction from ores. Leach solution with and without surfactant was fed to the ores. The presence of surfactants was noted to increase the overall copper recovered by approximately 2-3%. Interfacial tension measurements were performed to determine the changes imparted onto the acidic leach solution by the surfactants. Hanging drops were used to determine the activity at the air-liquid boundary. It was found that at the surfactant concentrations used in heap leaching, the interfacial tension of the fluid changed very little, from about 71 mN/m to 69.5 mN/m.

The contact angle was determined to better understand the interaction between the acidic media and the ore. This was obtained using capillary wicking and Washburn's equation. Ore was finely ground and packed into particle beds. Leach liquid with surfactant was introduced

to these beds. The rate of permeating fluid flow was monitored against time. The affinity of the liquid for the solid surface dictated the rate of uptake. Washburn's equation allowed for the contact angle to be calculated from these results. It was found that surfactants lowered the contact angle of liquid on solid by up to 3 degrees.

The combination of results indicated that the surfactants increases the affinity between the solid and liquid by reducing the contact angle. In a heap, this allows acid to ingress further into sub-surface regions of ore particles. As a result, leachability of the ore is increased as harder to reach minerals can be accessed.

Lay Summary

Copper is an important material for daily life. It needs to be produced cheaply so it remains affordable. Heap leaching is a method of production that allows copper ores to be turned into copper metal. It is a low cost and environmentally friendly process. This is important as copper ores are declining in grade.

The production process involves piling ore together in a heap. It is then irrigated with acid solution which dissolves copper minerals. The solution flows through the heap and is collected and processed for copper recovery. The process is often slow and inefficient and copper recovered from the heap can be low. Surfactants have proven capability to make the process more efficient. Surfactants increase the affinity between the acid leach solution and the ore. This increases the amount of copper that can be dissolved. This means more copper can be produced from the same process.

Preface

The work in this thesis is original, independent and intellectual work performed by the author, Kush Shah, except as noted in the text.

Table of Contents

List of Tables

List of Figures

List of Chemical Formulas

$KAlSi_3O_8$	Microline	146
$KAlSi_3O_8$	Orthoclase	146
SiO_2	Quartz	146
$FeCO_3$	Siderite	146
Cu	Copper	
H_2SO_4	Sulfuric Acid	

List of Abbreviations

Abbreviation	*Definition*
AAS	Atomic Absorbance Spectroscopy
DI	De-Ionized
PLS	Pregnant Leach Solution
PSD	Particle Size Distribution
ppm	Parts Per Million
P_{80}	80% Passing Value
ROM	Run-of-Mine
XRD	X-Ray Diffraction

Acknowledgements

This thesis would have been possible without the help of a true and dedicated support network who have been incredible in helping succeed with my work. I am unfortunately only able to give particular mention to a few names here, but I am duly grateful for all the help.

I would like to thank my supervisor, Dr. David Dreisinger, for providing me this opportunity. This masters has given me great chance to learn and experience something new. Thank you for being patient and allowing me the opportunity to learn things in my own way. This has been an experience like no other.

I would like to extend a thank you to Dr. Jack Bender and BASF for furnishing everything from the tangible goods to the problem that needed a solution.

I would also like to extend my sincere gratitude to Dr. David Dixon for the assistance he provided during the course of my research. The endless questions and long office hours have certainly provided much food for thought.

I wish thank: Dr. Marek Pawlik, Dr. Wenying Liu, Sally Finora and Jophat Engwayu for the assistance in the parts of this work regarding surface and interfacial tension. The access provided for analysis equipment as well as the assistance in providing knowledge to better understand the work is greatly appreciated.

I wish to extend a special thank you to my lab mates in Frank Forward, room 406: Monse, Pablo, Ryan and Prashant. Thank You for making the seemingly endless hours in the lab seem not so endless.

Lastly I wish to thank my family for the all the enduring support and who has stood by me all the way!

Dedication

"An investment in knowledge pays the best return," – Benjamin Franklin

I dedicate this thesis to my parents. Their unconditional love and encouragement has allowed me to achieve success in everything I have done till now. Their unwavering faith in providing a good education has taught me to truly value what it can give. To the greatest teachers in my life, this thesis and all that it encompasses, tangibly and intangibly, is only a microcosm of how much you have helped me accomplish in life. You gave up a lot and never asked for much. For everything, I wish there was a better was to say THANK YOU.

Chapter 1: Introduction

1.1 Thesis Background

Heap leaching has provided an economically favorable route of production of metals from low grade ores. The use of heap leaching to produce copper, uranium, gold and silver has been successfully practiced and applied on a commercial scale (Padilla, Cisternas, & Cueto, 2008). Over time, the promise shown by existing applications has led to development of the technology to other metals and minerals. For this thesis and discussion, the topic of heap leaching is specifically applied to the heap leaching of copper ores.

Heap leaching technologies have gained a significant role and focus in the world of hydrometallurgical copper extraction. By far the largest application of the heap leaching technology is in the production of copper. Around 20% of the copper produced globally is through hydrometallurgical treatment, of which more than 15% is extracted using heap leaching (Bartlett, 1997)

Copper is versatile and is used in numerous applications. Some of the properties that make it highly sought after are: (a) its superior ability to conduct heat and electricity, (b) high resistance to corrosion, and (c) ease with which it can be fabricated and shaped into different products. The global production of copper has steadily been increasing (see Figure 1.1) and the demand for it has been shaped by the myriad of uses in which it has proven itself useful (Moskalyk & Alfantazi, 2003).

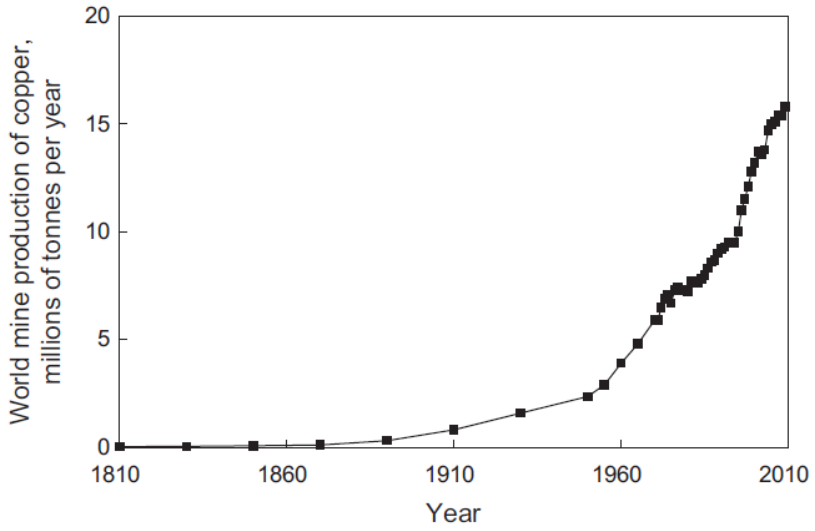

Figure 1.1 – Total copper produced worldwide. *©(Schlesinger, King, Sole, & Davenport, 2011c). (Reproduced with permission from Elsevier)*

Because of the demand placed on copper metal, the methods of production used bear significant consideration. Without meeting the key criterion of economic feasibility, no production method can be considered successful. The type of treatment applied relies very much on the source material being supplied to the process. In the case of the production of copper from its ores, the grades encountered dictate the available treatment options.

In general, the world over, the grades of copper in ore bodies have been in decline. Average grades of copper in open pit mines are approximately 0.4-0.5% and underground mining produces grades of approximately 1%-2%. (Schlesinger, King, Sole, & Davenport, 2011a). The heap leach process has been instrumental in economically extracting copper from low-grade ores.

The general heap leach process entails the following steps:

(a) A minimal amount of preparation is performed on the ore. This involves crushing to a suitable size and possibly agglomerating the ore.

(b) Ore material is piled together to produce a heap which is irrigated with acidic lixiviant.

(c) Metal values are leached from the heap and the solution is collected from the bottom of the heap.

(d) Further processing can recover the soluble metals and transform them into high purity metallic materials, ready for use.

The biggest limitations in the heap leach process are the long extraction times and low and/or variable recoveries from a heap. This stems from issues relating to the exposure of mineral grains to the necessary reactants that facilitate leaching (e.g. limited exposure to acidic solution, oxygen, etc…). Referring to Figure 2.1 (page 6), in a heap leach the size of particles used is on the order of approximately 25mm. The valuable mineral grains that need to be leached are located within these larger pieces of ore. This means that lixiviant needs to permeate through a labyrinth of heaped particles and needs to permeate into ore pieces laden with minerals to dissolve available copper.

Often the main culprit limiting the rate of extraction tends to be poor wettability and limited contact of ore with the acidic phase. This could be due to the poor distribution of acidic lixiviant as is often noted in heap leach operations (Dixon & Petersen, 2007). This could also be due to the limited extent to which acidic media can diffuse into the particles. The

dissolution of the mineral grains in the ore particles occurs at the surface and sub-surface regions which are only accessible by pores and fissures (Ghorbani, 2012).

This poses a problem for operators of heap leach systems as a balance needs to be struck to maintain operational viability. A heap needs to produce a certain amount of copper to justify the investment taken to prepare and operate it. This, however, may limit the ability of an operator to be efficient if the time taken for a heap to produce the minimum required copper is too long. In order to increase the rate at which copper can be extracted and reduce the operational time for a heap, other modes of optimization are necessary. A possible means to achieve this is the use of surfactants.

Surfactants are molecules whose function is designed to change the surface tension of a liquid in contact with a secondary phase (either solid, liquid, or gas). They are designed to adsorb at the interface between the hosting fluid and the secondary phases (Rosen, 2004a). The surfactants alter the interaction between them. Their functionality is discussed in greater detail in chapter 4 (section 4.1.2).

The work in this thesis was performed based on work performed by BASF (Bender, Hight, Emmerich, & Brewer, 2016) as well as with their cooperation. BASF developed surfactants for use primarily in heap leach systems for use with low grade copper ores. Work performed by them to test surfactants in heap leach systems found that the overall amount of copper leached in a heap was greater with surfactants as compared to a heap in which no surfactants were present.

1.2 Research Aims and Objectives

Using the surfactants developed by BASF, the focus of this thesis was to better understand how the surfactants behave within an irrigated heap. More specifically the objectives set-out for the work in this thesis were to:

- Understand where exactly in the heap leach system the surfactants act to increase the overall leachability of the ores, outside of performing comparative extractions with and without the presence of surfactants.
- To create a systematic and repeatable method through which the activity of the surfactant can be reliably quantified and measured. Heap leaching is conducted using different ore types and leaching solutions, depending on the operation. By creating a reliable experimental method that can incorporate these variables, accurate measurements and observations can be obtained. Depending on the ore type and solution type the experiments can provide a better picture of how strong the effect of the surfactant is.

These objectives were directed at providing a better understanding of the underlying mechanisms of the changes imposed on the system to improve the results of the heap leach.

Chapter 2: Literature Review

2.1.1 Copper Hydrometallurgy

The separation practices employed to process and refine ores for the production of metals is a crucial consideration when aiming to make a process economically viable. With respect to the production of copper from its ore, the separation practices employed are generally encompassed within the realm of: (a) pyrometallurgy, or (b) hydrometallurgy. The general penchant for the production of copper in the world has been in favor of pyrometallurgy. Its dominancy has reigned strong for well over a century (Dreisinger, 2006) and still accounts for about 80% of the production of copper in the world today (Schlesinger et al., 2011a). It is no surprise then, that pyrometallurgical processes have the advantage of being a successfully proven technology, with an abundance of them having been developed over time (Moskalyk & Alfantazi, 2003).

Proven technologies boast a minimized risk factor for companies that operate copper production lines, and allow for predictable and favorable returns on investment. However, a limitation imposed by pyrometallurigcal technologies are the high capital costs associated with processing ore. (Dreisinger, 2006). Because of this a minimum ore cut-off grade is usually required to ensure that the economic feasibility of the process is maintained. The grade of ore usually needs to be concentrated to about 30% copper, which also impacts the economics of the process (Schlesinger, King, Sole, & Davenport, 2011b). Because of this it has been pertinent to find suitable alternatives to supplement conventional methods of copper extraction.

In the last few decades, the practices associated with hydrometallurgical extraction of copper have been garnering greater popularity. They have been able to provide more cost effective ways of processing bulk ore without the need for expensive capital investments by permitting extraction without the need for a concentration step, in most cases (Schlesinger et al., 2011b). Additional advantages offered by hydrometallurgical processing relate to their environmental impact. They are more environmentally friendly as these processes tend to be less polluting than smelting (high SO_2 emissions). They are also suited to processing ores with moderate to high levels of contaminants (arsenic, antimony, phosphorous, etc…) that smelters are unable to handle. (Dreisinger, 2006).

Different methods, procedures and flowsheets have been developed that economically apply the principals governing hydrometallurgy to the extraction of copper. The overall recovery method applied depends on the type of ore being processed (e.g. copper oxide vs. copper sulfide) and the grade of copper in the ore (Scheffel, 2002).

Where high grade ore types are available, high cost extraction(s) can be utilized without greatly affecting unit profits as the resulting higher recoveries can justify the cost. This is exemplified in Figure 2.1 where some of the different hydrometallurgical processes are shown and the different particles sizes at which the extractions are realized. Ore with higher grades can be subject to pre-leach processing steps such as size reduction by grinding to fine sizes, which entail higher operational cost, but whose grade can justify it. Where lower grades are predominant, the process needs to be adjusted accordingly.

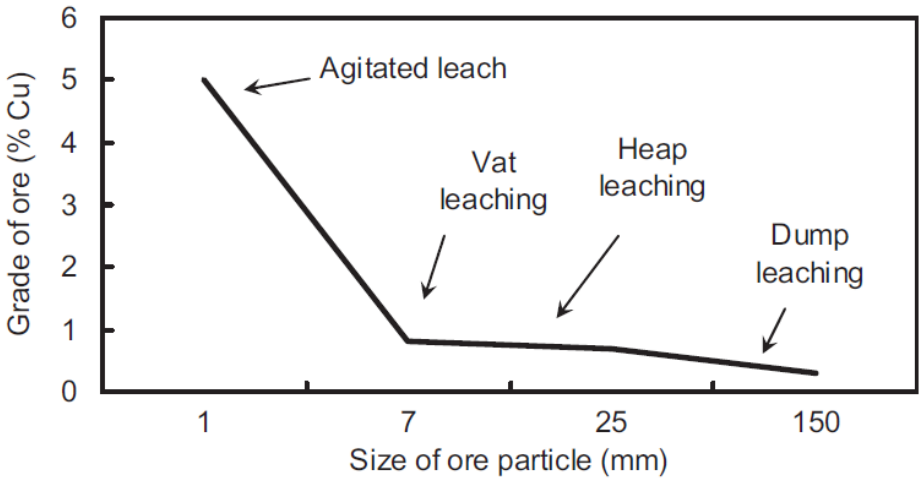

Figure 2.1 – Size fractions of particles as a function of copper grade. *The higher the grade of the ore the more processing it can endure (from a cost perspective) prior to a leach. This is to ensure that the recovery is maximized such that the cost to process is justified. ©(Schlesinger et al., 2011a). (Reproduced with permission from Elsevier)*

2.1.2 Heap Leaching & Dump Leaching

Heap and dump leaching collectively fall under the banner of percolation leaching. As the name suggests, the process involves the percolation of a lixiviant (for example sulfuric acid solution) through a permeable mass of ore under normal atmospheric conditions. The lixiviant percolating through the ore leaches soluble minerals in its path, and exits the mass as a solution rich in solubilized minerals (e.g. copper and other minerals that may be present in the material).

Heap leaching and dump leaching are intrinsically similar in nature with a major exception being the level of control exerted in each. The reason for this difference is due to the type of material processed in each one. Heap leaching can treat ore containing up to 2% copper.

Dump leaching is used to treat ore with less than 0.5% copper content. (Schlesinger et al., 2011a)

In a heap leach the level of control exerted on the process is much greater than compared to a dump leach. The heap is optimized to attain maximum copper extraction. The optimization protocols typically involve ore crushing and sizing, ore dressing and a careful and controlled approach to heap construction and irrigation. These stages are necessary and the extra investment to exert more control on the process is justified by the higher, comparative, copper grade. In the heap leach process overall, the time scales for extraction can vary from about approximately 3 months to a year or more. This depends on the type of ore being subject to treatment.

A dump leach is used to treat material of very low concentration that would otherwise be considered waste. Run of mine ore material [ROM] (raw ore, with little to no sizing) is piled together into a dump and treated with lixiviant. The time scales for extraction can be years. The low grade makes it uneconomical to perform extensive processing on the ore prior to leaching. (Schlesinger et al., 2011a; Schlesinger et al., 2011b). Dump leaching allows for better utilization of the ore as a whole as any extra copper leached is a bonus that can be added to the downstream processes to boost copper production.

While the underlying fundamentals to heap and dump leaching are intrinsically the same, the discussions in this thesis are focused largely on the former. It should be noted however, that

the surfactants developed by BASF for the heap leaching process can also be used in the dump leach process.

2.1.3 Heap Leaching and Copper Extraction

The low cost of copper production from heap leaching stems from the design circuit typically used. (See Figure 2.2 and Figure 2.3).

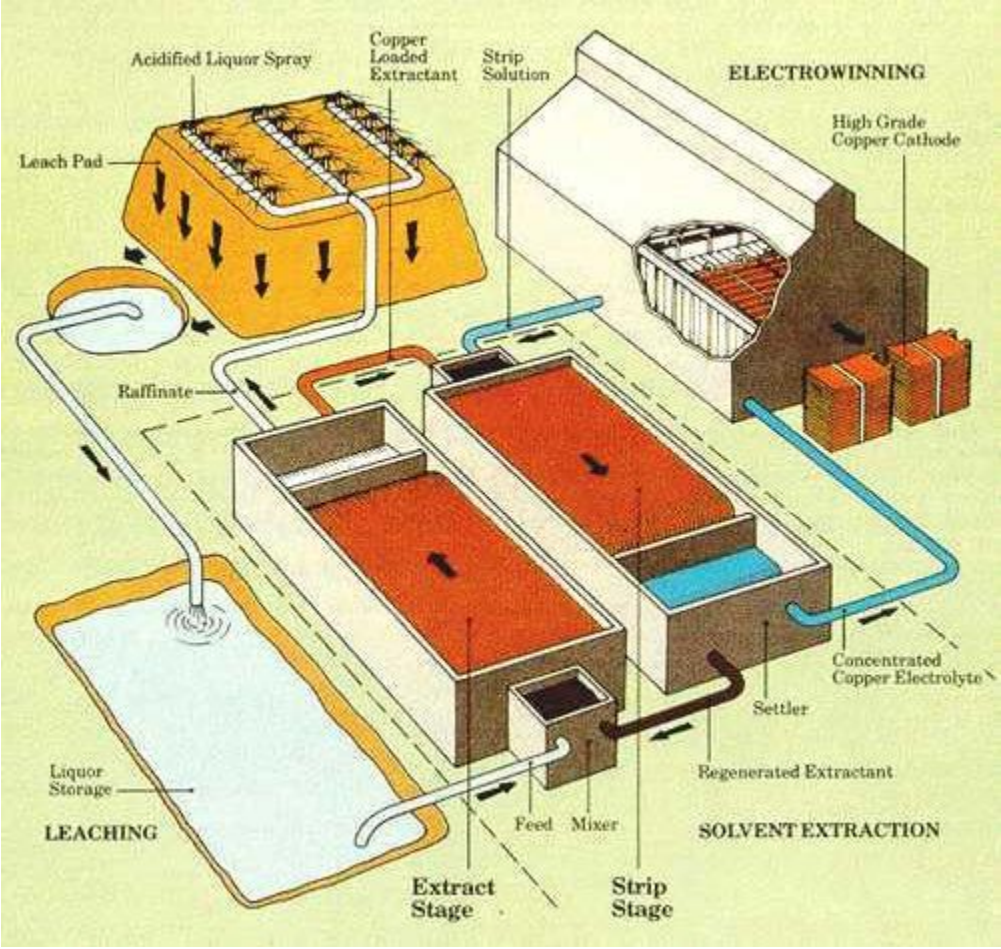

Figure 2.2 – Heap Leach circuit for the treatment of copper ores. *The circuit above depicts the typical circuit designed to extract copper from a heap leach. Pregnant Leach Solution (PLS) exits the bottom of the heap and is forwarded to a stripping and extraction circuit to increase the amount of copper in solution. The copper rich solution is run through an electrowinning plant to produce pure copper metal plates. Copied by permission from the "Electrochemistry Encyclopedia" (http://knowledge.electrochem.org/encycl/art-m02-metals.htm) on 11/5/2017. (Woods, 2010)*

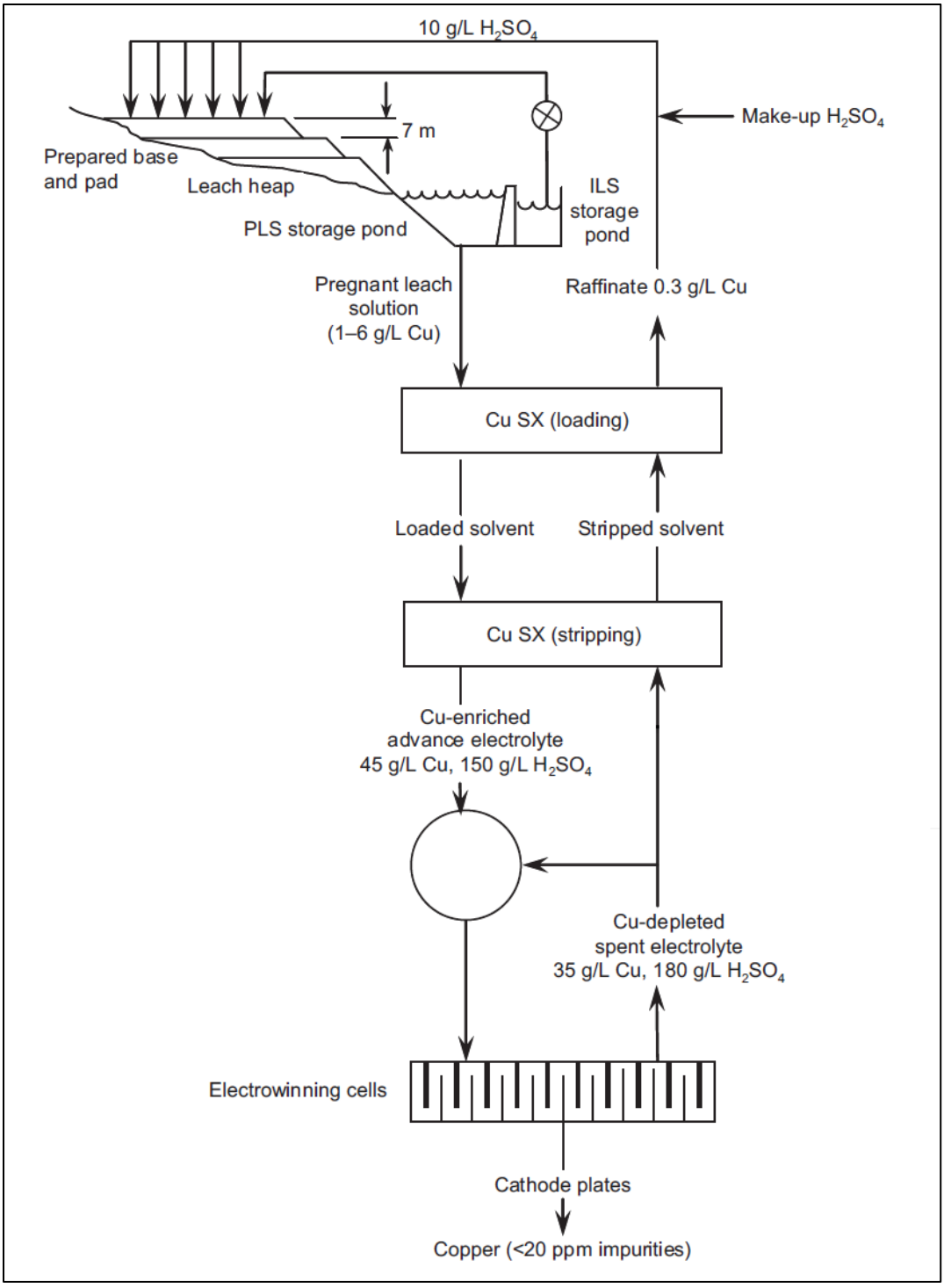

Figure 2.3 – Basic flow sheet of heap leach process. *Pregnant leach solution exiting from the heap is too low in copper concentration for direct electrowinning to produce copper. The copper in solution needs to be stepped up in a series of stages such that the feed stock to the electrowinning cells is high enough in copper to ensure economical and efficient copper production. .©(Schlesinger et al., 2011a) (Reproduced with permission from Elsevier).*

A copper heap leach and extraction circuit is depicted in Figure 2.2. The basic flow sheet associated with the process in Figure 2.2, is depicted in Figure 2.3. The process starts with the irrigation of the heap with lixiviant containing sulfuric acid. As the leach liquid passes through the heap it leaches mineral species in its path and exits as a solution rich in dissolved copper (aka pregnant leach solution (PLS)), in the form of copper sulfate solution. The production of copper metal from the leached ore is achieved through electrowinning. However, the solution produced directly from the heap is too low in concentration for economically feasible copper production in a cell house, and may have too many deleterious species that hinder efficient production.

To create a feed stock more amenable to copper electrowinning an intermediate step is required. The purification of the copper solution involves the use of a stripping and extraction circuit (see Figure 2.4). In the extraction stage, the copper rich solution from the heap is contacted with an organic phase with a high affinity for the copper in solution. The organic phase selectively complexes with the copper and extracts it from the aqueous solution. The loaded organic is separated from the now barren aqueous phase (raffinate). In the stripping stage, the copper loaded organic phase is contacted with spent electrowinning solution, typically at high acid concentrations. The opposite reaction occurs and copper is loaded back into the aqueous phase but at a significantly higher concentration and purity (see Figure 2.4). (Schlesinger et al., 2011b). The freshly loaded copper electrolyte is fed into an electrowinning cell house where copper ions are reduced to copper metal at the cell cathodes.

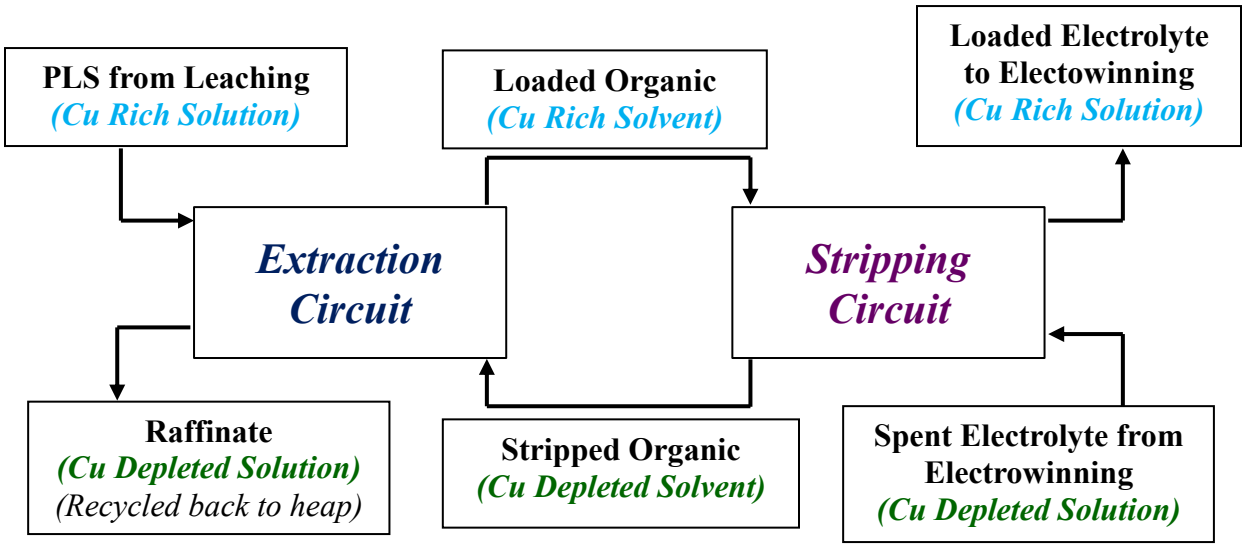

Figure 2.4 – Stripping and Extraction circuit. *In an extraction and stripping circuit, the copper concentration in solution is stepped-up prior to electrowinning. Leach solution from the heap is contacted with an organic phase that selectively targets aqueous copper to produce loaded organic. The copper is then stripped from the organic by contact with strong acidic solutions produced by electrowinning. This results in the reproduction of aqueous copper but at a higher concentration and purity for efficient production of copper metal.*

Often metal grades of leachable copper ores are too low to effectively support costs associated with certain extraction processes. Heap leaching technologies have been able to overcome this limitation by introducing low capital requirements to treat low-grade ores. Additionally pre-concentration can be avoided as copper can be leached from ores whose grade is too low for processes such as floatation (Bartlett, 1997). Also operation costs can be reduced as the system allows for the recycling of solutions and solvents between different stages of the circuit (see Figure 2.2).

Overall, by using relatively few stages in the production process heap leaching has provided an advantageous production method and created economic value where raw material would have once been considered waste.

2.1.4 Heap Leaching Chemistry

One of the major limitations encountered in the heap leach system is the time scale of operation. The biggest factor controlling this is the type of ore being processed on the heap pad. Heap leaching of copper minerals vary with type and composition. The minerals that are typically subject to extraction in a heap leach are copper oxides and/or copper sulfides. The extent to which will copper solubilize varies with leach chemistry and reaction kinetics. The lixiviant typically used in heap leaching is sulfuric acid solution. This is also combined with the fact that heaps are operated in large open spaces, and so the conditions for the leaching are at atmospheric temperature and pressure. In light of this the process requirements need to be carefully considered, depending on the type of ore being treated. For example, ores inherently not amenable to leaching may require significantly longer times to ensure enough copper extraction to maintain operational viability, which may affect downstream operations.

Leaching of Copper Oxide Minerals

Copper leaching is more readily achieved in copper oxide ores. Referring to Figure 2.5 it can be seen that copper and its oxides readily dissolve to the Cu^{2+} under acidic conditions. The reactions below exemplify some of the reactions that copper oxide minerals undergo under atmospheric conditions with acid (*Reactions adopted from (Schlesinger et al., 2011a)*).

$$CuO + H_2SO_4 \longrightarrow Cu^{2+} + SO_4^{2-} + H_2O \text{ (Tenorite Leach)}$$

$$2CuCO_3.Cu(OH)_2 + 3H_2SO_4 \longrightarrow 3Cu^{2+} + 3SO_4^{2-} + 2CO_2 + 4H_2O \text{ (Azurite Leach)}$$

$$CuCO_3.Cu(OH)_2 + 2H_2SO_4 \longrightarrow 2Cu^{2+} + 2SO_4^{2-} + CO_2 + 3H_2O \text{ (Malachite Leach)}$$

$$Cu_2O + H_2SO_4 \longrightarrow Cu^{2+} + SO_4^{2-} + Cu + H_2O \text{ (Cuprite Leach)}$$

$$CuO.SiO_2 + H_2SO_4 \longrightarrow Cu^{2+} + SO_4^{2-} + SiO_2.nH_2O + (3\text{-}n)H_2O \text{ (Chrysocolla Leach)}$$

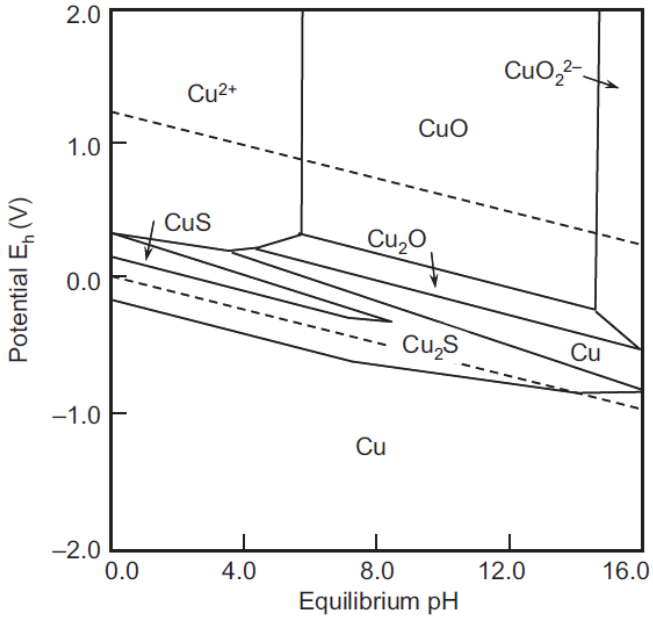

Figure 2.5 - Pourbaix diagram showing the Cu-O-S system at 25˚C. *[Cu]=[S]=10^{-4} M. Copper oxide minerals are more readily dissolved under mildly acidic conditions.©(Schlesinger et al., 2011a) (Reproduced with permission from Elsevier*

Leaching of Copper Sulfides Minerals

Copper sulfide minerals do not solubilize copper as readily as copper oxide minerals, though the rate of success is highly dependent on the type of ore being treated. In general the oxidation of copper sulfides to soluble copper ions requires the use of oxidizing agents in addition to acidic conditions (Sherrit, Pavlides, & Weekes, 2005). However, at atmospheric conditions, even in the presence of these, the extent to which copper sulfide minerals react

depends on the chemistry of the ore; namely whether the ore is a primary or secondary sulfide.

Primary sulfides are typically encountered deep within the earth's crust. Their formation occurs due to the movement of aqueous solutions which originate below the crust of the earth. The high temperature and pressure in the sub-surface regions of the earth provide the driving force for the fluid to diffuse through the crust. The subsequent lower temperatures and pressures encountered cause dissolved species in the aqueous phase to precipitate out. These newly formed minerals are termed primary minerals. When sulfur is predominant, these minerals are termed primary sulfides. Secondary sulfides are formed from the oxidation of primary sulfides. The movement of groundwater through zones of primary sulfides causes them to be oxidized and dissolved. As the mineral rich solution permeates away from the main zone, the minerals may re-precipitate elsewhere. Depending on the conditions at the point of re-precipitation (i.e. reducing or oxidizing) the type of minerals formed vary. However, these re-formed minerals are termed as copper sulfides. (Rakovan, 2003). All copper sulfides require the presence of Fe^{3+} and O_2 for leaching to occur (Schlesinger et al.,

2011b). Referring to Figure 2.6 it can be seen that the zone where this occurs (top left of diagram) shows that highly acidic and oxidizing conditions are necessary.

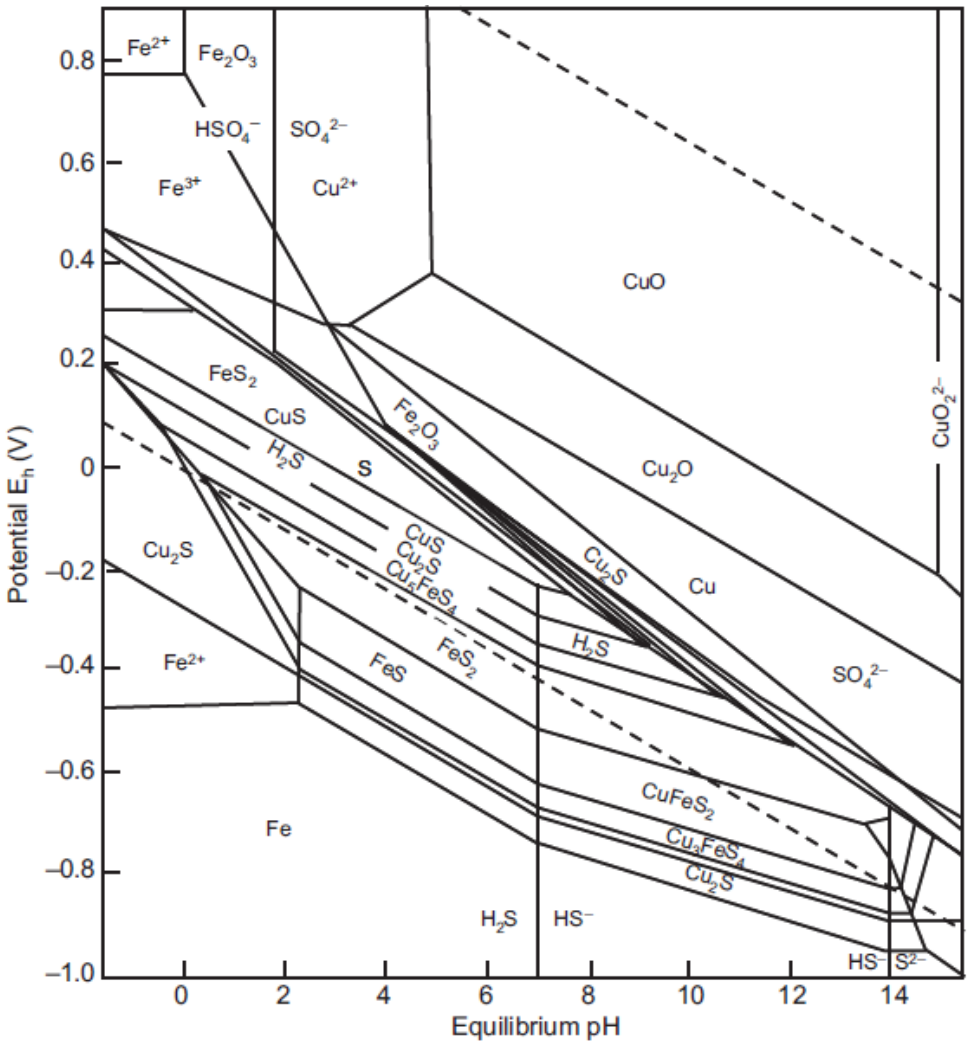

Figure 2.6 - Pourbaix diagram showing the Cu-Fe-O-H-S system at 25˚C. *[Cu]=10^{-2}M, [Fe]=[S]=10^{-1} M. Copper sulfide minerals require more aggressive conditions to solubilize copper as compared to copper oxide minerals. Copper sulfides require both acidic conditions and oxidizing agents to achieve the same state of dissolution. ©(Schlesinger et al., 2011a) (Reproduced with permission from Elsevier)*

Primary sulfides are significantly less amenable to leaching at atmospheric conditions, such as those in a heap leach. Minerals like chalcopyrite are very refractory in nature and need higher temperature and pressure conditions to break down their crystal lattice to produce

soluble copper. While Fe^{3+} and O_2 are used to break down the mineral, the reactions are performed in high temperature and pressure autoclaves. As a result they undergo little dissolution in a heap. (Schlesinger et al., 2011a)

Secondary sulfides are more amenable to heap leach treatments. In the process of leaching copper from these minerals, Fe^{3+} is used as the oxidizing agent and is reduced to Fe^{2+} in the process. The Fe^{3+} is regenereated by the oxidation of Fe^{2+} with O_2 (which is reduced to water). The reactions below exemplify some of the reactions that copper sulfide minerals undergo under atmospheric conditions with acid (*Reactions adopted from (Schlesinger et al., 2011a)*).

Chalcocite Leaching

(i) $Cu_2S + Fe_2(SO_4)_3 \longrightarrow Cu^{2+} + SO_4^{2-} + CuS + 2FeSO_4$

(ii) $4FeSO_4 + O_2 + 2H_2SO_4 \longrightarrow 2Fe_2(SO_4)_3 + 2H_2O$

(*overall*) $Cu_2S + 0.5O_2 + H_2SO_4 \longrightarrow Cu^{2+} + SO_4^{2-} + CuS + H_2O$

Covellite Leaching

(i) $CuS + Fe_2(SO_4)_3 \longrightarrow Cu^{2+} + SO_4^{2-} + 2FeSO_4 + S$

(ii) $4FeSO_4 + O_2 + 2H_2SO_4 \longrightarrow 2Fe_2(SO_4)_3 + 2H_2O$

(*overall*) $CuS + 0.5O_2 + H_2SO_4 \longrightarrow Cu^{2+} + SO_4^{2-} + H_2O + S$

In these reactions the Fe^{3+}/Fe^{2+} redox couple behaves in a catalytic manner. The reaction sequence that depicts the ferrous oxidation to ferric is (Schlesinger et al., 2011a):

Ferric/ferrous couple

(i) $4Fe^{2+} \longrightarrow 4Fe^{3+} + 4e^-$

(ii) $O_2 + 4H^+ + 4e^- \longrightarrow 2H_2O$

(*overall*) $4FeSO_4 + O_2 + 2H_2SO_4 \longrightarrow 2Fe_2(SO_4)_3 + 2H_2O$

Bacterial Leaching of Copper Sulfides Minerals

Heap leaching operations have found success in using bacterial micro-organisms to increase the rate of oxidation (Brierley, 2001). While the copper leaching reaction above can be carried out on their own, the bacteria act as natural catalysts increasing the reaction rates by orders of magnitude. The bacteria themselves are not directly involved in the leaching process. When Fe^{3+} is reduced to Fe^{2+} the bacteria act as an intermediary in the regeneration of Fe^{2+} to Fe^{3+} and the simultaneous reduction of oxygen to water.

The exact mechanism by which they function is still a subject of debate within the realm of bioleaching applications. As depicted in Figure 2.7 there are two proposed mechanisms by which they interact with the phases in the heap (Watling, 2006). The mechanism of indirect contact with the ore surface entails that aqueous species migrate to the surfaces of the bacteria from where the redox reactions are carried out. The mechanism of direct contact seemingly entails that the bacteria are in contact with the ore surface and from where the redox reactions are carried out on a thin membrane between the bacteria and the ore.

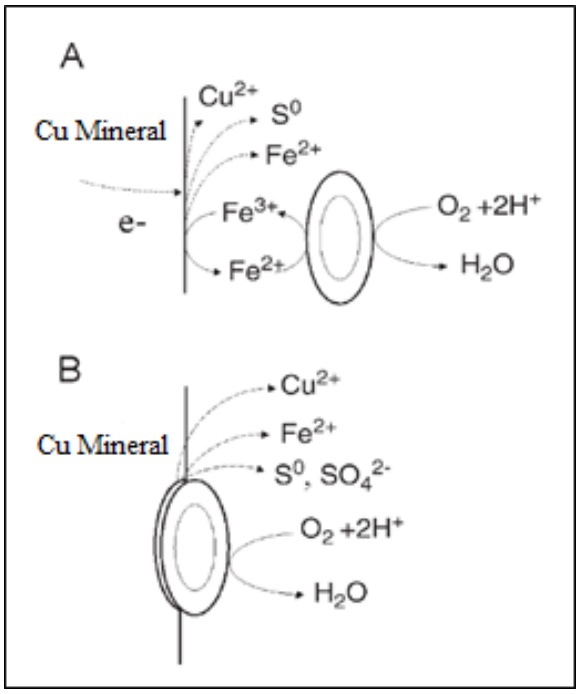

Figure 2.7 – Bacterial function in oxidation of copper sulfides. *The possible methods by which leaching of copper sulfide takes place are explained by two theories. Illustration A represents indirect contact mechanism where bacteria oxidizes ferrous ions to ferric ions. Ferric ions then further the dissolution of the copper sulfide by acting as an oxidizing agent. Illustration B represents a direct contact mechanism whereby the bacteria is in direct contact with the sulfide. The oxidation of ferric to ferrous occurs on a thin layer on the interface between them. The ferric then oxidizes the copper sulfide into soluble copper and sulfate. For either mechanism the presence of ferric is vital to enhance the leach process. ©(Watling, 2006) (Reproduced with permission from Elsevier)*

Whatever the mechanism of the type of interaction used by the bacteria success has been found in using them to increase the rate of reactions in heaps. There are several different types of bacteria and strains that the catalytic actions are typically attributed to. At low to moderate temperatures (approximately 20°C to 40°C) catalytic activity is commonly attributed to mesophilic bacteria such as Acidothiobacillus ferrooxidans, Leptospirillum ferriphilumooxidans, and Acidothiobacillus thiooxidans. At higher temperatures (40°C to 45 °C), Acidothiobacillus caldus is more prevalent. At elevated temperature (greater than 60 °C), thermophilic bacteria such as Sulfolobus metallicus and Metallosphaeraspp are believed to be the dominant bioleaching strains. (Watling, 2006).

As the bioheap leach technology has developed, numerous strains of bacteria have also been developed to optimize the leaching of copper. However, bacteria that best assist in leaching of the ores are typically native to the ore and their surroundings. These are developed more due to increased adaptability. When a heap leach is initially established bacterial introduction to the heap leach can be performed during the agglomeration stage, where an appropriate bacterial inoculum is mixed with the ore prior to leaching (Brierley, 2001). Nutrient delivery to bacteria also needs to be considered in the initial leaching stages, but as the leaching continues the bacteria are able to survive primarily on the host ore. Once the leach is established and the bacteria are able to continuously catalyze the regeneration of ferric, the reaction becomes autogenous and the bacteria are able to survive on the energy released for their cellular functions. Additionally the bacteria are able to convert sulfur produced from the leachate into sulfuric acid providing the bacteria with fuel and the heap with acid.

The use of bacteria imposes the need for stricter operational control. In order to ensure the survival of the bacteria, the temperature and conditions in the heap must be within the temperature and pH ranges that allow the bacteria to function at their prime. Lixiviant feed stock to heap needs to be carefully controlled such that deleterious species to the bacteria are not added into the system (e.g. recycled raffinate solution may contain some organic species that in sufficient amounts could be toxic to the bacteria). In addition to this, the nature of nutrients added into the heap needs to be managed well. While meeting the needs for bacterial development, the nutrients added need to be controlled such that their introduction into the heap doesn't result in the precipitation of species that are more difficult to deal with in downstream processing. (Brierley, 2001). Whilst not mandatory, bacterial assisted

leaching provides beneficial advantages over regular lixiviant heap leaching, by increasing the rate dissolution of copper sulfides. (Schlesinger et al., 2011a).

2.1.5 Heap Mechanics

An important aspect of the heap leaching process is the irrigation process and leachate flow through the heap. The physical contact of the liquid with the solid phases is necessary for the leaching of the minerals to take place. The permeation aspect of heap leaching is discussed in further detail in Chapter 3, section 3.2.

2.1.6 Heap Construction and Preparation

The heap preparation and construction are crucial steps that dictate how well optimized the heap is for fluid permeation. To maximize copper leaching the contact between the acidic solution and ore particles needs to be maximized. The following few sections highlight some of the commercially adopted practices used in preparing heaps.

Heap Foundation

The heap is constructed on a base with a slight gradient. It is vital to note that for successful extraction the heap leach pads need to be constructed atop a base which is impermeable (see Figure 2.8). This is to ensure no PLS is lost to the permeable ground underneath as it may contaminate the water table. Additionally the loss of PLS equates to a loss in revenue, so ensuring no PLS is lost is crucial. This also adds a constraint to the heap pile construction. The gradient on which the pile is constructed cannot be too steep (maximum slope is around

5˚) as this may cause the solids in the heap to slip and fall in the PLS storage pond. (Schlesinger et al., 2011a)

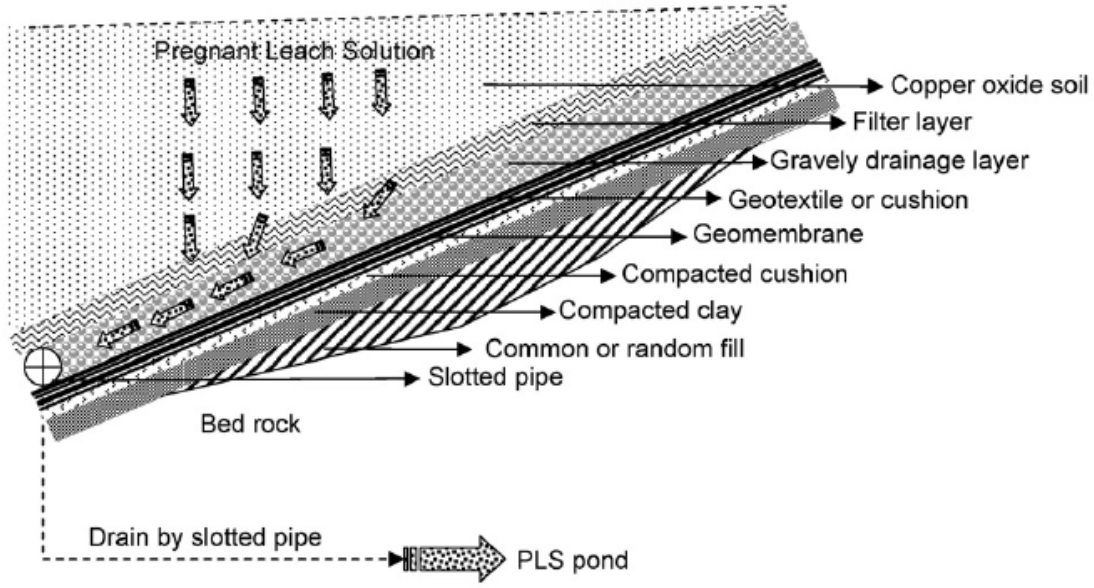

Figure 2.8 – Drainage mechanism for heap leach system. *Heaps are constructed atop impermeable bases with a slight gradient. Percolated fluid can be drained from the heap in due to the effect of gravity. ©(Majdi, Amini, & Chermahini, 2009). Reproduced with permission from Elsevier*

Ore sizing

Mined ore typically contains ore particles which greatly vary in size (see Figure 2.9). In a heap this would cause the problem of non-uniform application of acid to the leach surfaces, which would greatly limit the acidic solution from leaching all potentially reachable copper minerals.

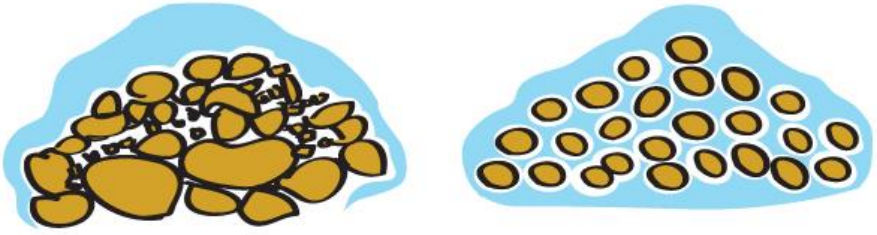

Figure 2.9 – Effect of sizing on fluid dispersion and wetting. *The figure depicts the difference when ores in a heap leach operation are not subject to a crushing and agglomeration (left) and when they (right). By subjecting an ore to crushing and agglomeration extraction leach kinetics can be improved as there is more uniformity of acid to ore surface. Fines in the ore reduce extraction kinetics due to localized saturation. Agglomeration helps bind the fines into larger particles, increasing heap permeability and reducing the limitations caused by fines. ©(Captaine & Carlson, 2017)*

The image on the left of Figure 2.9 is emblematic of a pile in dump leaching. As the ore is too low in grade to justify further size reduction the pile is irrigated as is. The permeation of fluid is not well controlled and leaching is not optimized. Crushing and agglomerating more evenly can produce shaped particles thereby ensuring more uniform application of acid to particle surface and hence faster leaching.

In heap leach systems, ore is typically crushed to between 10-50 mm in size. Below 10 mm the size of the particle has little benefit on copper extraction (Schlesinger et al., 2011a). In heap leaches the particle size used is controlled to ensure that the heap has sufficient permeability. A heap with too many oversize particles has poor wettability characteristics. A heap with too many fines may hinder fluid percolation and may cause localized oversaturation within the heap (Schlesinger et al., 2011a). The crushing and size reduction of the ore can be performed with the aid of conventional crushing equipment such as primary crushers (e.g. jaw crusher, gyratory crusher) as well as secondary crushers (e.g. HPGR's)

(Dhawan, Safarzadeh, Miller, Moats, & Rajamani, 2013; Ghorbani, 2012). The use of crushers and the circuits employed for size reduction are dependent on ore type and desired final particle size.

Agglomeration

Another practice adopted prior to the heap leach is the agglomeration of the ore. A major problem for the heap leaching process is the presence of fine material which tend to hinder fluid flow. Fines are introduced into the heap from crushing of the ore, but the degree to which they are liberated is dependent on the ore. Ores that contain a large portion of soft clay like material may produce may many fines by virtue of the fact that softer materials are more amenable to size reduction. However, if overall, the ore is processed too much in a crush cycle then too many fines may also be produced, regardless of type.

They pose a limitation in leaching as mobilization of fine particles cause localized saturation and reduce heap permeability. (Dhawan et al., 2013) (see Figure 2.10). Fine material has a higher tendency to migrate within the heap, especially toward the bottom. This causes them to segregate and settle into spaces between larger particles. The result is blinding of the particle surfaces, as permeation of the fluid through these dense layers of segregated particles is severely limited. Over the scale of a heap this causes valuable and accessible mineral particles to be locked out to leaching and overall reduces the efficiency of extraction. To minimize this agglomeration is used.

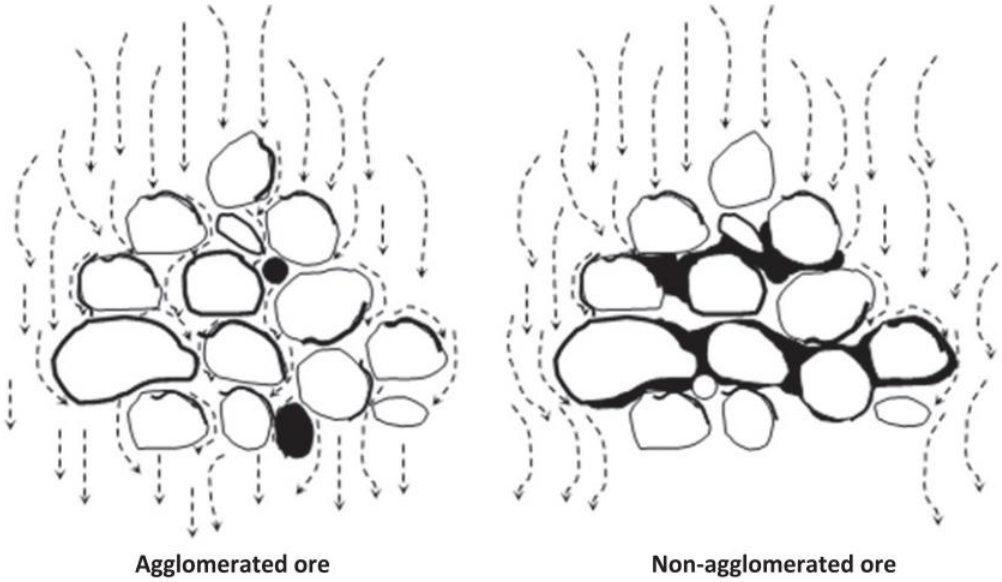

Figure 2.10 – Effect of agglomeration on particles in heap. *Fines in a heap have a tendency to move downward. This can reduce the efficiency of the heap leach process. Segregated particles can cause blinding of the solution to ore surfaces, locking out valuable mineral from leaching. ©(Dhawan et al., 2013). Reproduced with permission from Elsevier*

During heap leach operations, extraction is usually limited by diffusion of acid through the heap rather than reaction kinetics (Schlesinger et al., 2011a). Combined with the problem of solution channeling and blinding, permeation through the heap may become hindered especially in the presence of too many fine materials. (Marsden & House, 2006a). Agglomeration helps to improve the permeability of the heap aiming by creating a more uniform distribution path for the leach media to the particles and exposed surfaces (Schlesinger et al., 2011a).

Agglomeration of ore material can take 2 forms: (a) the binding of fine material to each other, or (b) the binding of fine material to the ore larger particles. In the case of the former the particles form small clumps or granules with no defined core/nucleus. In the case of the

latter the fine materials adhere to the larger ore pieces form a rim around them. The rim structures are preferred in heap leaching as they are more stable. (Dhawan et al., 2013).

Agglomeration is performed by keeping particles in motion (e.g. using a rotating drum), and by gradually introducing the necessary media to cement the particles together (namely water, and leaching media). The agglomeration of the particles is akin to the construction of a snowball. As the drum is in motion the contact between the particles allows them to adhere together through liquid bridges. The liquid acts a binder as allows the finer material to adhere to the larger particles through capillary action and surface tension. (Dhawan et al., 2013) In the case of copper ores, concentrated acid and water are usually added for agglomeration (Schlesinger et al., 2011a). Raffinate can also be added as part of the agglomeration media. Additionally for sulfidic ores, bacterial inoculums can also be added into the agglomeration stage. This allows the bioleaching to get a fast start compared with no bacterial inoculum directly added during agglomeration.

Depending on the type of ore and the presence of fines the residence time in the agglomerator and the media used need to be controlled. In the case where hard ore material is being used and the percentage of fines is relatively low, long residence times would not be necessary and water and/or weak acidic media would usually be sufficient to bind the fines into rims on the larger particles. In the case where soft clays and a large percentage of fines are present, long residence times as well as binding agents such as cements (Dhawan et al., 2013), or polymer matrices (Underwood, 2000), may be necessary to improve agglomeration. The addition of

acid during agglomeration also has the benefit of dissolving readily accessible copper from the mineral. Overall the agglomeration procedure is a well established practice to minimize the movement of fines and the associated problems that it causes (Marsden & House, 2006a), and has been found to have an overall positive effect on the heap leachability (Bouffard, 2008).

Heap Construction

This aspect of heap leaching is essential as the majority of the costs that arise are as a result of this. In stacking a heap pad, a major variable is the pile height. There is a tradeoff between pile height and cost. (Connelly & West, 2009). A lower pile height may demand a greater capital as there is a greater surface area to irrigate and may also produce a lower grade pregnant leach solution. This however, would be off-set by greater overall recovery and effective aeration may be more easily achieved. (Schlesinger et al., 2011a)

Stacking height is an important factor for consideration during heap construction. There are 2 main methods by which heap pads can be constructed, dynamic and multi-lift pads. Dynamic pads consist of a single-lift (single stack) whose contents are replaced with fresh ore after leaching has occurred. Multi-lift pads consist of a single stack of ore which is leached and subsequent lifts are built atop the initial one. While multi-pad lifts offer ease of operation as ore simply needs to be added, the increased height may introduce extraction difficulties (e.g. aeration and irrigation may get strained with an increase in volume of material). Additionally as pads get taller, acid added may begin to increasingly leach gangue as lower heights of the

pads would consist of mostly leached material. (Schlesinger et al., 2011a). Single lift pads offer increased leach effectiveness with the downside of increased logistics for constructing and dismantling a pad. This doubling handling of the ore can add significant cost to the operation. (Lupo, 2006). The stacking of the ore is performed with mechanized loaders and conveyors, wherein the material is fed on a base and systematically layered until the desired heap height is achieved.

Heap Irrigation and Aeration

A constructed heap needs to be irrigated with acidic solution in order for leaching to occur. The irrigation of the heap is typically achieved with the use of interconnected dispersion system laid atop the heap. The points of irrigation need to be laid out in such a way that irrigation is maximized but does not oversaturate the heap. The lixiviant is dispersed at a low rate to avoid pooling at the surface and to allow for free movement of air through the pile. Typically raffinate is added as the lixiviant as well as fresh acid to make up for acid loss in previous leaches. The fluid is added to the heap at approximately 10 $L.m^{-2}.h^{-1}$, but the rate is typically adjusted based on the hydraulic conductivity of the ore. (Schlesinger et al., 2011a)

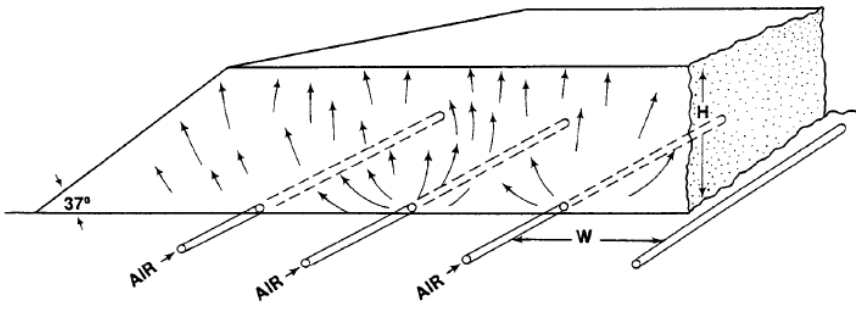

Figure 2.11 – Heap Aeration. *(© (Bartlett, 1997), adapted with permission of Springer).*

Heap aeration is typically applied as depicted in Figure 2.11 with the aid of pipes, which span the heap. The aeration is typically applied to increase the flow of oxygen through the heap when sulfide leaching is performed or when bacterial activity needs to be enhanced (Watling, 2006). The aeration is performed depending on the grade of the copper in heap. When the grade is high enough to justify the extra cost of forced air supply it is typically applied. (Schlesinger et al., 2011a).

The heap irrigation and transportation also serve as control mechanism for the heat dissipation through the heap. The exothermic reactions need to be controlled. This is especially important when bacteria are involved as the temperature needs to be maintained to where the bacteria are able to function at their optimal level.

2.1.7 Heap Leaching and Surfactants

Surfactants have been proposed as a viable alternative to enhance the leachability of the ores and improve extraction from the heap overall. Research into the use of surfactants in heap leach systems has been performed at a lab scale (Bender et al., 2016; Vest, Lüzerath, Freidrich, & Seelmann-Eggebert, 2009). The research involved studying the impact on copper extractions using column leaches. The effectiveness of the surfactants are made by comparing overall extractions against columns in which no surfactants are present.

Surfactants are soluble molecules and so their introduction points into the heap leach are achieved where leach fluid is introduced into the system. They can be added into the system

in the agglomeration stage (Underwood, 2000; Vest et al., 2009) or with the leach liquid that is fed into the heap (Bender et al., 2016; Vest et al., 2009).

However a review of the literature has found that the use of surfactants in heap leaching has not been widely explored or discussed as an operational consideration. Additionally, the use of surfactants in industrial heap leach settings is not yet an adopted practice. Outside of comparing the improvements in copper leaching, the effects of the surfactants imposed on the heap leach system are not well understood.

The aim of the research in this thesis is to better understand and characterize the role of surfactants in the heap leach process. Their primary function is to alter the behavior of a liquid in contact with a secondary phase (this is reviewed in greater detail in section 4.1). In the heap leaching process the dissolution of copper occurs where the acidic media and the ore come into contact. Through a series of carefully designed experiments, the goal of this thesis is to produce a systematic study further detailing where the influence of the surfactants is the strongest and how this allows for increased extraction in a heap.

Chapter 3: Heap Leach Testing

To begin investigating the effect of surfactant on leaching and extraction, heap leach columns were set-up. Determining the impact of surfactants required exposing ore to leachate loaded with and without surfactant and comparing copper extraction. To simulate a heap leach at a laboratory scale, ore is packed in columns and irrigated with acid. For these experiments, the operating conditions are further elaborated in the following sections.

3.1 Experimental Basis

The column experiments that were performed for this thesis were based on prior work done by BASF (Bender et al., 2016). For their work, BASF used 6ft columns and a low grade copper ore (~0.42% copper concentration) with 91.2% of the copper present as acid soluble copper (Bender et al., 2016). Using a pre-determined: particle size distribution, agglomeration procedure and leachate composition – the BASF columns were loaded with a set amount of material and run in a manner that simulated a heap leach.

The ore and the surfactants used for the work in this thesis were supplied by BASF and were the same ones used by them for their experimental work. Using the BASF experiments as a frame of reference, the column work performed for this thesis was set to closely mimic as many of the same working conditions as possible. Having previously worked with the same

ore type and surfactants, the decision to use their preparation methods and experimental conditions was made in order to best optimize the experiments.

The biggest difference between the work conducted by BASF and the working methodology for this thesis was the direction of flow of the acidic leach media. BASF columns operated with fluid flow going from top to bottom, whereas, the columns employed here were operated from bottom to top (i.e flooded vats). This was to overcome wetting issues commonly encountered in heaps operated in down flow mode. To better understand why this occurs, the characteristics of fluid permeation in heaps need to be understood.

3.2 Wetting Issues in Heap Leach Systems

Heap leach operations work via the irrigation of a heap with leachate dispensed from the top and collection of the resulting pregnant leach solution at the bottom. Simulated heap leaches in columns are operated in the same manner. However, the experimental work carried out for this thesis, involved ore being placed in columns with leachate being pumped in from the bottom **(**see Figure 3.8). The leachate essentially flooded the reactor before exiting as pregnant leach solution from the top of the column. The reason for this centered around wetting issues common to heap leach systems.

3.2.1 Leachate Flow in Heaps

When irrigated the dispersion of leachate is done from a point source. Fluid movement is predominantly vertical through the heap, with solution flow typically in "main" channels along the point source where leachate is being introduced into the heap (see Figure 3.1). However, not all leachate introduced into the heap remains in motion and percolates its way through the system. A large portion of the fluid added is retained within the heap itself (Dixon & Petersen, 2007). The fluid is retained between particles in crevices, cavities, pockets and other such voids that can accommodate pools of leach solution (see Figure 3.1). The continuity of the heap leach process is facilitated in those zones where the moving fluid comes in contact with stagnant fluid. The contact allows for the exchange of constituent aqueous species to and from the ore particles (Dixon & Petersen, 2007).

The retention of stagnant fluid against particle surfaces allows for acidic media to penetrate the pores and cracks in ore particles. As it does so the voids in the particles get filled by the fluid. This creates a diffusion pathway for both reactants to travel to the mineral surface and reacted products to travel outside the ore particle (see Figure 3.2).

These stagnant pools of solution also play a vital role in the exodus of leached/dissolved copper from within the heap at large. The moisture trapped between the pore spaces of particles creates a network of liquid pathways through which dissolved species can migrate. Ionic and other aqueous species migrate across this network of stagnant solution pathways via molecular diffusion. In this way species move across this "network" along concentration

gradients to zones where flowing solution comes in contact with stagnant solution (Dixon & Petersen, 2007). As mentioned before, these areas of contact allow for the exchange of species. In this way dissolved copper is removed from the heap at large.

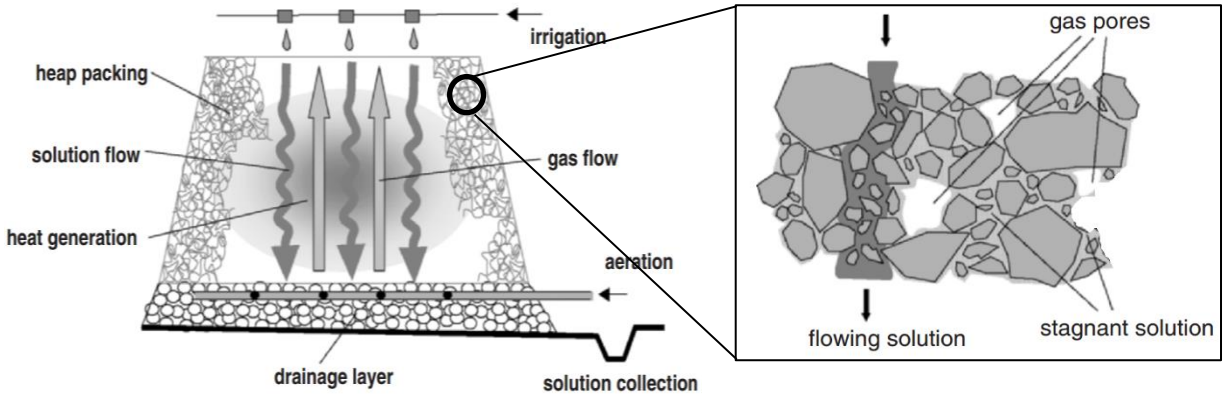

Figure 3.1 - A heap indicating the major heap-scale transport effects (left). A cluster of particles within a heap bed (right). *Solution introduced into the system percolates its way through the bulk phase but a significant portion remains as stagnant solution between ore particles. The pools of stagnant solution serve an important role in creating diffusion pathways for dissolved mineral ions. Dissolved species migrate into the stagnant pools, from the ore particles. Aqueous species are able to migrate through the heap across these inter-connected pools of stagnant solution. Flowing leach solution comes into contact with these stagnant pools and is able to exchange dissolved constituents with it.©(Dixon & Petersen, 2007), reproduced with permission of Springer)*

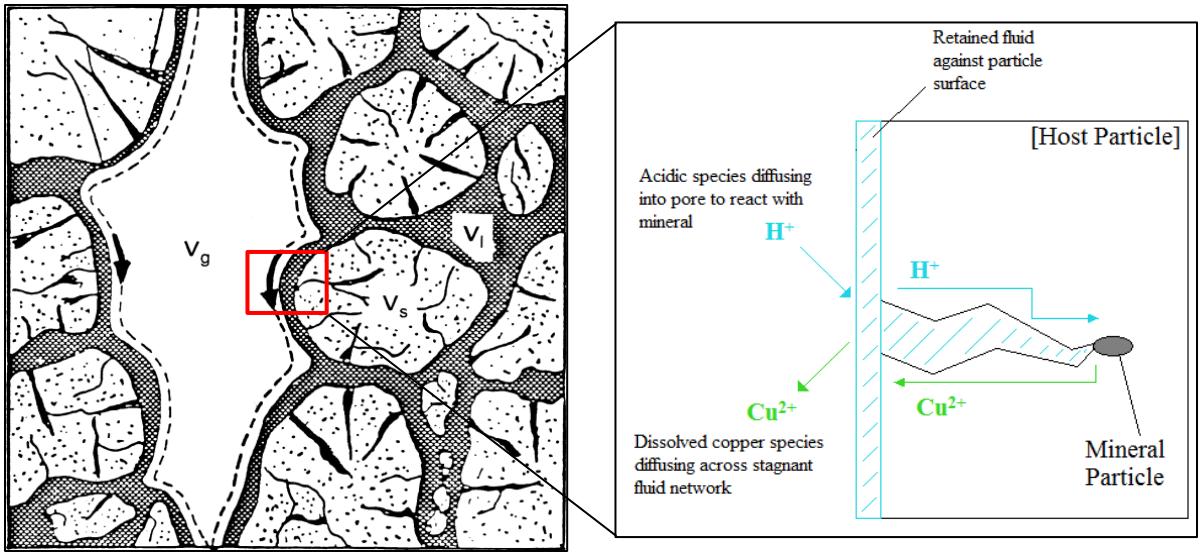

Figure 3.2 - Schematic of a heap showing space occupied by solids, rock porosity, solution void space and air void space (left). *Fluid is retained in stagnant pools against the surface of mineral particles. This is important as it allows for the solution to penetrate the particles via its cracks, flaws and pores. Once inside, acidic media can react with leachable mineral surfaces. Dissolved species can then diffuse out of the micro-pores of the host particle into the stagnant solution pools. From there it can diffuse across the network of solution pools into channels of flowing solution where it can exit the heap.©(Bartlett, 1997), reproduced with permission of Springer).*

3.2.2 Wetting Issues Associated with Heaps

A common issue associated with heap leaches is the wetting of particles from leachate percolation. The rate of extraction and movement of dissolved species depends on how effectively wetted the heap and particles within them are (Dixon & Petersen, 2007). Depending on the particle size distribution and packing procedure employed the final porosity / spacing between particles may limit the degree to which fluid can percolate through the heap. This can directly impact the geometry of the stagnant solution zones, which in turn can directly affect the movement of aqueous species (Dixon & Petersen, 2007). Additionally, solution flow channels may be impacted, both in terms of flow direction as well as their proximity to stagnant solution zones.

When a heap is initially irrigated, leachate is generally applied from localized applicators at certain points on the heap (e.g drip irrigators on a large grid). Whilst fluid flow would be considered vertical through the heap, the delivery of acidic media laterally is achieved through capillary action. As depicted in Figure 3.3, fluid added at the top of the heap would disperse both downward and outward as it percolated through from the point of introduction. In this way a heap could be perceived as a bulk phase with the spaces between particles as a matrix of pores through which solution permeates (Dixon & Petersen, 2007). As fluid occupies these pores, the subsequent migration and exchange of aqueous species can take place.

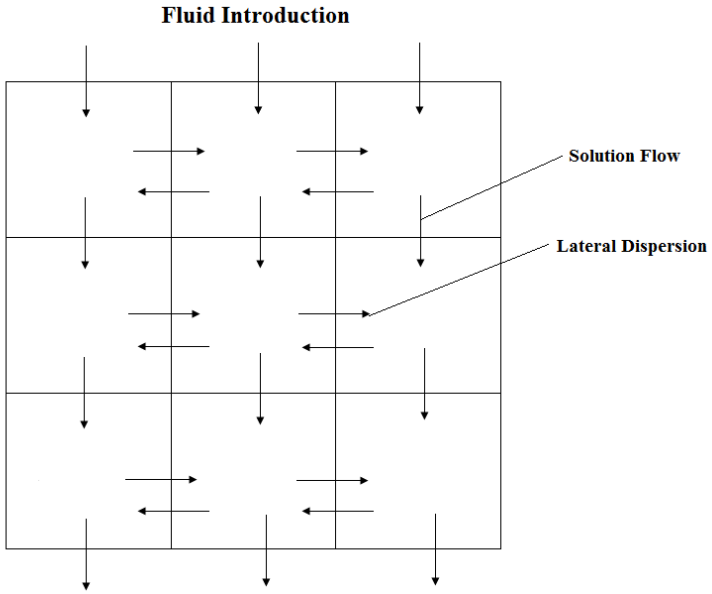

Figure 3.3 - The figure depicts the movement of fluid in a heap as it gets irrigated. *The heap can be envisioned as bulk of particles with the spaces inbetween them as a matrix of pores through which solution permeates. Solution is only added a fixed distances from each other and solution flow would typically be considered vertical. However, with the aid of capillary action, the fluid can still permeate laterally to particles located in between the irrigation points.*

The fluid application must be administered and maintained carefully. If the distances between irrigation points is too large, solution delivery may be hindered. While lateral dispersion does occur to wet particles perpendicular to solution flow, the degree to which this occurs may vary considerably. With an increased distance between irrigation points, the ability of a fluid to disperse further sideways (to reach particles in the center of the irrigation points) considerably decreases (Dixon & Petersen, 2007). As distance limits the extent to which capillary action can effectively wet particles, a limit on the effective exchange of ionic and aqueous species is also likely. Particles suffering from inadequate delivery of acidic media, will also suffer from inadequate access to flowing solution. This poses a limitation on the overall system, as leachable copper maybe relegated as "waste" by virtue of the fact that the acidic media is unable to or has limited contact with the host particle.

Additionally with top down flow, forced solution channeling may also pose a challenge. Fluid may be forced to flow down certain channels/spaces between particles. This forced diversion may occur due to the presence of excessive fines, or poor agglomeration or particle packing (Schlesinger et al., 2011a). This creates dead zones with no fluid flow or fluid permeation and by extension no leaching is able to take place. Just as before, this results in same overall system limitation.

3.2.3 Flooded Heaps & VAT Leaching

Heap leaches operate through a complex combination of physical, chemical (and some cases biological) processes. In addition to the wetting issues highlighted in the previous section,

optimizing the conditions for successful heap leaching requires understanding the long and complex chain of sub-processes that comprise the leach process (Dixon & Petersen, 2007). Often the efficiency of operation is dictated by how successful transport of the acidic media to the exposed mineral particle surfaces. Operating a heap leach as a homogenous mixture, with the necessary solid-solution contact to achieve optimum extraction is not always possible. Because of how heap leaches are prepared and operated, factors such as inadequate mixing, limited solution flow and other rate limiting attributes can and do occur (Marsden & House, 2006b).

In a test column, attributing differences in extraction solely from the presence of surfactant may not be entirely definitive if wetting issues are unaccounted for or if complete wetting is not a certainty. By operating the column as a flooded vat all particles in the column are immersed in the leachate. This results in an even wetting of all particle surfaces and eliminates the limitations that may be present from columns operating in top-down flow. In addition by maximizing solid-liquid surface area contact, the contact time is also maximized thereby ensuring that all particles are exposed for the same amount of time as the leachate flows through the column.

Leachate upflow is typically uncommon as a representation of heap leaching. However, for this work the aim of the leach experiments was not to replicate the heap leach process. The aim was to more definitively attribute differences in extraction solely to the presence of surfactant in leachate. The inherent wetting issues created from normal irrigation could be

minimized using the leachate up flow method, if not entirely eliminated, for the reasons mentioned in the preceding section(s).

3.3 Experimental Set-Up

3.3.1 Ore Preparation

3.3.1.1 Ore Selection and Particle Size Distribution

The ore was shipped from BASF in Tucson, Arizona, and was delivered pre-screened into the following size fractions:

- -0.254 mm
- +0.254, -6.35 mm
- +6.35, -12.7 mm
- +12.7, -19.05 mm
- +19.05, -25.4 mm
- +25.4, -38.1 mm
- +38.1 mm

The mineral processing (crushing & grinding) and size verification was performed and confirmed by SGS in Tucson, Arizona (Bender et al., 2016). The ore being present in separate size fractions and within the typical sizes used in leaching, meant that additional mineral processing in the form of crushing or grinding was unnecessary. As the ore was

separated prior to the commencement of the test work, the procedures established by BASF called for the needed amount of each size fraction to be weighed out, agglomerated and then loaded into the columns.

For the work performed by BASF the particle size distribution employed by them for their various columns was as follows (see Table 3.1):

Particle Size (mm)	***Mass Percent (%)***	***Weight per Column (kg)***
-0.254 mm	8.41%	7.64
+0.254, -6.35 mm	9%	8.17
+6.35, -12.7 mm	8.23%	7.47
+12.7, -19.05 mm	8.64%	7.84
+19.05, -25.4 mm	10.3%	9.35
+25.4, -38.1 mm	35.5%	32.21
+38.1 mm	19.94%	18.1

Table 3.1 – Proportions of size fractions used by BASF for their heap leach columns. *Each column employed used approximately a total of 90kg of ore material. The various size fractions comprising the bulk mixture were added in the portions listed as shown. Values obtained from BASF published literature "Leaching Aids for Dump and Heap Leach; SX Compatibility, Biocompatibility and Recycle of Lixiviant" - (Bender et al., 2016)*

When plotted as cumulative function the particle size distributions yielded the following:

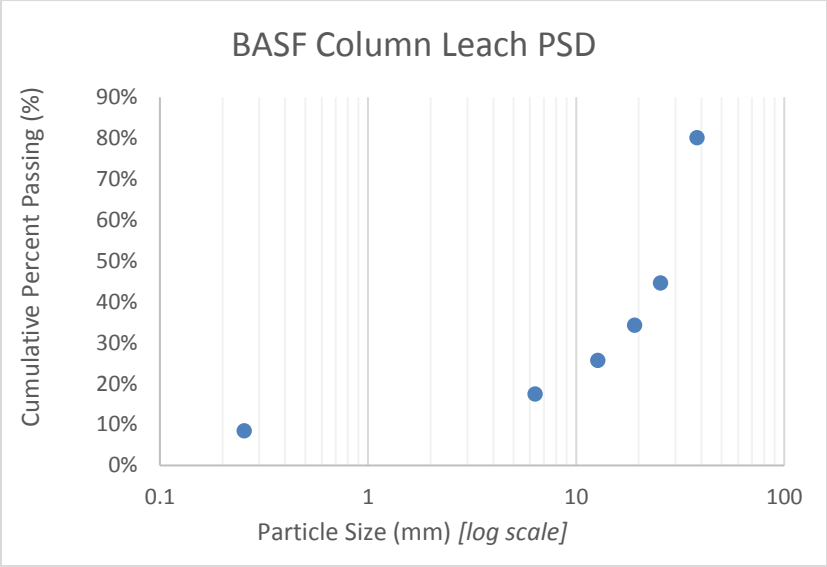

Figure 3.4 – Cumulative Particle Size Distribution used in BASF columns.

The P_{80} value for the size distribution used by BASF was roughly 38.1 mm. The P_{80} references the 80% passing value in a particle size distribution. In other words, 80% of the particles in the mixture are smaller than the P_{80} value. Columns employed by BASF each measured 6ft. in height with a diameter of approximately 1.5ft. Each column was loaded with approximately 90kg of material (Bender et al., 2016). The size of the columns (each with an internal volume of ~10.6ft^3/~0.3m^3) had the capacity to support a larger amount of materials with a wider particle size distribution with a P_{80} as large as 38.1 mm.

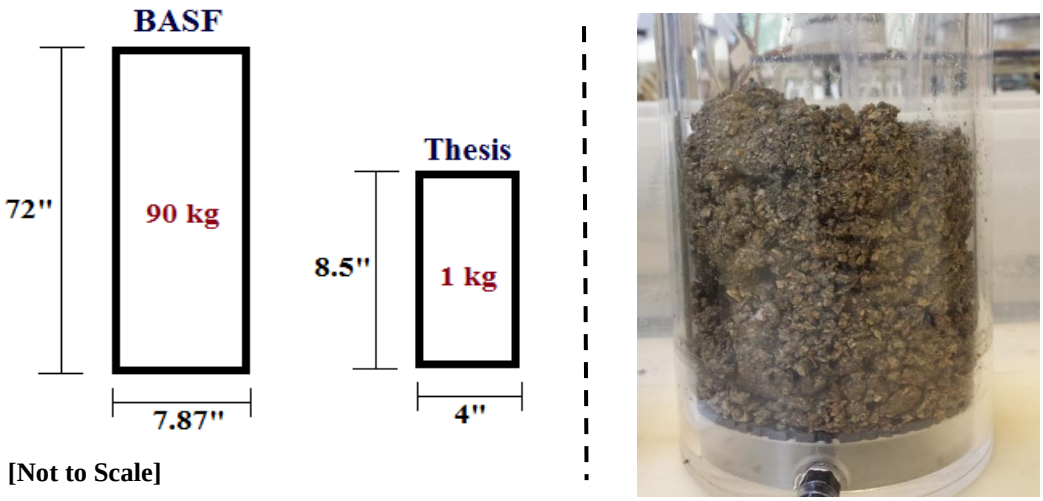

Figure 3.5 – Comparison of columns used by BASF and work for this thesis (left). Photo of column in this work loaded with ore (right). *The columns used in thesis were significantly smaller than the ones used by BASF. The columns used by BASF had an approximate internal volume of roughly 0.3m^3. The columns in this thesis had an internal volume of roughly 0.0017m^3. Comparatively, the columns used by BASF were able to accommodate a significantly larger amount of ore, as well larger sizes. For the test work in this thesis, the material fed into the columns was limited to 1 kg of material and the particles used were limited to the smaller size fractions*

For the work performed in this thesis, the particle size distribution of the material employed was not as large as the one employed by BASF. The reason for this was the difference in size of the columns employed. As highlighted in Figure 3.5, the size of columns used for this thesis were acrylic columns measuring 8.5" in height by 4" in width. A total mass of 1 kg of ore was introduced to the column owing to the size limitation. Replicating the exact particle size distribution as used by BASF in smaller columns was not feasible. The main limitation causing this was that the larger particles were limited to a few, if any, that would fit in the column. When limited to 1 kg of material the physical number of ore pieces sized 1" or above would have been limited 1 or 2 that could fit. This would also have created a statistically biased particle distribution.

To overcome this limitation, for the small columns in this thesis, the particle sizes employed were up to +19.05, -25.4 mm in size. Larger size fractions were not employed for these columns. The mass that was to be occupied by these size fractions was replaced in equal parts by the smaller fractions. When identified as mass percentages, in the BASF columns, the +24.5, -38.1 mm and +38.1 mm size fractions accounted for roughly 55% of the mass input. When replaced, an additional 11% of each preceding smaller size fraction was added to normalize the mass. This resulted in a particle size distribution as follows:

Particle Size (mm)	***Mass Percent (%)***	***Per Column (kg)***
- 0.254	19.50%	0.195
+ 0.254	20.09%	0.2
+ 6.35	19.31%	0.193
+ 12.7	19.72%	0.197
+ 19.05	21.38%	0.214

Table 3.2 - Particle size distribution used for the test work in this thesis. *As compared to the BASF work, the amount of material used was significantly reduced and so the particle size distribution had to be adjusted accordingly. The reduced mass also meant that smaller particles had to be used. Due to the size and mass of the columns employed in thesis, sizes above 1" could not be accommodated in the columns.*

When plotted as cumulative function the particle size distributions yielded the following:

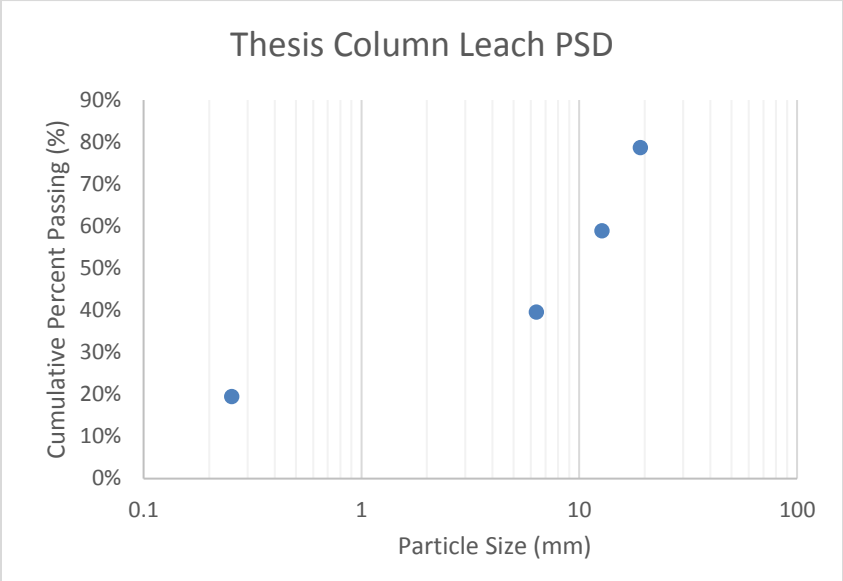

Figure 3.6 - Cumulative Particle Size Distribution used in columns for this thesis.

3.3.1.2 Ore Dressing

Prior to the ore being loaded into the column it needed to be prepped and dressed. For this concentrated acid and water were used. According to procedures and tests established by BASF the amount of acid added for the agglomeration was calculated to be 25% of total acid consumption as determined by the bottle roll test (Bender et al., 2016). This amounted to 1.52kg of acid and 1.75kg of water were used for every 90kg of ore. Per kilo of ore this was roughly 16.7g of acid and 19.3g of water. Concentrated sulfuric acid (98% by purity as manufactured by BDH chemicals) along with DI water was used for agglomeration.

The agglomeration was carried out using a tarp roll. The weighed fractions were placed in the middle of a laid tarp/sheet. The edges of the tarp were lifted in turn to allow the material in

the middle to roll over itself. Once mixed, but still dry, the pile was sprayed with water until lightly covered and once again rolled lifting the tarp edges. This was repeated with controlled water addition so as to allow the fines to stick to the larger particles, but without causing the mixture to become overly saturated. When completed, the concentrated acid was added with an applicator and the mixture once again rolled. When completed, the agglomerated mixture was carefully added to the columns.

3.3.2 Reagent Preparation

The 3 columns were set up to have nearly identical conditions save for the leachate composition. As per the work performed by BASF the acid concentration used for the leach liquid was 10g/L sulfuric acid (1% H_2SO_4), with additional acid added to correct for purity. This was prepared using reagent grade sulfuric acid (98% purity H_2SO_4 manufactured by BDH chemicals) and DI water.

The aim of running column leach tests was to compare and contrast the effect of surfactant in the leachate. To this end the sulfuric acid solution used for each feed line was produced identically. For these columns two surfactants were tested to observe their effect on the leach. The first surfactant, referred to as MC1000, was present at 50ppm. The second surfactant, referred to as DP-HS-1002, was present at 25ppm. [The details of their usage was highlighted by BASF in a paper published in Copper 2016 with the title “Leaching Aids for Dump and Heap Leach; SX Compatibility, Biocompatibility, and Recycle of Lixiviant”. In it surfactant MC1000 was referred to LA-A and DP-HS-1002 was referred to LA-B (Bender et al.,

2016)]. The addition of surfactant into the lixiviant was calculated and added on a mass basis.

The following were the lixiviant conditions employed for the 3 columns:

Column 1 [Control]	**Column 2** MC1000	**Column 3** DP-HS-1002
1% H_2SO_4 - (10g/L H_2SO_4)	1% H_2SO_4 - (10g/L H_2SO_4) MC1000 (50ppm)	1% H_2SO_4 - (10g/L H_2SO_4) DP-HS-1002 (25ppm)

For their tests and comparisons, BASF ran the 2 surfactants at 25ppm and 50ppm each in a number of different columns (Bender et al., 2016). While keeping in line with their tests and through discussions held with them prior to the test work commencing, the conditions in the table above were deemed the best conditions to use for the lab scale leaches.

3.3.3 Reactor Set-Up

To create a flooded leach environment, the reactors were set up to have fluid flow run vertically upward through the column (see Figure 3.7 and Figure 3.8). Buckets with the respective leachate were set as input/feed reservoirs, which fed into the individual columns. The columns were operated in a one-pass manner, whereby fluid was pumped once through the system and no re-circulation was done. The input reservoirs where checked daily for leachate level and topped up as necessary to ensure constant leachate flow through the column for the duration of the experiment.

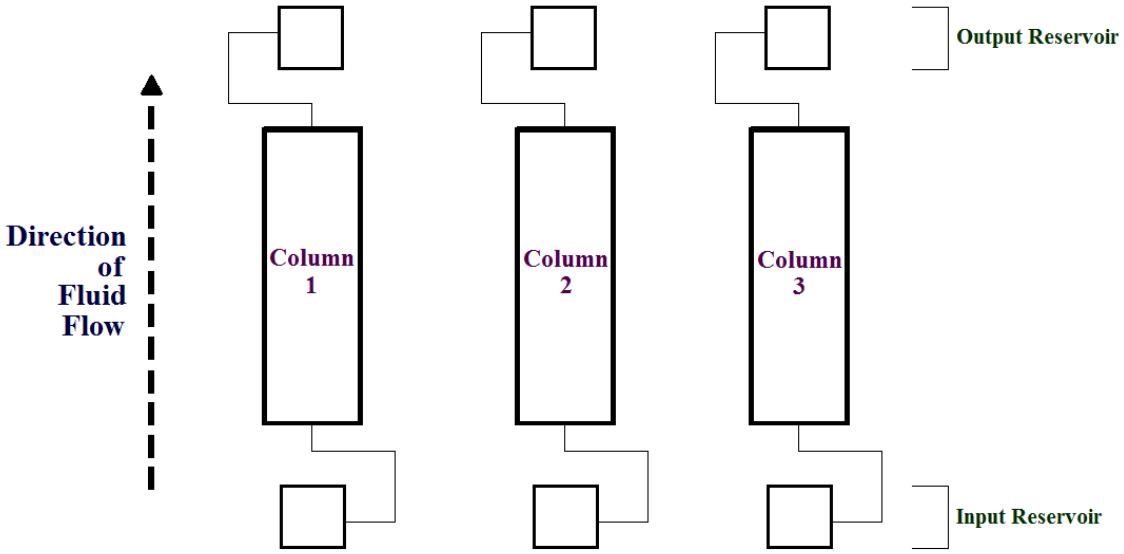

Figure 3.7 – Leaching column configuration. *The "input" reservoirs were buckets with fresh acid (1% H_2SO_4) which were connected to the bottom of the column. The acid was fed in and flowed vertically upward through the heap. The "output" reservoirs were collection receptacles for pregnant leach solution (i.e. copper rich solution) that flowed out of the top of the column.*

The lixiviant feed into the columns was facilitated with the aid of a peristaltic pump. A Masterflex L/S pump drive with standard clear case polycarbonate pump heads were used for this. Each column was fitted to an individual pump head, with all pump heads being accepted by one pump drive. In this configuration the same flow rate could be ensured for all the columns.

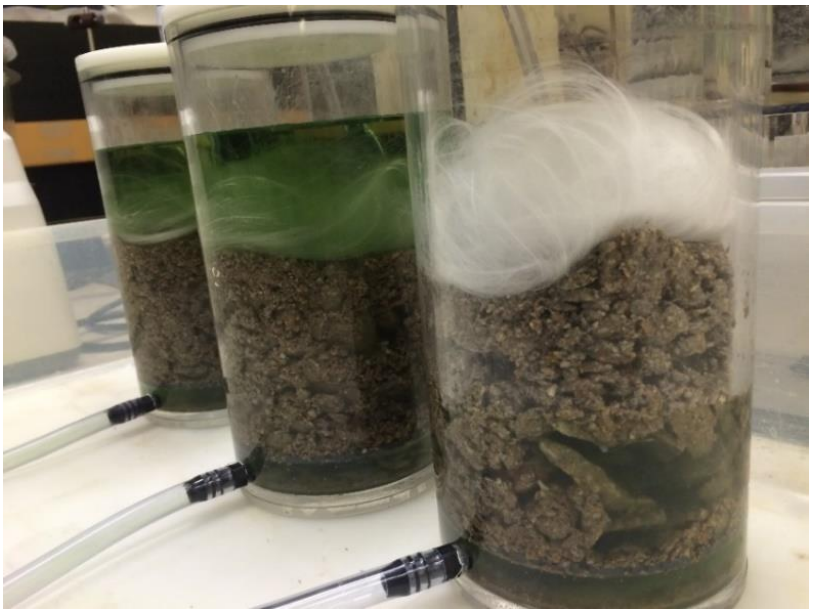

Figure 3.8 - Flooded VAT columns with leach flow upward through column. *The picture shows the columns during the first few hours of leaching. The deep rich green color results from the dissolution of copper from the agglomeration stage. Pregnant leach solution exited from the top of the column.*

The flow rate employed by BASF for their individual columns was 8 $ml.min^{-1}$ (Bender et al., 2016). By taking the size of their columns into account the lixiviant flux rate equated to 14.8 $L.m^{-2}.h^{-1}$. Based on this, and re-calculating and re-adjusting it to the columns for this work the flow rate was calculated to be 2 $ml.min^{-1}$. The pump drive and pump heads were calibrated and checked for flow rate using a stopwatch and a measuring cylinder to ensure accurate fluid throughput.

3.3.4 Sampling and Primary Data Collection

The pregnant leach solution (PLS) was collected in an output reservoir which flowed out of the top of the column once it made a pass through the ore (see Figure 3.7). The columns were run for approximately 55 days. The output reservoirs were checked daily. Samples were also

collected daily for analysis. In addition to sample collection, the weight of each output reservoir was recorded. This, along with the data from Atomic Absorbance Spectrometry, allowed for the calculation of daily copper extracted. pH and oxidation-reduction potential of the PLS were also recorded daily.

Figure 3.9 – Pregnant Leach Solution in output reservoir collection buckets. *The PLS samples were collected in buckets as shown in the picture above. The weight of the collected sample was recorded daily. A sample of the solution was also collected to determine copper concentration. The dark green color is the result of the easily reachable copper being leached first. The color of the collected fluid becomes lighter over time as leachable copper in the ore gradually diminishes.*

3.4 Sampling and Analysis to Calculate Copper Extraction

The progress of the columns was monitored via the extraction profile generated by each column. Daily samples were collected and analyzed to measure the copper leached. The cumulative total was calculated from this to determine the rate and overall extraction.

3.4.1 Analysis of Pregnant Leach Solution (PLS)

The PLS samples, collected from the output reservoirs, were analyzed using a Varian AAS 240 Atomic Absorbance Spectroscopy analyzer (see Figure 3.10). The samples were analyzed using a copper lamp which emitted light at a wavelength of 324.8 nm. The AAS allows for the determination of the concentration of an aqueous species. Samples obtained from the output bucket of the columns were collected and analyzed using AAS to check for copper concentration.

Figure 3.10 – Varian AAS 240 Atomic Absorbance Spectrometer

Samples of pregnant leach solution needed to be diluted before they could be fed to the AAS for analysis. All solution preparations were done by dilution in 1% nitric acid (reagent grade HNO_3 as supplied by BDH Chemicals).

To facilitate the analysis, copper standards were prepared and used to create a calibration curve before the analysis was performed. Copper standard as manufactured and supplied by SCP Science (1001 μg/ml in 4% nitric acid solution [i.e. Cu^{2+} at a concentration of 1001 ppm in solution]) were used to prepare the standards. Fresh standards were prepared prior to each spectroscopy run that was performed. A total of 6 standards were used each time to create the calibration curve. The standards used were as follows:

Cu^{2+} Concentration	**0 ppm**	**1 ppm**	**2 ppm**	**3 ppm**	**4 ppm**	**5 ppm**
Vol. of Cu^{2+} (1001 ppm) Used	0 ml	0.1 ml	0.2 ml	0.3 ml	0.4 ml	0.5 ml
Overall Standard Volume	100 ml					
Solution Matrix	1% HNO_3					

Table 3.3 – Calibration standard used for the atomic absorbance spectroscopy. *The individual standards were prepared by diluting a main solution of 1001ppm Cu^{2+} into 100ml volumes of 1-5ppm Cu^{2+}. The spectrometer was calibrated against these standards. Once the spectrometer was able to create an absorbance spectrum based on these standards, samples with unknown concentrations of copper could be fed in to determine their respective concentrations.*

The samples from the output buckets were diluted depending on expected concentration of copper in the pregnant leach solution. They needed to be diluted to ensure that readings obtained through the spectrometer provided readings were within the calibration range. Readings that fell above the calibration range, returned an error. These samples were re-diluted at a larger dilution factor and re-analyzed in the spectrometer. Conversely, readings that fell between 0 and 1 ppm, while technically still in the calibration range, were re-diluted at a lower dilution factor. The aim was to ensure that all readings fell between 1 and 5 ppm for the most accurate reading. Each time a sample was analyzed, the spectrometer

automatically took 3 readings of the samples and returned an average as the final reading of the sample.

3.4.2 Analysis of Solids Residue

After the leaching experiments had been terminated, the residual copper in the ore had to be determined. This ensured that all copper in the mineral was accounted for and permitted calculation of the mass balance for copper extraction.

The determination of the copper values in the barren ore was performed by Bureau Veritas at their commercial laboratory in Richmond, British Columbia. The method of determination was through multi-acid digestion followed by atomic absorbance spectroscopy. The exact procedure was not provided, though multi-acid digestion usually involves digesting a sample of ore in a mixture of nitric acid (HNO_3), hydrochloric acid (HCl), perchloric acid ($HClO_4$), and hydrofluoric acid (HF) (Bureau Veritas, 2017). A ground solid sample is added to a particular mixture of these acids and placed in a mild heating environment. The resulting liquid, which contains dissolved mineral species, is separated and further analyzed for metal(s) of choice. The use of strong and highly oxidizing acids allows for almost complete digestion of the solid materials. This permits an accurate level of detection of metal values that may be fairly low in the material. A total of 3 individual multi-acid digestions and atomic absorbance analysis were ordered for the solids in each of the columns.

3.5 Column Leaching Results

The amount of copper extracted daily was determined from the copper concentration in the samples as well as the recorded weight of the output bucket. Using the values obtained from the atomic absorbance, the daily amount of copper extraction was calculated as follows:

$$\textbf{Copper Extracted (g)} = \underbrace{\frac{\textbf{PLS Weight (kg)}}{\rho_{H_2SO_4}\left(\frac{\text{kg}}{\text{L}}\right)}}_{\text{Solution Volume (L)}} \; x \; \underbrace{\frac{\textbf{dilution factor} * \textbf{AAS Conc. Value}\left(\frac{\text{mg}}{\text{L}}\right)}{1000\left(\frac{\text{mg}}{\text{g}}\right)}}_{\text{Copper Concentration (g/L)}}$$

From this the cumulative extraction profile of the 3 columns could be plotted. These are shown in Figure 3.11 and Figure 3.12. Figure 3.11 shows the absolute copper extracted over the lifetime that the columns were run. Figure 3.12 shows the columns in the final stages of extraction.

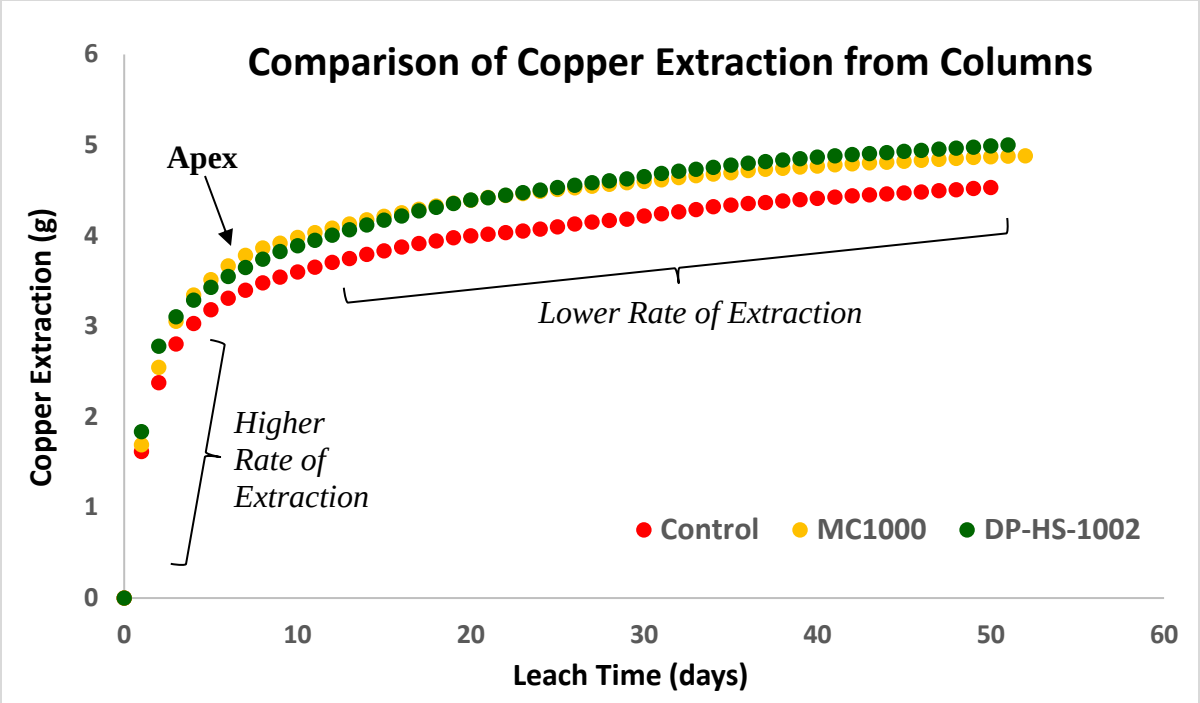

Figure 3.11 - The extraction curves for the 3 columns are depicted in the graph above. *The values shown in the graph are only cumulative daily extraction values obtained from AAS over the lifetime of the column*

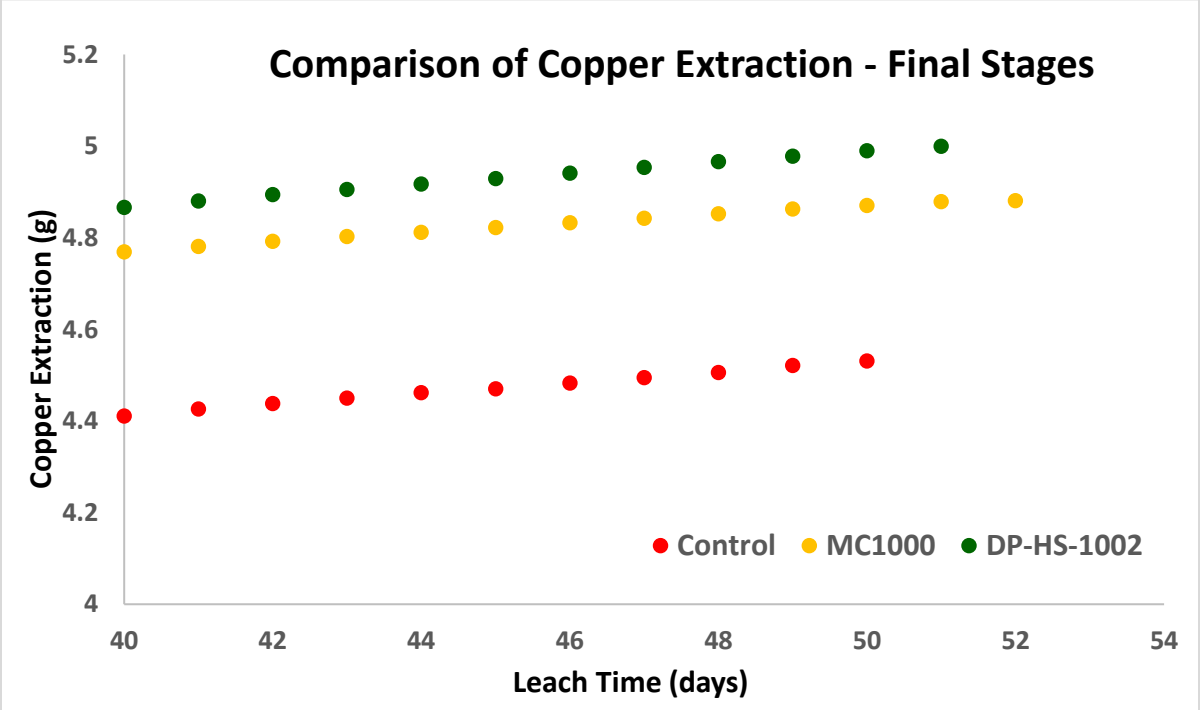

Figure 3.12 –Cumulative extraction for the different columns operated in thesis. *The graph is an extension of (Figure 3.11), showing the columns in their final stages of leaching. From the profiles above, there is a considerable difference in the total extraction with and without the presence of surfactant in the leachate.*

The graphs above only depict the rate of absolute copper extracted from the ore on a daily basis. The copper extracted varied by slight amounts in each column, but overall showed that the leachate containing the surfactant showed greater extraction at termination. However, in order to more accurately and definitively compare leaching rates and amounts, the extractions needed to be translated into copper recovery profiles for each respective column. To do this the copper balance needed to be determined for each column. The results from the copper balance allowed for the total copper input per column to be determined:

	Control	***MC1000***	***DP-HS-1002***
Total Cu Extracted from Columns (g):	4.531	4.881	5.0000
Cu in column drainage (g):	0.006	0.011	0.0084
Cu in solid residue (g):	0.5338	0.472	0.472
Total Copper Input (g):	5.071	5.363	5.480
(Days Leached):	(50)	(52)	(51)

Table 3.4 - Copper balances for each table, ultimately showing the total copper in each column.

In Table 3.4, the values of "Copper content in the solid residue" were determined from solid residue analysis performed by Bureau Veritas. The details of the procedure are provided in the "Sample Analysis" section. The results from the residue analysis performed by Bureau Veritas are as follows:

	Control	*MC1000*	*DP-HS-1002*
%Cu – Test 1	0.06	0.05	0.05
%Cu – Test 2	0.06	0.05	0.05
%Cu – Test 3	0.05	0.05	0.05
%Cu - Average	0.00567	0.05	0.05
Mass of Residue (g)	942	944	944
Mass of Copper in Residue (g)	0.5338	0.472	0.472

Table 3.5 - Mass of copper left in tailing / solid residue after the leach columns were terminated. *This was necessary to calculate as it showed what copper was not extracted by the acidic media.*

Additionally, in Table 3.4, the "Column Drainage" value referred to the residual fluid in the column after the leach experiment was terminated. Because the columns were run as up flow columns, when the pumps were stopped to terminate the experiment, some fluid did not exit the column into the output reservoirs. It was collected separately, but still analyzed for copper. This was necessary as some dissolved copper was in fact present in this fluid.

By determining the copper that was removed from the ore and the copper that was still in the ore, the total copper content of each column could be determined. Based on this, the cumulative daily copper extracted could be determined as follows:

$$\textbf{Copper Recoverd}\ (\%) = \frac{\textbf{Copper Extracted}\ (\textbf{g})}{\textbf{Total Copper}\ (\textbf{g})}$$

Because the copper input varied amongst each column, a recovery comparison allowed for easier assessment of extraction amongst the columns. The recovery as percent extraction of total copper is shown in Figure 3.13 and Figure 3.14.

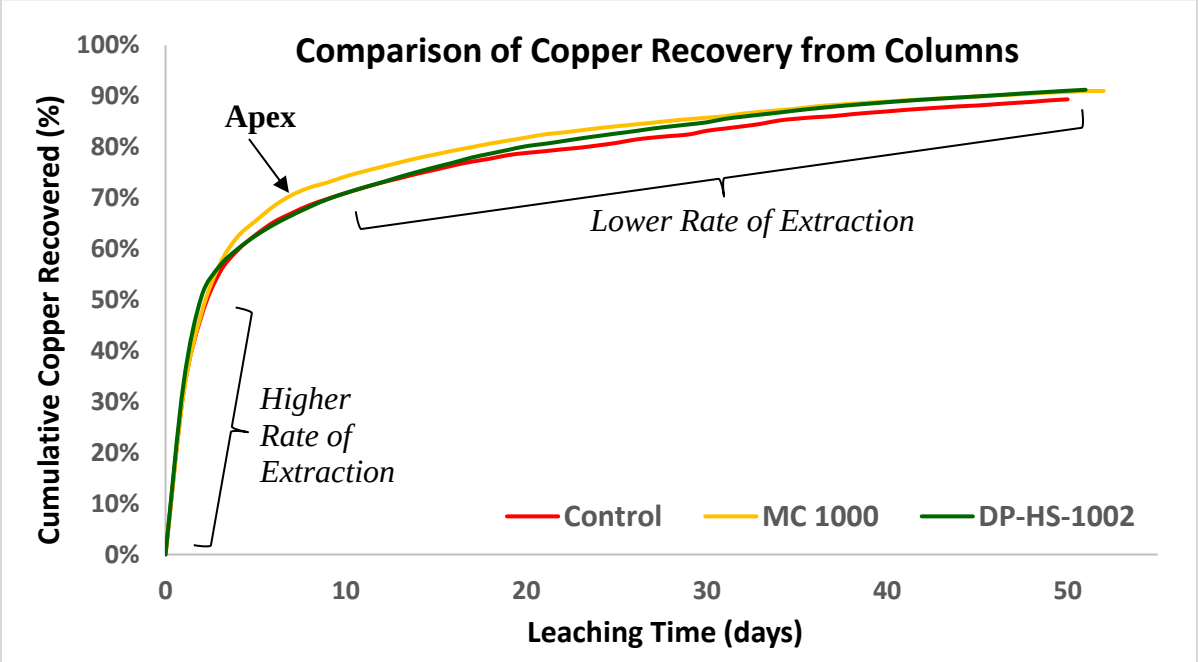

Figure 3.13 – Total copper recovered for each column. *The graph shows the daily cumulative leached copper from each of the columns, but as a percentage of the total copper content of each column. The recovery profiles shown in this graph are an extension of (Figure 3.11) and (Figure 3.12). The daily cumulative amounts were divided by "Total Copper" value in Table 3.4.*

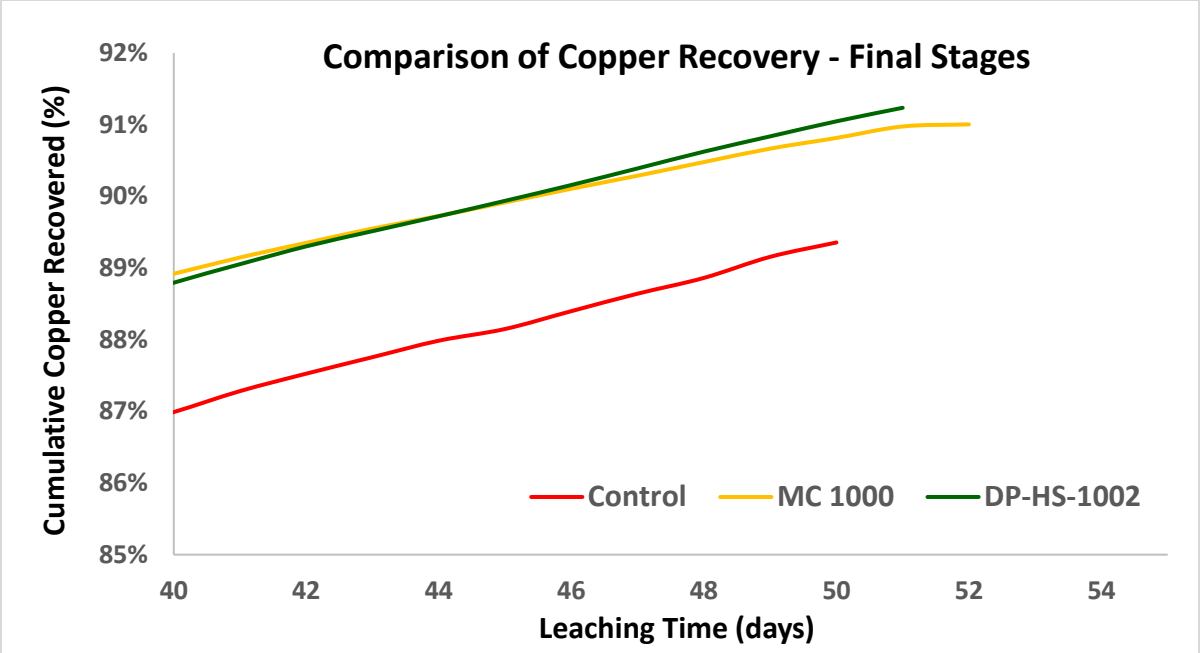

Figure 3.14 –Cumulative percentage extraction of copper over leaching time. *The graph above is an extension of (Figure 3.13). Like (Figure 3.12), the graph shows the percent recovered from the columns in the last stages of the extraction. The columns with surfactant were both shown to have achieved approximately 91%-92% of copper extraction as compared to 89% for the column without surfactant.*

3.6 Discussion

From the results the presence of surfactant in the leachate plays a role in furthering the extraction of copper from the ore. Starting with Figure 3.11 and Figure 3.12, there is a difference in the total cumulative copper extracted from the columns with surfactant, than without surfactant. The data collected over the lifetime of the column showed that as the experiments were terminated, the columns with surfactant had leached more copper from the ore than the column without any surfactant. Furthermore, from Figure 3.11 and Figure 3.12, it can be seen that all 3 columns reached their apex in approximately 2-3 days. Prior to reaching the apex of leached copper, the rate of extraction is relatively high. At the apex, the leaching of copper continues to occur but the rate at which this occurs considerably reduces. Overall the columns with surfactant have a higher established apex than the column without

surfactant. This means that in the first few days when the greatest amount of leaching is taking place, the columns with surfactant are able to leach more copper. Once the leaching has reached its apex, the rate of extraction is roughly equal for all the columns.

However, because the copper content of each column varied to some degree (as confirmed by Table 3.4), the profiles developed in Figure 3.11 and Figure 3.12 needed to be normalized. This was achieved by taking the cumulative copper values and dividing them by the total copper value for each column. This resulted in the profiles established in Figure 3.13 and Figure 3.14. From these 2 figures it can be seen a greater amount is still recovered with the presence of surfactant. This is also backed by the results of the residue analysis. The copper in the residue for MC1000 accounted for 8.8% of the total copper in the column. Additionally the copper in the residue for DP-HS-1002 was 8.6% of the total copper. In the control column the copper in the residue accounted for 10.5% of the total copper in the column.

In these profiles it can be seen that all 3 columns reach their apex at roughly the same time. However, MC1000 establishes a slightly higher apex in terms of percent extracted. The control column and surfactant DP-HS-1002 establish their apexes at roughly the same extraction amounts. The rates of extraction beyond that for MC1000 and the control column are roughly the same. However, the rate of extraction climbs for DP-HS-1002 to meet the extraction that MC1000 achieves. Overall the control column has roughly 88-89% copper extraction versus 91%-92% for the columns with surfactant.

This result presents a find in favor of surfactants within the heap leach process. For these experiments all the particles present in the columns were fully submerged in leaching fluid for the duration of the experiments. The particles were therefore exposed for the same amount time to the passing leach fluid. This meant that the mass transport of species to and from the particle surface were ensured to not be a rate limiting factor in the extraction of copper from host particles.

The leach columns were optimized to eliminate rate limiting factors. Keeping all other conditions identical there was still a discernable difference with and without the presence of surfactant. The columns with surfactant reached higher overall extractions of soluble copper. Within the same period of time the columns without surfactant achieved lower extraction of soluble copper. From the columns it was seen that surfactants had some effect in increasing the amount of copper extracted. Further investigation was needed to determine this effect.

Chapter 4: Surface Tension Analysis

The test work in the previous chapter has showed that the presence of surfactants in leach solution had an impact on the overall yield and rate of extraction of copper. These results were first seen in and confirmed by the test work conducted by BASF (Bender et al., 2016).

The work performed by BASF had columns in which fluid flow was top-down much like a regular heap leach. To ensure wetting issues and mass transport to and from the particles were not a limiting factor, in the column set-up for this thesis all particles were submerged in leaching fluid. With the variations in methodology, but similar overall results in extraction, there was a clear effect brought on by the use of surfactants.

The surfactants were introduced into the column was through the leach solution. They were dissolved into the sulfuric acid solution just prior to use. The columns operated by BASF also used this method of introduction for the surfactants. The aim of this chapter was to observe the changes that the surfactants imparted on to the host solution, especially because the method of introduction was the same for both studies.

The changes imparted by the surfactant on leach solution was studied by measuring the interfacial tension or surface tension of the fluid. This method helped better discern the reaction at the air-liquid interface and how the presence of the surfactant altered it.

4.1 Surface/Interfacial Tension of Liquids

The surface/interfacial tension, as the name suggests, is the tension of a fluid surface when in contact with a secondary phase. It can also be thought of as the measure of the work required expand or create another unit area of a fluid when in contact with a secondary phase. The surface tension is also the ability of a fluid to hold itself together or the free energy of a fluid to expand against external forces that may be acting on it (Rosen, 2004a). Essentially the surface tension of the fluid is an important property as it predicts how well a fluid responds against external forces and secondary phases.

The use of surfactants play an important role in this aspect. Surfactants (or Surface Active Agents) as chemical agents function by primarily adsorbing at liquid interfaces to alter the behavior of the host liquids when in contact with other phases (Rosen, 2004a). When dealing with surfactants in solution, the interfacial tension is an important quantity to know and understand. It is directly measureable and the reduction of interfacial tension as a function of surfactant concentration is used to judge how effective the surfactant is (Rosen, 2004b).

4.1.1 Understanding Surface/Interfacial Tension

In a droplet (or given volume) of a liquid (for example, water) the fluid is composed of many molecules. Within the volume of water, the molecules are held together via hydrogen bonding due to the naturally occurring polarity of water molecules. These molecules are loosely bound to each other such that it allows the liquid to have a malleable form (unlike a solid), but not completely unbound that all molecules exist separately (like a gas).

Within the body of the fluid, the molecules are present within the bulk of the fluid as well as at the surface of the drop. The surface / interfacial tension of a liquid arises as the molecules at the surface of the fluid are at a higher potential energy as compared to their counterparts within the bulk of fluid (Rosen, 2004b). Molecules within the bulk of a body of fluid are at an overall lower potential energy. This is because within the bulk volume of the fluid molecules can interact, attract and act on each other, with equal measure. Overall, across all the molecules in the internal bulk of the fluid, they experience a net overall minimal force as the interactions with surrounding molecules minimize each other (see Figure 4.1).

On the other hand, molecules at the surface of the fluid are limited in their interactions. The interaction is limited to those adjacent molecules also at the surface of the fluid and those in the bulk just next to the surface (see Figure 4.1). This means that the forces acting on surface molecules are not balanced out. Molecules at the surface are also in contact with molecules of the opposite phase across the interface. Depending on the secondary phase, the greater the dissimilarity in nature between two phases in contact, the lesser the inclination to be in contact. This results in a greater tension along the interface as the two phases seek to minimize contact. (Rosen, 2004b).

In a system such as a drop of water surrounded by air, for example, the surface interactions with molecules of the same phase are much greater in magnitude than those interactions with the opposite phase. The dissimilarity between the two phases means that the interactions with the fluid and air molecules are not strong. Interactions of the surface water molecules with

other molecules of the same phase are much stronger due to the higher presence of these molecules near the surface. (Rosen, 2004b).

Because of the nature of the inter-molecular attraction for particles at the surfaces of a fluid, they experience an overall greater net force acting on them (see Figure 4.1). For a body of liquid to exist the molecules in the liquid need to be at their equilibrium state (or lowest energy state), including the surface molecules. The attractive forces between molecules on the surface cause the liquid to contract until the inter-molecular forces is at its minimum. At that point the surface molecules are in equilibrium with each other as well as the internal molecules and secondary phase molecules acting on them. This minimization of the surface area will assume the smoothest shape of the liquid surface that can support the minimization of the surface energy.

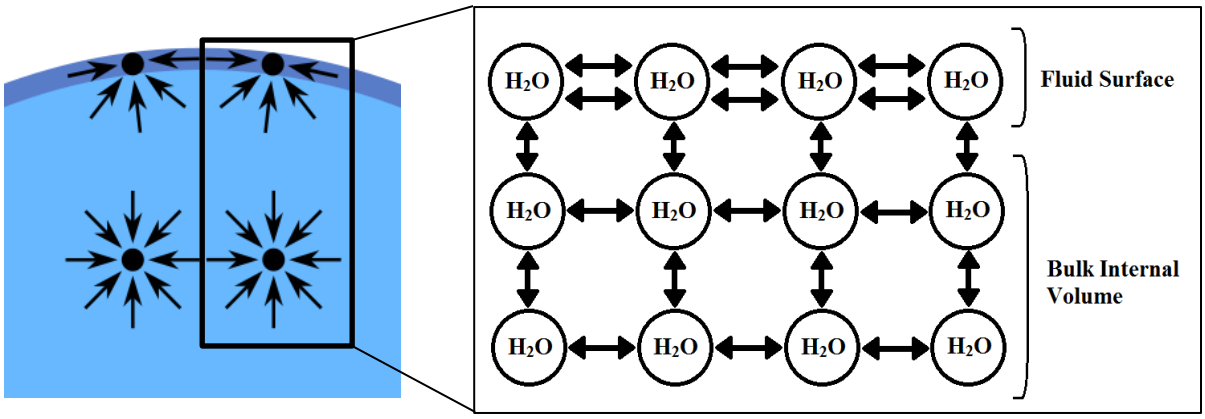

Figure 4.1 – Molecular structure of water at the surface. *Molecules at the surface of a fluid experience greater inter-molecular interaction and thus play a greater role in the determination of surface tension of a fluid. The interfacial tension is a measure of the force required to pull apart the molecules at the surface of the fluid to permit the presence of more molecules at the surface. The figure to the left was adapted from wikimedia commons digital media repisatory (Wikimedia Commons, 2012). The figure to the right was adapted from the US Geological Survey Water Sciences website (United States Geological Survey, 2016),*

This is also where the interfacial tension measurement derives its value. As mentioned the molecules at the surface of the liquid have a different potential energy to the molecules in the internal bulk of the volume. When summed, the molecules at the surface have a net greater force of attraction acting on them. Because of this potential difference some work must be done to bring molecules from the internal volume of the fluid to the surface. The surface tension is a measure of this work. It measures the force required to pull apart surface molecules to permit the expansion of the fluid surface and allow molecules from the bulk phase into it. (Rosen, 2004a).

4.1.2 Surfactants and Interfacial Tension

When using a solution containing surfactants, the role of the surfactants is to adsorb at the surface of the liquid. By doing so they offer a means of altering the surface properties of a fluid. For example, in a freshly formed surface of a solution (like a droplet of liquid) the surfactant would initially be present as dispersed monomers throughout the bulk of the fluid. As the fresh surfaces are formed the surfactant monomers diffuse through the bulk fluid to these new surfaces and adsorb there (see Figure 4.2).

When a new fluid surface is initially formed, the migration of surfactants to the new surfaces is not instantaneous. The rate at which surfactants migrate and adsorb at the liquid surfaces is dependent on a variety of factors including the type hosting solvent and surfactant being used. Generally, when a new surface is created the surface tension is initially close to that of the solvent but decays over time to a stable value. This indicates that the surfactant migration and presence at the surface has reached equilibrium. (Eastoe & Dalton, 2000).

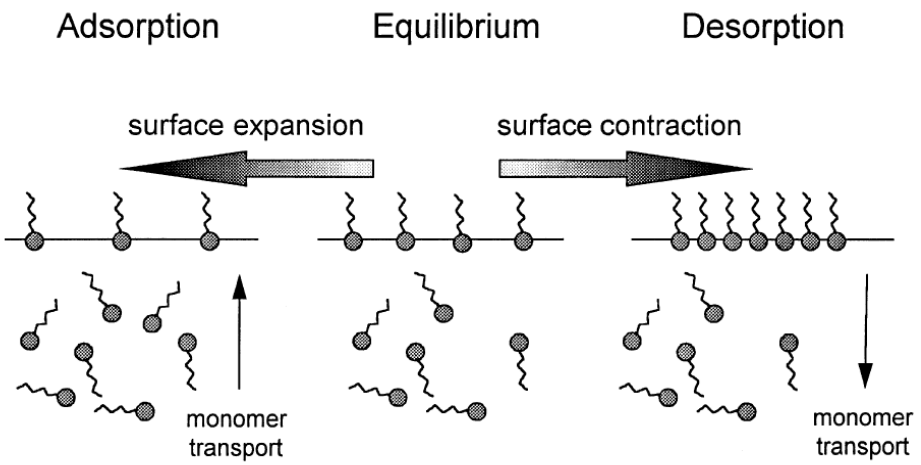

Figure 4.2 - Diffusion of surfactant monomers to the surface of the fluid. *Surfactants diffuse from the bulk fluid to the surfaces of the fluid. The natural structural difference in the monomer provides a driving force for the monomers to the surface of the liquid. The activity of the surface is such that surfactants decrease the work required to increase the volume of the surface by a given amount. The figure was reproduced from "Dynamic Surface Tension and Adsorption Mechanisms od Surfactants at the Air-Water Interface" © (Eastoe & Dalton, 2000) (Reproduced with permission from Elsevier).*

The adsorption of the surfactant monomers at the surfaces of the fluid takes place because of the way they are chemically structured. They are typically organic molecules that have long chain "tails" and a "head" that can be polar and behaves akin to functional group (see Figure 4.3). The "head" and "tail" of the surfactants have different functionalities with respect to their host fluid and so are also known as amphipathic structures. This means that part of their structure has a strong attraction to the solvent (aka as the lyophilic group) and the other part has a weak affinity for the solvent (aka as the lyophobic group). (Rosen, 2004a).

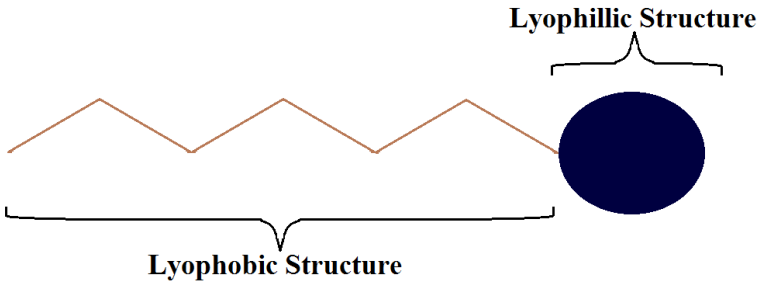

Figure 4.3 – A typical surfactant structure. *Surfactants structures contain a lyophilic group with a strong affinity for the host solvent and a lyophobic structure with a weak affinity for the host solvent.*

In the case of a surfactant dissolved in an aqueous solution the lyophobic structure would be known as the hydrophobic group of the surfactant, and the lyophilic group would be the hydrophilic part. The driving force for the diffusion and adsorption of surfactant monomers at the surface of the liquid occurs due to this difference within the same structure. The repellent nature of the hydrophobic group provides the driving force for the surfactant monomers to diffuse to the surfaces of the fluid.

Once at the boundary the surfactant monomers re-orient themselves in such a way that the lyophobic groups are in minimal contact with the host solvent (Rosen, 2004a). As seen in Figure 4.2 the lyophobic structures stick outward from the surface of the fluid. The lyophilic structures on the other hand, with a very high affinity for the host solvent, remain just at the boundary of the fluid, attracted to the solvent molecules at the surface. In the case of an aqueous solution the hydrophilic groups re-structure the fluid by breaking the hydrogen bonds between water and occupying the spaces in between. This strong affinity for the solvent molecules stops the surfactant from being completely expelled from the fluid (Rosen, 2004a).

The drastically different behaviors of the 2 structures within the same molecule keep the surfactants concentrated at the boundary of the fluid. In addition to this the lyophobic groups that stick outside the surface of the fluid, create a new surface layer of surfactant tails atop the original fluid layer. These surfactant tails that stick out have greater similarity with the secondary phase than the original host solvent. This increases the interaction between the surfactants and the secondary phase. The overall surface tension of the fluid reduces (Rosen, 2004b). Because the effect of surfactants is predominantly at the surface of a liquid, surface tension and any changes to it can be readily measured.

4.2 Interfacial Tension Measurements

A convenient way to determine the surface tension of a fluid is through the use of the drop shape method. (Woodward, 2000). In this method a drop of fluid is suspended against a source of light and an image of the drop using a camera is obtained (see Figure 4.4).

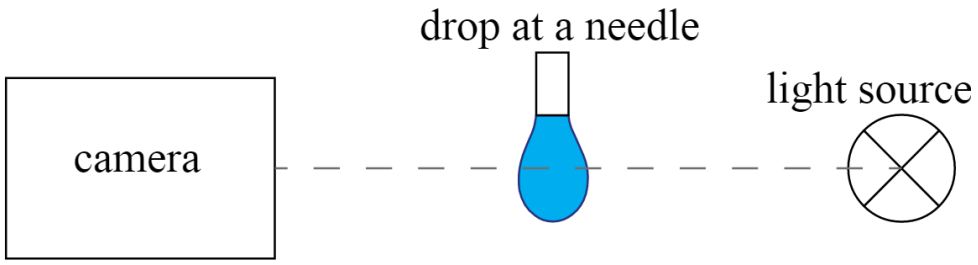

Figure 4.4 – The drop shape analysis method. *The pendant drop method involves suspending a drop of fluid against a light source and using a camera to obtain a profile of the drop. The shape of the drop can be analyzed to determine the interfacial tension of the fluid. Image obtained from Data Physics Instruments GmbH (Data Physics Instruments GmbH, 2017).*

As highlighted in the section 4.2.1, in a droplet of fluid there are molecules throughout the fluid, including at the surface. These surface particles dictate the behavior of the fluid in contact with secondary phases. The hanging drop exploits the attraction between the surface molecules and bulk internal molecules (see Figure 4.5).

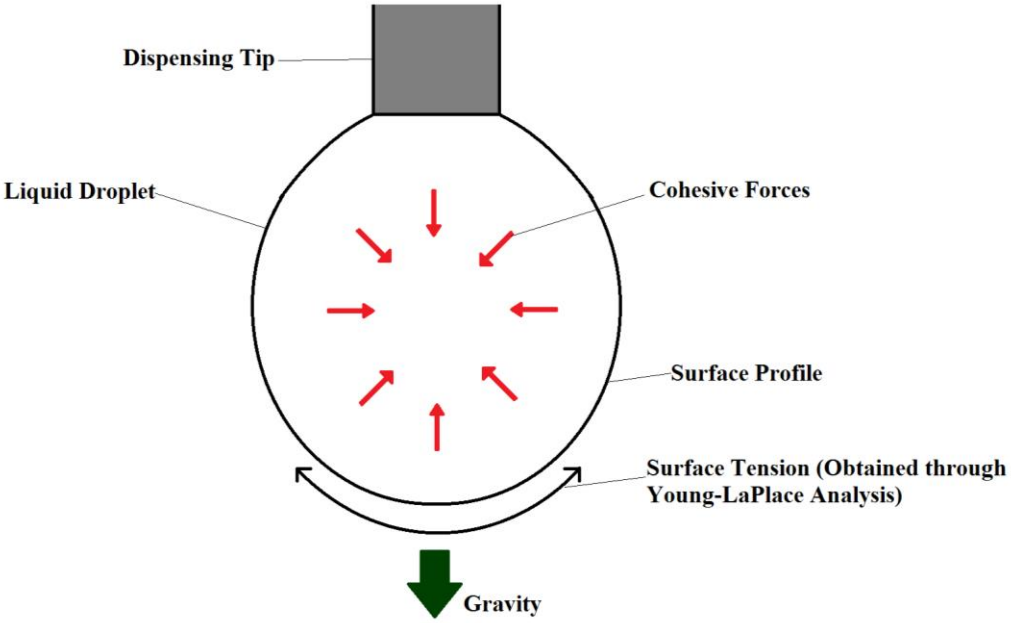

Figure 4.5 – Drop Shape Capture method. *Using a drop shape analyzer and drop shape capture equipment, the surface tension for a fluid can be determined. When a drop is suspended from a tip the main forces that act on shaping the drop are gravity and the intermolecular attractive forces between the molecules in the fluid. When suspended, the drop wants to take on a spherical shape to minimize the surface area and therefore be at a minimum surface tension. However, due to gravity there is a distortion that takes place, forming the drop into a pendant like shape. The surface tension can be measured from a set-up such as this as the degree of distortion shows how resistant the shape is to deformation despite the effect of external forces acting on the drop. The degree of distortion is measured from the curvature of the shape profile obtained.*

When a droplet of fluid is suspended such as in a hanging drop, the effect of interfacial tension becomes more starkly obvious. This is because the forces acting on the drop are the

cohesive forces between the molecules and gravity. The interfacial tension is the work done by the fluid to hold itself together while being pulled down on from gravity.

As a droplet is initially formed the liquid forms a spherical shape to minimize the tension over the surface. As more volume is added to the drop gravity begins to take effect and distort the drop into a tear/pendant shape. When fully formed and in equilibrium there is a balance between the intermolecular cohesive forces and gravity. The surface molecules "stretch" to contain the liquid despite gravity acting to pull the liquid down. A fluid with high interfacial tension is able to withstand distortion to a greater degree as the molecules in the fluid have a stronger tendency to stick together.

The analysis of surface tension requires suspending drops of fluid against a back light and a silhouette of the drop is created. The hardware used for the work in this thesis was the FTA 1000 B Class Drop Shape Analyzer (manufactured by First Ten Angstroms Instruments). The hardware used for image capture had its own software which performed surface tension calculations.

Once captured, the software was able to apply the Young-Laplace equation on the profile of the droplet curvature to determine the surface tension of the fluid. (Woodward, 2000). The Young-Laplace equation seeks to describe the difference in pressure sustained across an interface when 2 phases are in contact with each other. The drops analyzed need to be distorted by gravity in order for the Young-Laplace work (Woodward, 2000). This is because the Young-Laplace equation works by calculating the radius of curvature, of a drop, from a

given point. The equation used also takes the effect of distortion by gravity into account. Based on the calculated value of curvature, the surface tension is determined.

In a hanging drop experiment the effect of surfactants on a hosting fluid can be more easily identifiable. The primary effect of the surfactant monomers is to disperse through the liquid and toward the surface and adsorb there. As it does so the surfactants affects the intermolecular interactions at the fluid surface. In a hanging droplet the activity of the surfactants has a direct impact on the surface profile created. By comparing droplets of the same volume, the surfactant effects can be determined by the comparing the differences in the obtained profiles.

4.3 Experimental Preparation and Set-Up

The following sections detail the testing conditions and preparation procedures used for the measurement of interfacial tensions. For these particular tests only the air-liquid interface was being tested and so no solid preparation was required.

4.3.1 Solvent Preparation

For this experiment the solutions used were 1% sulfuric acid with increasing concentrations of surfactant. Both surfactants used in the column leaching experiments (MC1000 & DP-HS-1002) were also used for testing in this experiment. The concentrations of solution used in this experiment are summarized below.

	MC1000	DP-HS-1002
0 ppm	✓	✓
25 ppm		✓
50 ppm	✓	✓
100 ppm	✓	✓
200 ppm	✓	✓
500 ppm	✓	✓
1000 ppm	✓	✓

Table 4.1 - The concentrations of surfactant solutions used for interfacial tension testing. *All surfactant solutions were prepared by dissolving the surfactant in a matrix solution of 1% sulfuric acid (10g/L H_2SO_4).*

The solutions were all prepared by dissolving the surfactants in a matrix of 10g/L sulfuric acid (98% purity as manufactured by BDH chemicals). The sulfuric acid solution was prepared by dilution in DI water.

The surfactant solutions in Table 4.1 were prepared in the following manner:

- A bulk solution of surfactant was prepared by initially dissolving 1g of the respective surfactant in 1L of 1% sulfuric acid to create a 1g/L surfactant solution.
- The density of 1% sulfuric acid at room temperature (~20°C) is 1.0049 g/cm^3 according to CRC's Handbook of Chemistry and Physics (Lide, 2008). Because of the close proximity of the density of 1% sulfuric acid to that of water, it was assumed that the density of sulfuric was 1g/L. This meant that to create a 1000ppm surfactant solution, 1g for every 1L of sulfuric acid was needed. (In reality, assuming the density of 1% sulfuric acid to be 1.0049g/cm^3, to create a 1000ppm surfactant solution, 1.0049g of surfactant solution would have been needed. This was very close to the original amount used).
- The ingredients to prepare the bulk solution were placed in a volumetric flask and stirred thoroughly to ensure complete dissolution of the surfactant.

- For the drop shape analyzer, the volumes of solution required were quite small (highlighted in section 4.3.3). To prepare the solutions according to the concentrations listed out in Table 4.1, the 1 g/L surfactant solution was further diluted in 1% sulfuric acid solution. This was done using auto-pipettes and 10mL volumetric flasks. The dilutions were prepared as shown in the table below.

	0 ppm	25 ppm	50 ppm	100 ppm	200 ppm	500 ppm	1000 ppm
Dilution Factor	-	40	20	10	5	2	1
Bulk Solution Per 10mL	-	0.25 mL	0.5 mL	1 mL	2 mL	5 mL	10 mL

Table 4.2 - Dilution factors and final concentrations for solution testing. *The final solutions for testing were prepared by diluting a bulk sample of 1 g/L (1000 ppm) surfactant solution down to the final concentrations as shown in the table above. The needed amounts of the bulk solutions were measured out using an auto-pipette and placed in a 10mL volumetric flask. The rest of the volume was filled with 1% sulfuric acid solution.*

- All solutions were made just prior to performing drop shape analysis testing.

4.3.2 Image Capture / Machine Preparation

As mentioned in section 4.2, to begin the process of collecting interfacial tension measurements, a droplet of fluid needs to be suspended in between a camera and a backlight (see Figure 4.4). For the work in this thesis the instrument used was an FTA 1000B Series Drop Shape Analyzer (see Figure 4.6). The hardware unit consisted of a camera to obtain images, a fluid dispensing syringe and a backlight for the capture of drop profile. The hardware was connected to a computer loaded with software needed to operate the instrument. The software controlled the number of photos obtained from the camera as well

as the rate of photos obtained. The software also controlled the pumps that dispensed fluid through the syringe. The software analyzed the images obtained through the hardware.

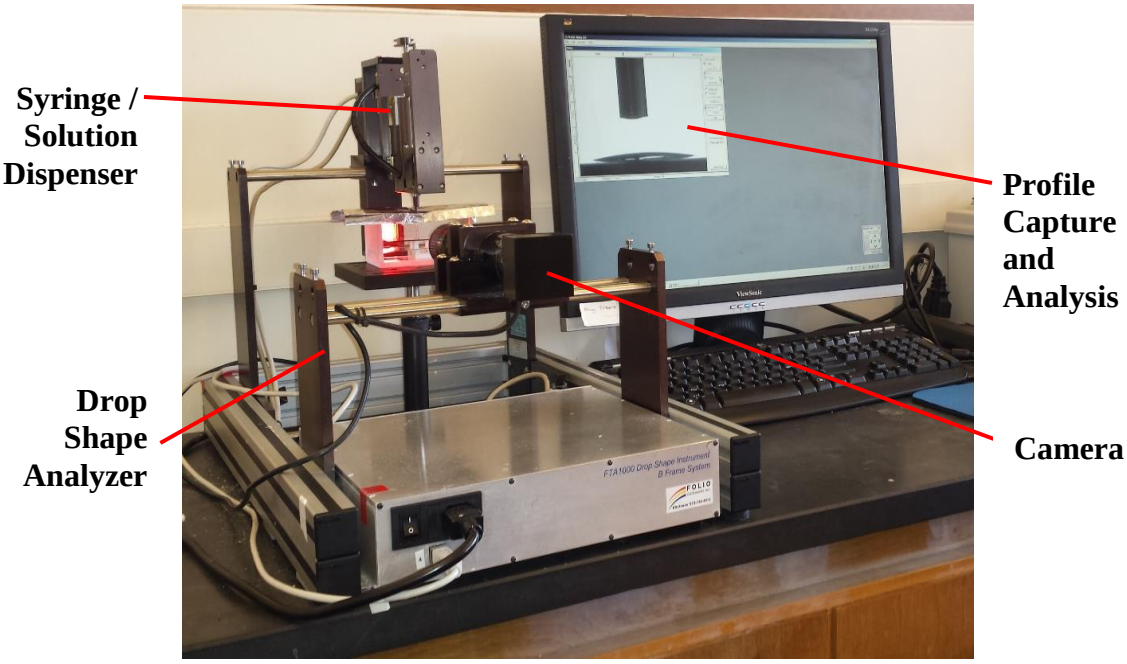

Figure 4.6 - FTA1000 B Series as manufactured by First Ten Angstroms Instruments used for the drop shape analysis. *The machine consisted of a syringe which dispensed solution from the tip of a needle and which was held as a droplet at the tip of the needle. The unit also consisted of a camera which was able to take photographs of the profiles of the droplet. The software associated with the machine was used to control a number of factors such as fluid dispensation rates through the syringe, to the number and rate of photographs taken. The software was also able to automatically analyze and calculate the interfacial tension of the fluid.*

An example of the type of images obtained are shown in Figure 4.9. The fluid is dispensed from a needle tip. The backlight creates a silhouette of the droplet on the camera. This silhouette effect is important as it allows the software to more clearly identify between the droplet and the surrounding phase. The shape of the droplet (i.e. the shape of the silhouette) is what the software uses for determining the interfacial tension.

When collecting images the needle was encapsulated in a sealed cuvet with the bottom partially filled with water (see Figure 4.7 and Figure 4.8). This acted to protect the droplet from evaporation as the water in the cuvet created a saturated environment to stop evaporation (Liu, Pawlik, & Holuszko, 2015). An unprotected droplet exposed to open air would have seen the hanging drop evaporate with time, with the consequence being the drop changing shape with time. This would have interfered with the interfacial tension reading as the software uses the profile of the drop for this purpose. Prior to starting the experiment cuvet was filled with water and sealed with Parafilm. The cuvet was then allowed to sit for 20 minutes for a saturated environment to be established.

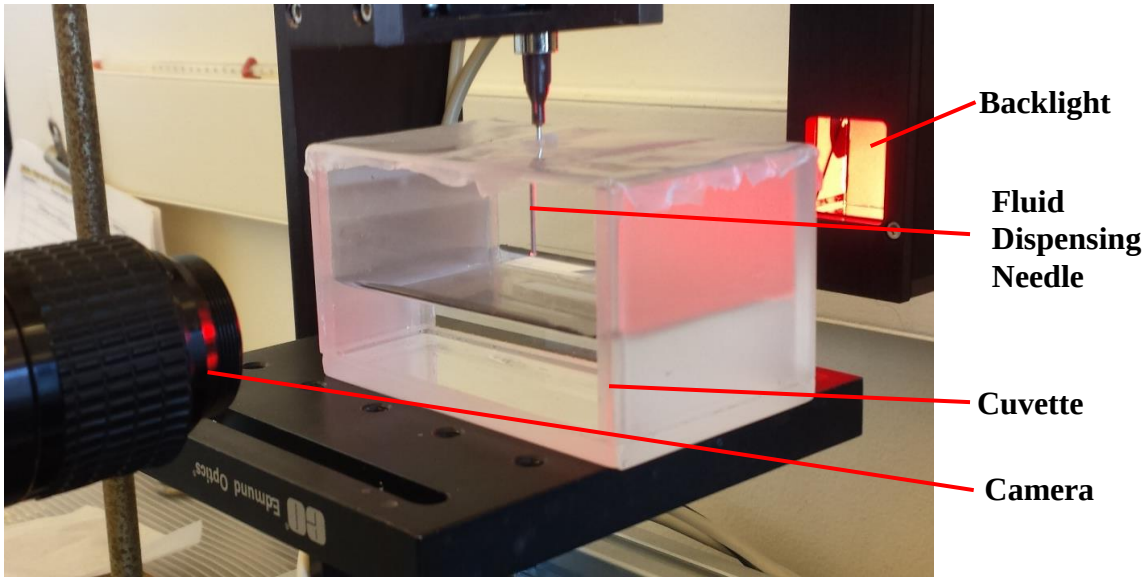

Figure 4.7 – Needle set-up for image capture. *The needle tip and droplet formed are encapsulated by a saturated environment in a cuvet with water. This acts a protective chamber preventing evaporation that may occur from an unprotected drop (Liu et al., 2015).*

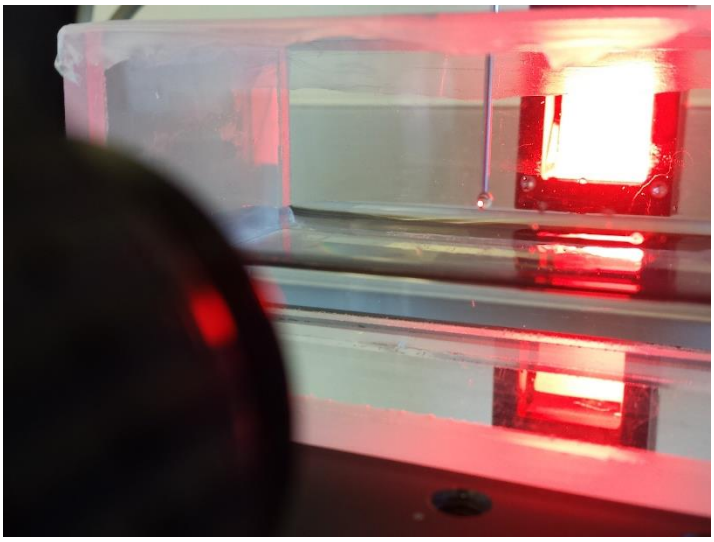

Figure 4.8 – A fully prepared cell set-up to collect drop profiles for interfacial tension measurements. *The height of the needle and water needed to be adjusted such that the formed droplet did not interact with the water, nor did the water level affect the final images obtained through the camera.*

4.3.3 Operating Procedures

Dispensing Apparatus

For the drop shape analyses a glass syringe (Hamilton Co. Gastight #1710 syringe) was used to hold and dispense the fluid while the experiment was running. The syringe had a barrel volume of 100 μL and had a plunger connected to a motorized pump. The pump was controlled by the computer and dispensed the fluid within the syringe at a user specified rate depending on the dimensions of the syringe.

Prior to starting each experiment the syringe the internal part of the syringe barrel was thoroughly rinsed with distilled water. This was subsequently followed by a flush with ethyl alcohol to remove/dissolve any organics that the water could eliminate. The barrel was once again flushed with distilled water thoroughly to ensure no ethanol remained behind. The syringe was then placed in a mild heating oven to allow for the evaporation of water.

The syringe tips/needles used for the experiment were gauged needles (as manufactured by Howard Electronic Instruments Inc).

Drop Volume

For all experiments the drop volume used was 12 μL. In order to gain accurate measurements using the drop shape optical capture large pendants need to be formed. In addition to this it is necessary to have pendants with a distorted pear shape to measure surface tension. Droplets with small volumes are more spherical and the software is unable to accurately determine surface tension as a spherical shape means that distortion by gravity has little to no effect. (Woodward, 2000) To optimize for interfacial tension calculations the pendant drops needed to be symmetric around a central axis, with the height of the drop taking up 75% of the vertical height of the optical capture space. (Woodward, 2000).

All experiments were performed by loading solution into the syringe and creating droplets. The optical calibration was also carried out at the same drop volume (further elaborated below).

Optical Calibration

Prior to performing any experiments with fluids of unknown surface tension, the image capture software needed to be calibrated against a fluid of known surface tension. The analysis applied by the software involves the fitting of a curve to the pendant drop generated at the needle tip.

Based on the image captured (see Figure 4.9) the image applies a profile based on the color difference at the boundary. The backlight allows the software to discern between the dark pixels and the light pixels indicating a phase difference. At this boundary the profile is applied and interfacial tension is calculated. Prior to starting any test work the software needed to be calibrated for distance measurements. This allowed for the software to identify distances based on the pixels occupied by the droplet.

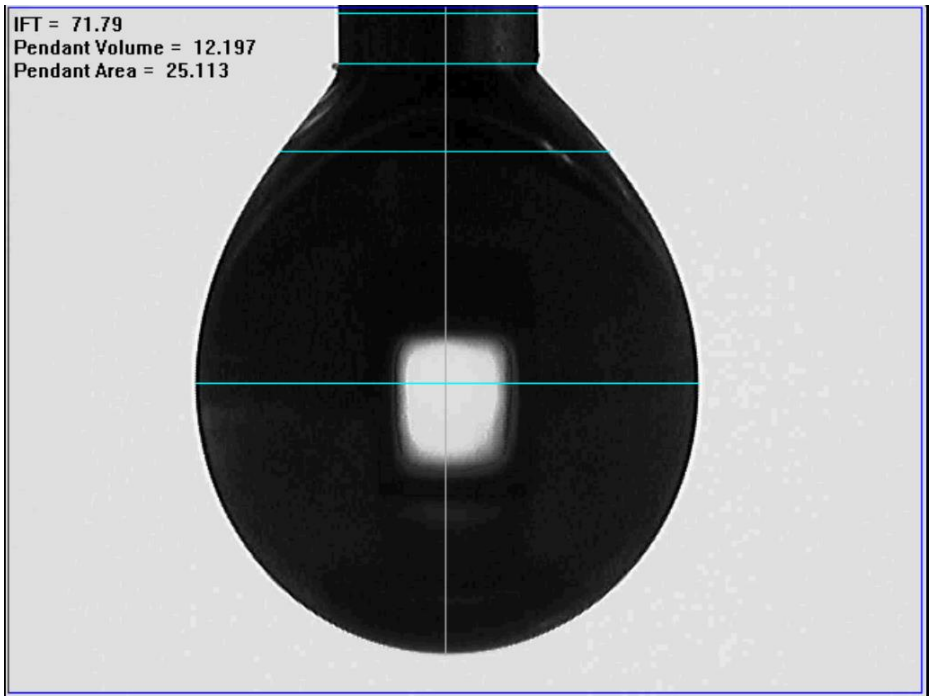

Figure 4.9 – Pendant drop image as obtained by the drop shape analyzer. *The surface tension is calculated automatically by the software by measuring the distortion of the droplet from a central point along the central axis. The software is able to apply a profile at the boundary and return a value of surface tension. It does this by discerning the difference in the pixels and applying a boundary when the pixels go from dark to light.*

In order to calibrate the software to obtain accurate measurements two types of calibration were applied: “Calibration by known distance” and “Calibration by known IFT (interfacial tension)”.

Calibration by known distance was applied by using an object of known length. In this case the needle tip was used. In the calibration setting of the software the known distance being measured was input into the software (outer diameter of the needle tip). An image of a needle tip (with no fluid) was captured by the camera. A measurement was made, using the software, from one corner of the tip to the other. The measured distance as obtained by the software, was then put in the calibration tab for the software to re-calibrate itself. The measurement was re-made. The process was repeated until the known distance of the needle tip matched the distance being measured.

Calibration by known IFT involved using a fluid of known interfacial tension for calibration purposes. In the case of this work pure distilled water was used as it had a known interfacial tension of 72.5 mN/m at room temperature. Distilled water was loaded into the syringe. Using the cuvet as a protective casing, a 12 μL drop was created. This was to ensure consistent measurement and no droplet evaporation. In the calibration tab the known interfacial tension was put in. Just as with the linear calibration, the interfacial tension had to also be measured. The process of re-entering and re-measuring was done until the measured IFT provided by the software matched the known IFT input into the software.

Data Measurement and Collection

For the interfacial tension measurements for each surfactant solution listed in Table 4.1, two separate rounds of testing were performed. The testing regime was as follows:

Round 1:

- Five runs per surfactant
- Approximately 300 images were captured per run
- A total running time of approximately 1000s was maintained for each run

Round 2:

- Five runs per surfactant
- Approximately 300 images were captured per run
- A total running time of approximately 500s was maintained for each run

4.4 Results and Discussion

A sample of the results collected from the drop shape analyses are shown in Figure 4.10, Figure 4.11 and Figure 4.12. The figures show the interfacial tensions vs. time, for the 2 rounds of testing, for the droplets formed from 1% sulfuric acid solution, 50ppm MC1000 solution, and 25ppm DP-HS-1002 solution, respectively.

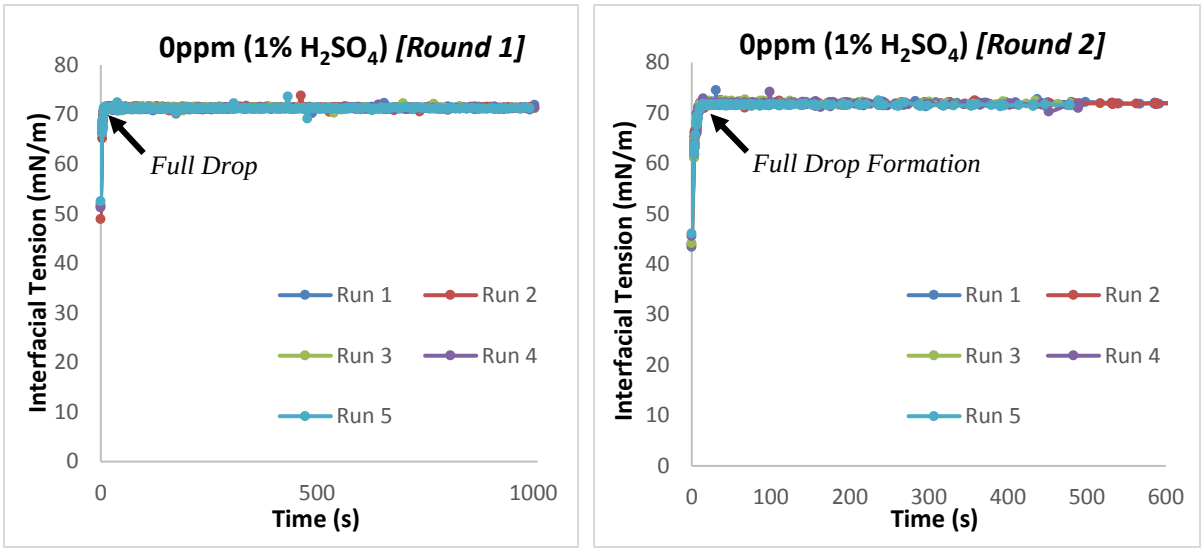

Figure 4.10 - Interfacial tension graphs for 1% sulfuric acid solution with no surfactant. *The surface tension plateaued as the full specified volume of liquid had been dispensed at the tip. This indicated that the equilibrium surface tension had been reached upon full drop formation.*

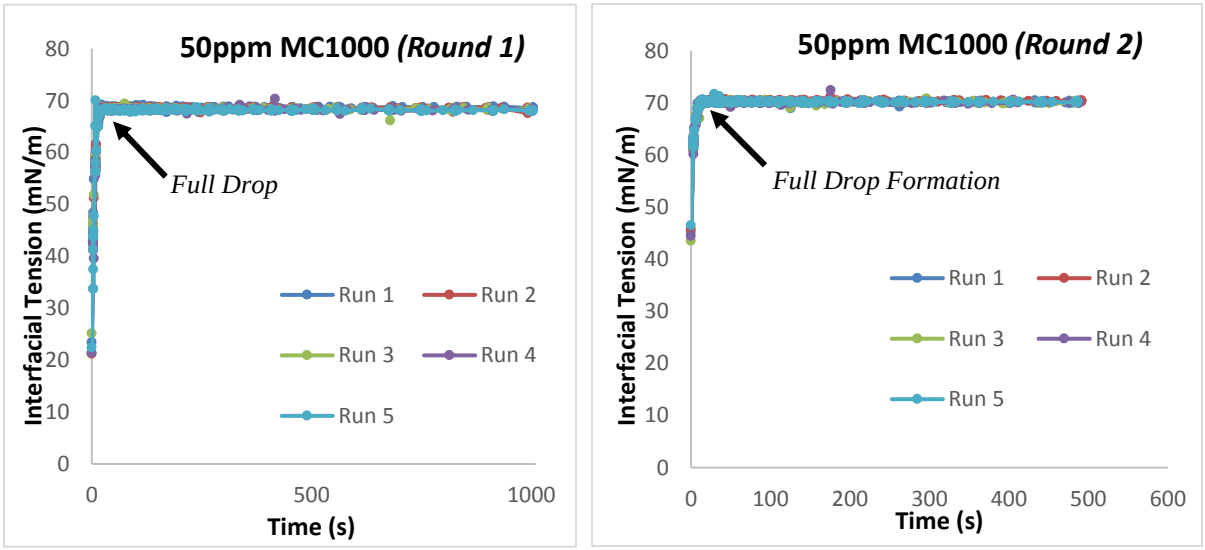

Figure 4.11 - Interfacial tension graphs for 50ppm MC1000 in1% sulfuric acid solution. *The surface tension plateaued as the full specified volume of liquid had been dispensed at the tip. This indicated that the equilibrium surface tension had been reached upon full drop formation.*

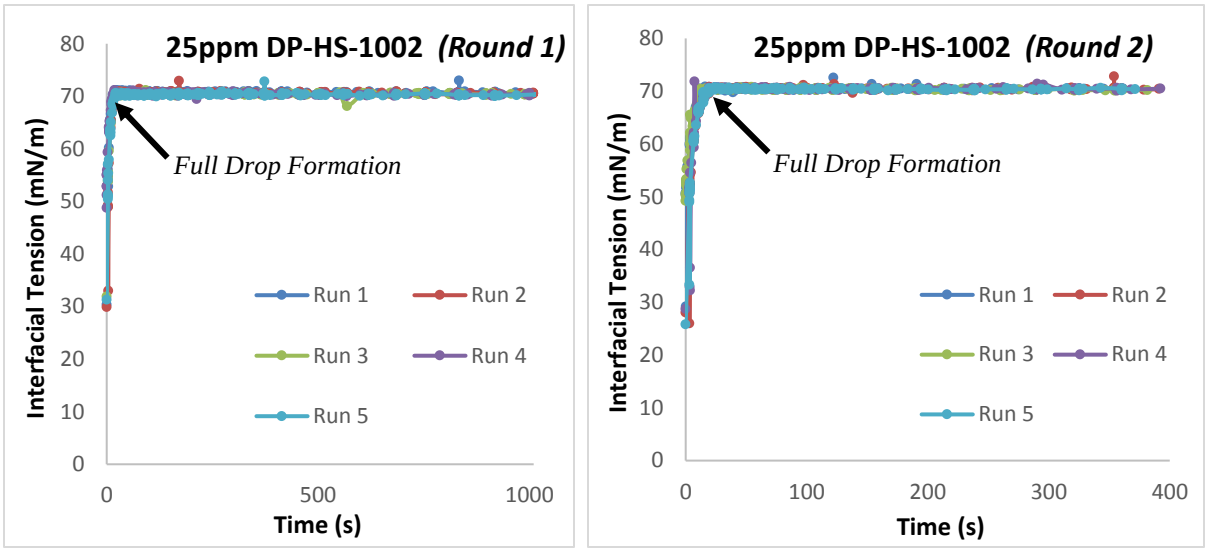

Figure 4.12 - Interfacial tension graphs for 25ppm DP-HS-1002 in 1% sulfuric acid solution. *The surface tension plateaued as the full specified volume of liquid had been dispensed at the tip. This indicated that the equilibrium surface tension had been reached upon full drop formation.*

For each graph in the figures shown above there is a trend whereby the interfacial tension systematically rises to a plateau point. From there the measured tension value remains constant about the plateau value. The rising value of interfacial tension occurs due to the formation of the droplet at the needle tip. The fluid was set to be dispensed from the syringe at a throughput rate of approximately 2 µL/s. This is in turn meant that the full droplet formation to 12 µL took some time. The image capture software took images of the droplet as it was forming. The analyses of these droplet profiles during the formation stages showed subsequently increasing values of surface tension. This is because the smaller fluid volumes creates smaller, virtually spherical drops that are not affected by gravity. This results in small values of interfacial tension as the drops initially form. As the volume delivered to the fluid droplet increases, the distortion by gravity becomes more evident. The interfacial tension values increase in value because the cohesive nature of the molecules in the fluid combat the

distortion to keep the droplet together. At full drop formation however, the interfacial tension was found to remain constant.

For solution loaded with surfactant the same trend was noted. The interfacial tension was seen to increase as the fluid volume was increased until full drop formation. Thereafter the interfacial tension was maintained at a constant value. For the solution loaded with surfactant this meant that the migration of surfactant monomers to the fluid surface / interface was very quick. The equilibrium surface tension was achieved in a very short time when the fluid drop was fully formed. This trend held steady for all solutions tested using the hanging drop mechanism. For this reason the duration of the tests was reduced from round 1 (approximately 1000s) to round 2 (approximately 500s).

The surface tension for each run was determined by calculating an average value of the plateaued section of the interfacial tension profile. This meant that the average was determined only using values at which full drop formation had occurred until the end of the test. The initial part of the profile was ignored as the drop formation did not represent the true interfacial tension of the fluid.

For each run of testing approximately 290 images (i.e. 290 calculated profile values) constituted each profile plateau. This meant that each run was the average of the points in the plateau. The final value of interfacial tension for a solution type was the average from the 5 individual runs. The final results for drop shape analysis method are shown below.

MC1000 loaded in 1% H_2SO_4 *(Round 1)*							
Surfactant Concentration *(ppm)*	**Average Individual Run Value**					**Final Average**	**Standard Deviation**
	Run 1	**Run 2**	**Run 3**	**Run 4**	**Run 5**		
0	71.47	71.34	71.32	71.24	71.28	71.34	0.09
50	68.66	68.49	68.36	68.26	68.20	68.39	0.18
100	70.62	70.47	70.30	70.31	70.16	70.37	0.18
200	67.61	67.95	67.74	67.48	67.14	67.58	0.30
500	64.25	63.59	63.27	62.70	60.36	62.83	1.49
1000	57.78	57.85	58.17	57.70	57.48	57.79	0.25

Table 4.3 - Summarized values for the interfacial tension values for MC1000 loaded solution for the first round of testing.

MC1000 loaded in 1% H_2SO_4 *(Round 2)*							
Surfactant Concentration *(ppm)*	**Average Individual Run Value**					**Final Average**	**Standard Deviation**
	Run 1	**Run 2**	**Run 3**	**Run 4**	**Run 5**		
0	72.03	71.86	71.83	71.79	71.59	71.82	0.16
50	70.22	70.35	70.14	70.12	70.20	70.21	0.09
100	69.59	69.36	69.24	69.38	69.54	69.42	0.14
200	67.76	67.44	67.32	67.36	67.21	67.42	0.21
500	62.97	64.20	63.22	63.78	62.38	63.31	0.71
1000	59.26	57.77	57.19	56.99	56.52	57.55	1.06

Table 4.4 - Summarized values for the interfacial tension values for MC1000 loaded solution for the second round of testing.

DP-HS-1002 loaded in 1% H_2SO_4 *(Round 1)*							
Surfactant Concentration *(ppm)*	**Average Individual Run Value**					**Final Average**	**Standard Deviation**
	Run 1	**Run 2**	**Run 3**	**Run 4**	**Run 5**		
0	71.47	71.38	71.32	71.25	71.28	71.34	0.09
25	70.80	70.69	70.47	70.46	70.34	70.55	0.19
50	68.21	68.22	68.21	68.35	68.17	68.23	0.07
100	69.84	69.74	69.74	69.86	69.86	69.81	0.07
200	69.28	69.12	69.10	69.11	69.15	69.15	0.08
500	68.06	67.67	67.62	67.57	67.46	67.67	0.23
1000	65.88	65.65	65.34	65.28	65.14	65.46	0.30

Table 4.5 - Summarized values for the interfacial tension values for DP-HS-1002 loaded solution for the first round of testing.

DP-HS-1002 loaded in 1% H_2SO_4 *(Round 2)*							
Surfactant Concentration *(ppm)*	**Average Individual Run Value**					**Final Average**	**Standard Deviation**
	Run 1	**Run 2**	**Run 3**	**Run 4**	**Run 5**		
0	71.56	71.46	71.42	71.40	71.12	71.39	0.16
25	70.46	70.51	70.39	70.46	70.41	70.45	0.05
50	70.64	70.45	70.38	70.32	70.34	70.43	0.13
100	69.93	69.78	69.69	69.62	69.48	69.70	0.17
200	69.01	68.83	68.79	68.77	68.58	68.80	0.15
500	67.38	67.19	67.10	67.02	66.82	67.10	0.20
1000	67.38	67.16	67.15	67.11	67.07	67.17	0.12

Table 4.6 - Summarized values for the interfacial tension values for DP-HS-1002 loaded solution for the second round of testing.

Each surfactant concentration was tested in 2 separate rounds to the determine reproducibility of the results obtained using the testing method developed for these particular surfactant loaded solutions. The values of surface tension as a function of surfactant concentration are depicted in Figure 4.13 and Figure 4.14. The graphs shown compare final average values as shown in Table 4.3, Table 4.4, Table 4.5 and Table 4.6, for the 2 surfactants.

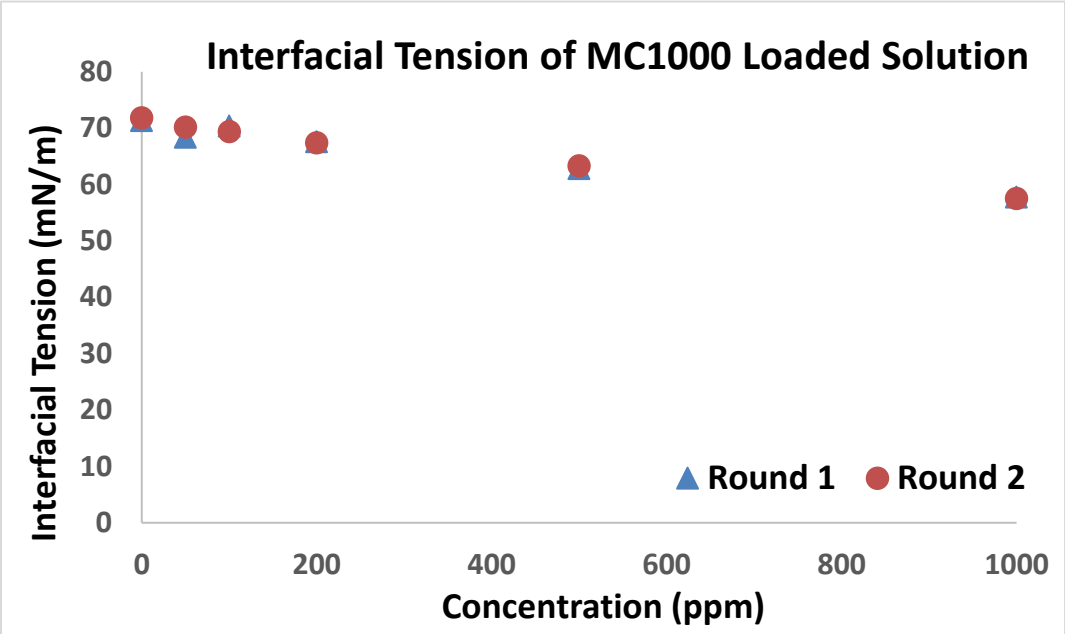

Figure 4.13 - Interfacial Tension for MC1000 loaded into 1% sulfuric acid solution. *The graphs depict the 2 separate rounds of testing performed on each solution. Each data point represents an average of 5 individual runs. Each run constituted an average of approximately 290 values from which the interfacial tension data was gathered.*

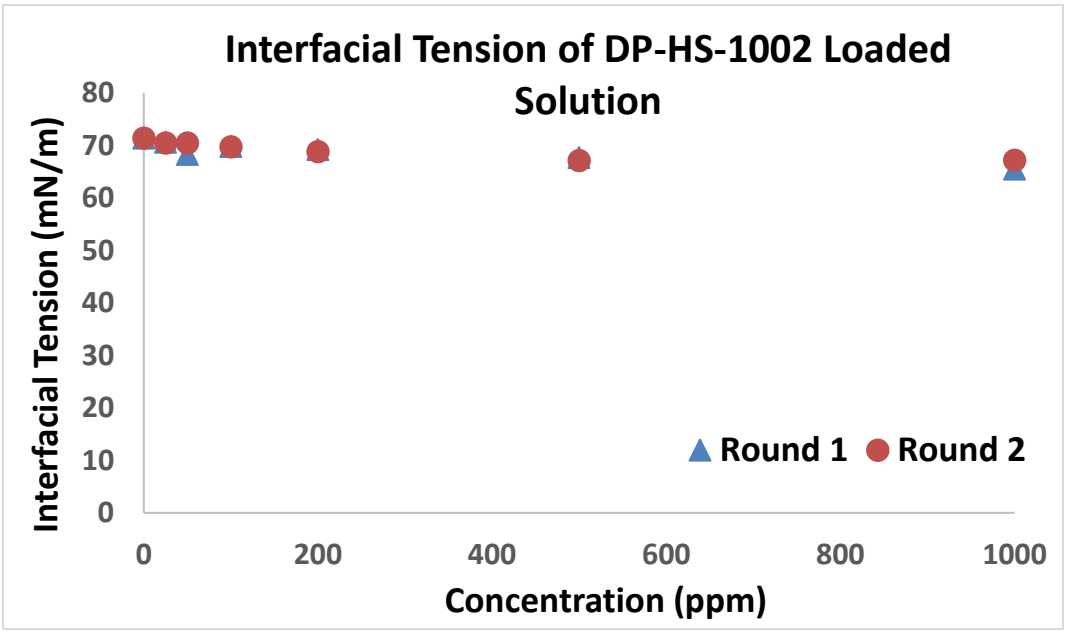

Figure 4.14 - Interfacial Tension for DP-HS-1002 loaded into 1% sulfuric acid solution. *The graphs depict the 2 separate rounds of testing performed on each solution. Each data point represents an average of 5 individual runs. Each run constituted an average of approximately 290 values from which the interfacial tension data was gathered.*

The two figures (Figure 4.13 and Figure 4.14) show that over the range of the surfactant concentrations tested the final values of interfacial tension for the 2 separate rounds of testing were quite close to each other. This indicated a high level of reproducibility for the testing method developed.

Overall the surfactants lowered the surface/interfacial tension of the fluid. As compared to DP-HS-1002, MC1000 had a bigger change in tension values as the surfactant concentration was increased from 0 – 1000 ppm (approximately 71 mN/m to 57 mN/m, respectively). DP-HS-1002 had a smaller change over the same concentration range (approximately 71 mN/m to 66 mN/m, respectively).

Solution not loaded with any surfactant solution (i.e. 1% H_2SO_4) had a fairly consistent value of interfacial tension that hovered around 71.5 mN/m with a standard deviation of 0.239 mN/m. The concentrations of surfactant used in the column leaching experiments were MC1000 at 50 ppm and DP-HS-1002 at 25 ppm. At these working concentrations the surface tension of leach fluid reduced to approximately 69 mN/m and 70.4 mN/m, respectively.

The surfactants had a bigger effect on the surface tension of the fluid at concentrations that were significantly higher than those used by working concentrations of the leaching experiments. For these experiments the interfacial tension of the fluid was tested along the the liquid-air interface. This finding indicated that the activity of surfactant, at the low concentrations used in leaching, had an overall low activity at this interface.

The aim of this chapter was to undertake a study to understand and classify the change imparted by the surfactant on the host liquid. For the typical leach solution of 1% sulfuric acid solution, it can be seen that the overall change in surface tension is not very large when these surfactants are added to it. The reduction in surface tension of the leaching fluid alone was not enough to fully attribute an increase in the amount leached copper. For this a further study to understand the activity of the surfactants at the solid-liquid interface was needed.

Chapter 5: Contact Angle Measurements

The determination of contact angle for this work was important to better understand where the surfactants acted within a heap leach system. From the initial experiment it was found that surfactants loaded into the leaching solution had a role to play in increasing the rate and yield in a heap leach. From the interfacial tension measurements it was found that the liquid-air interface seemed to be affected to a small degree in the working concentration ranges of the surfactants.

The next stage in attempting to determine where the surfactant had its biggest effect was studying the solid-liquid interface. For this the next set of experiments the aim was to measure the contact angle of the leaching solution (with increasing surfactant concentrations) on ore material.

5.1 Contact Angle Measurements

The contact angle of a liquid on a solid is the angle formed when a droplet of the liquid resides with and is equilibrium with a solid phase (see Figure 5.1). A convenient way of measuring the contact angle of liquids on solids usually makes use of the Sessile Drop Technique. This technique uses the same sort of set-up as the surface tension measurements. An image capture set-up is required to observe a body of fluid in proximity to another phase. However, the surface tension measurements only need a small volume of liquid to use as a hanging droplet.

The Sessile Drop Technique, on the other hand, requires the use of a solid material in which the liquid must be in contact with (see Figure 5.1). When in contact with the solid phase and gaseous phase alike, the interactions with each shape the drop as it reaches an equilibrium point. Using an image capture set-up the profile of a drop can be taken as it rests on a solid surface. From this the contact angle can be directly measured. In this method the contact angle provides a good reading for the affinity of the liquid phase to the solid phase.

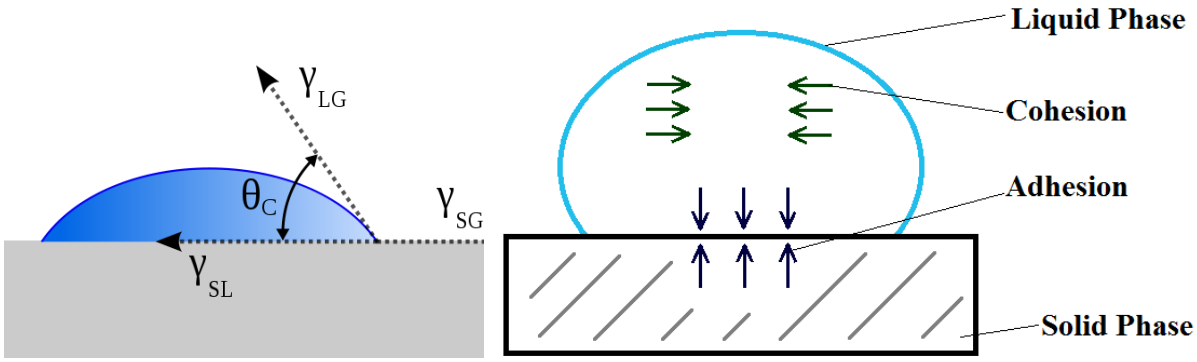

Figure 5.1 – Solid-liquid interactions in a Sessile Drop. *A convenient way to measure the interaction of a solid on a liquid is through the use of the contact angle measurement. A liquid at rest on a solid comes to rest at equilibrium and the contact angle (θ) provides a measure of the affinity for the liquid for the solid. The forces at play that shape the drop (and ultimately the contact angle) are the forces of cohesion (i.e. the intermolecular interaction between molecules in the liquid) and the force of adhesion (the affinity for the liquid on the solid). Image on the left was adapted from Wikimedia commoms (Wikimedia Commons, 2010).*

One issue associated with these measurements is the need for a homogenous solid phase upon which a solid can rest for direct angle measurements. A homogenous phase would mean that drops placed anywhere on the surface would return similar values. This ensures reproducibility and gives a more confident value for a solid-liquid contact angle. This poses an issue, however, for the measurement of contact angles using whole ore pieces as the solid surface. Ores are comprised of a multitude of different minerals interlocked with each other

to form a solid matrix (see Figure 5.2). The main limitation introduced by the natural non-homogeneity of an ore surface is the non-reproducibility of the contact angle measurements. The interaction of leach fluid with different minerals can yield different contact angle measurements. The random distribution of different mineral grains throughout an ore mean that a droplet of fluid can potentially report drastically different contact angle values, at different spots on the same surface!

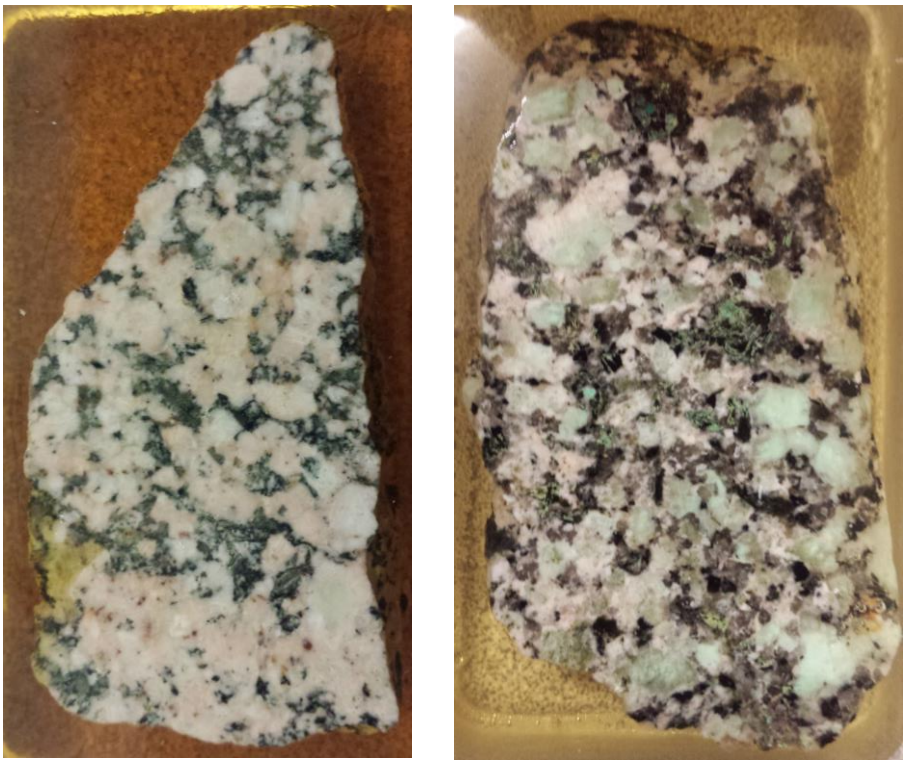

Figure 5.2 – Ore Surfaces. *The pictures shown above is the same ore as those used in the column leaching experiments in chapter 2. The ore pieces shown here were mounted in resin and the surfaces were sanded down with grit paper and polished with polishing paper. Flattened surfaces such as these can provide a level base from which a sessile drop can be placed to determine contact angle. However, the natural composition of the ore results in a non-homogenous surface. Placing sessile drops at different spots on the same surface can produce drastically different results, decreasing the reliability of the results. Hence, measuring conventional contact angles on ore surfaces can be challenging.*

This introduces an additional problem regarding value of the contact angle obtained. In a solid phase with a homogenous composition, the angle measurement can be confidently assumed to be the true value between that particular solid and liquid. However, with a multi-phase solid surface, wherever the liquid sits on the solid surface it is likely to encompass many different phases in the span that it contacts. Determining the degree of interaction with each mineral phase is not information that can be easily gleaned from a contact angle measurement. Additionally, a drop on spot of the surface may not provide a contact angle that would be representative of the whole ore.

The determination of contact angle for this work was important to better understand where the surfactants acted within a heap leach system. Because of the difficulty in using sessile drops to measure the effect on ore surfaces, another method needed to be used to determine contact angles. For this a method that involved capillary action was used.

5.2 Capillary Wicking and Contact Angle Measurements

The Sessile Drop Technique relies on the availability of a large enough solid phase with a non-porous sturdy surface on which a droplet can reside until it achieves equilibrium. The use of the Sessile Drop can be used on ore surfaces, but the reliability of the results remains in question. The method of capillary wicking provides a useful way to overcome this limitation by ensuring the equal contact of all mineral phases with a fluid of choice.

The capillary wicking method is typically used as a means to determine the contact angle and wettability of fluids on powdered material. For this, powdered material is systematically

loaded and packed into a holding receptacle (see Figure 5.3). As a result, the packed bed of powdered material forms a porous matrix. A reference liquid is introduced to one side of the porous matrix. The mechanism that drives the experiment to work is the ingress of fluid into the packed particle bed as a result of capillary action.

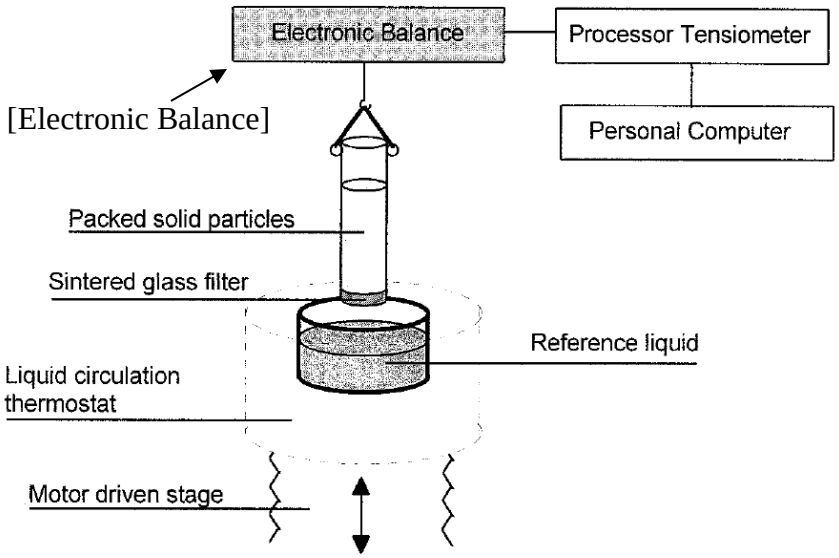

Figure 5.3 – Capillary Wicking through a packed bed of particles. *A packed bed of particles is loaded into a holding receptacle. One side of the bed is introduced to a liquid which. The liquid permeates through the packed bed due to capillary action. This occurs due to the attraction of liquid and solid phases and provides a way to calculate contact angle .© (Siebold et al., 1997). Reproduced with permission from Elsevier.*

5.2.1 Capillary Action

Capillary action (also known as capillarity) describes the tendency of a fluid to rise or fall within a capillary tube due to the attractive or repellent nature of the molecules in contact with a solid. On a sessile drop, the shape of a liquid droplet at rest on a surface depends on its interactions with its surrounding phases. As seen in (Figure 5.1) the main forces acting on a drop at rest are the forces of adhesion (i.e. the degree of interaction with the secondary phase) and the forces of cohesion (i.e. the degree to which the inter-molecular attraction attempts to

bind the molecules in the fluid together). A drop with a small contact angle can be considered to have a higher force of adhesion as compared to cohesion, as the molecules in the fluid have a high affinity for the molecules at the surface of the solid (see Figure 5.4). Conversely, a fluid with a high contact angle could be considered to have a higher force of cohesion as compared to adhesion as the molecules have a tendency to stick together.

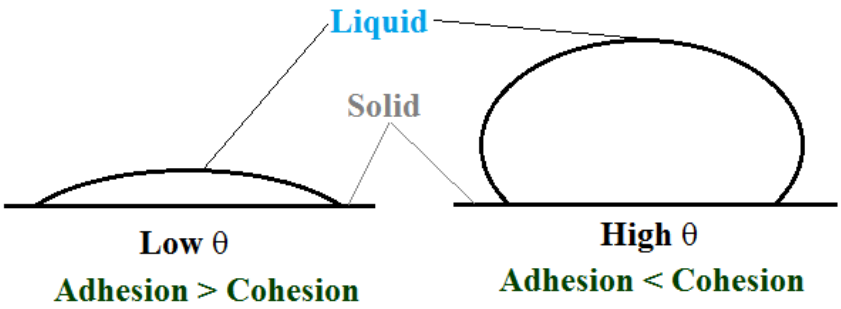

Figure 5.4 – Adhesion vs. Cohesion with respect to contact angle. *The forces affecting the shape of a drop when in contact with a solid phase are the forces of adhesion and cohesion. A liquid low contact would be considered to have a high affinity for the solid it is in contact with. This would mean that it has a higher adhesion force acting on it. Conversely, a liquid with a large contact angle would be considered to have a lower adhesion for the solid and a higher cohesion as the molecules in the liquid would rather bind together.*

The same forces of adhesion and cohesion control the motion of fluid in a capillary tube. When a tube is introduced to a body of fluid, such as in Figure 5.5, the cohesive and adhesive properties of the fluid come into play. A fluid with some degree of affinity for the solid it is in contact with would naturally adhere to the walls of the tube. This results in an upward force on the fluid head in the tube as the parts of the fluid in direct contact with the walls seek to maximize their contact area. However, the cohesive inter-molecular attraction

between the fluid molecules seeks to ensure that the fluid doesn't break up, and the surface tension keeps the surface of the fluid intact.

The effect of capillary rise occurs when the adhesive forces between the liquid and solid are stronger than the cohesive forces of the liquid. When the liquid has a high affinity for the solid there is strong inclination for the fluid to cling to the walls of the tube. As a result the fluid rises. The fluid front adopts a profile such that the height of the fluid in contact with the wall is higher than the height of the fluid at the center of the tube. While the surface tension keeps the fluid bound together, when the adhesive forces are greater than the cohesive ones, the surface tension is not minimal.

As was discussed in the previous chapter, the molecules at the surface of the liquid need to be in equilibrium for the liquid to be in equilibrium overall. Because of the adhesion to the walls, the fluid front continues to rise through the tube until the adhesive forces are balanced by the cohesive forces of the fluid phase. The cohesive forces attempt to minimize the forces between the molecules at the fluid front such that the difference in height at the walls and at the center of the tube is at a minimum.

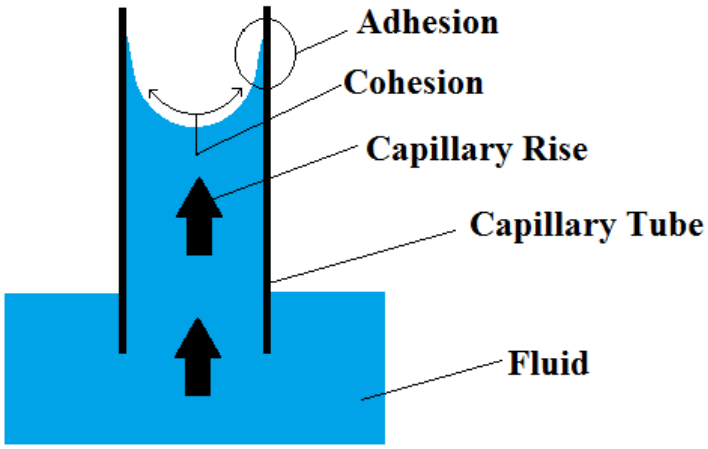

Figure 5.5 – Capillary Action. *In a capillary tube the rise of fluid is occurs almost spontaneously due to capillarity. A liquid with an affinity for a solid in the tube wall will naturally adhere to it. A liquid with a high degree of affinity will cause the liquid to rise through the tube as the fluid seeks to maximize its contact with the available wall surface. The intermolecular attractive forces in the liquid will present some resistance to prevent the liquid from breaking apart and the surface tension maintains the fluid front while the fluid rises. For capillary rise to occur the force of adhesion must be greater than the force of cohesion. The fluid stops rising when the two equal each other indicating the fluid is in a state of equilibrium.*

The radius of the tube the fluid is rising through directly affects how high the fluid will rise before adhesion and cohesion balance each other out. The smaller the tube the more pronounced the effect of capillarity. This is because the smaller tubes size means more fluid is directly in contact with the solid walls of the tube and the so force of adhesion is greater. Bigger tubes show less capillary rise as only a fraction of the fluid is in contact with the solid phase and so the cohesive force dominates more than the adhesive force. This effect plays a major role in the capillary wicking experiments overall.

5.2.2 Capillarity and Packed Particle Beds

In the packed particle beds as depicted in (Figure 5.3) the spaces/pores between particles can be thought of as capillary tubes that have been bundled together. The walls of the tubes are the particles themselves and the spaces in between them are where the fluid permeates

through (see Figure 5.6). The action of capillarity drives the fluid to permeate into the capillary bundles when it is introduced to a packed bed.

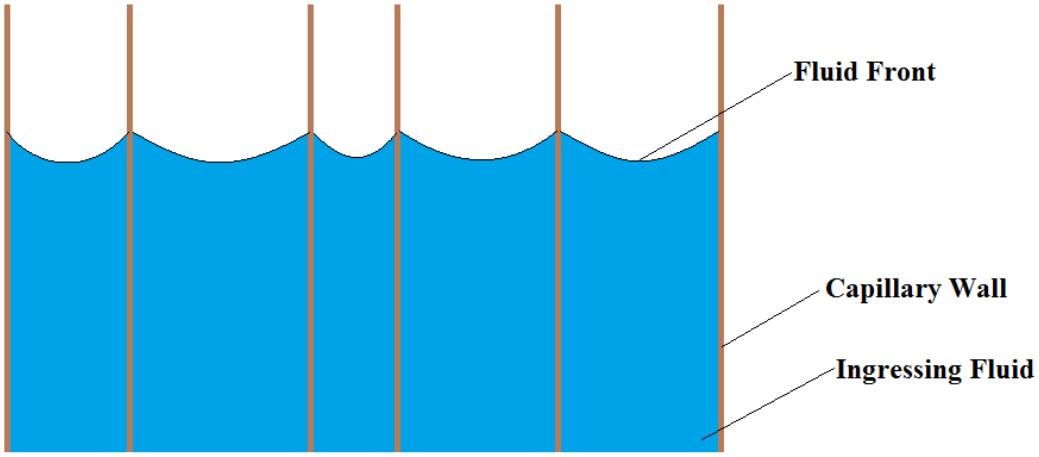

Figure 5.6 – Packed particle beds. *A packed bed of particles can be thought of as a series of capillary tubes bundled together in parallel. The rate at which fluid climbs through the bundles is a direct result of the affinity between the solid and liquid phases. The rate of ingress through the capillary bundles provides a useful tool to measure the solid-liquid contact angle. The rate can be measured through the weight gained in the bed over time of the height of the fluid over time.*

The rate at which the fluid rises through the capillaries and occupies the spaces between the particles provides useful data from which the contact angle can be calculated. This is because the rate is directly affected by the affinity the liquid phase has for the solid phase. The progression of the combined fluid fronts in all the capillaries of the packed bed are achieved by: (a) monitoring the height of the fluid against time as the fluid progress through or, (b) measuring the weight gained over time as the liquid displaces air to occupy the spaces in between particles. (Siebold, Walliser, Nardin, Oppliger, & Schultz, 1997).

5.2.3 Capillary Wicking and Washburn's equation

As was discussed the in the previous section the capillary rise of a fluid is the result of an attraction between the liquid and the solid phase of the capillary tube wall. As a liquid rises through a capillary tube, there is a linear relationship between the square of the height of the liquid front vs. time, over the duration the fluid remains in motion (Alghuniam, Kirdponpattara, & Newby, 2016). This forms the basis for the application of Washburn's equation for calculating contact angle. In most capillary rise experiments the general noted trend for the movement of fluid through a packed bed follows the regime as shown in Figure 5.8. The initial part of the profile is dominated by intertial effects where the momentum of the fluid is the driving force of the fluid. The second stage of profile, known as Washburn's regime, is driven by capillary action of the fluid in the tubes. The third and last part of the profile is when the force of gravity becomes too large for the adhesive and cohesive forces to resist at which point the fluid front can no longer rise. (Alghuniam et al., 2016).

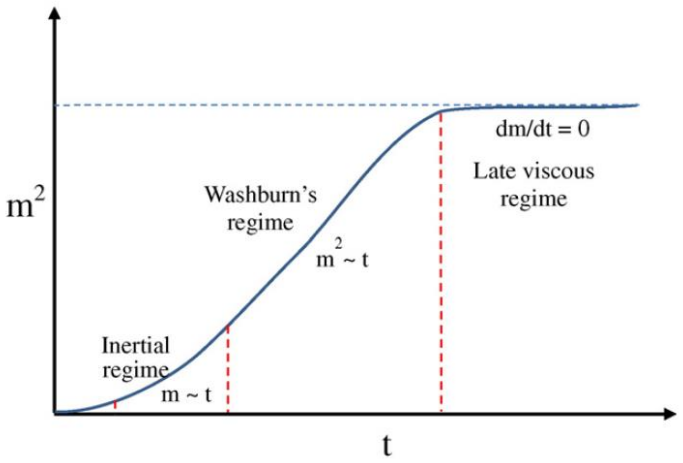

Figure 5.7 –Washburn's regime in typical capillarity graph. *©(Alghuniam et al., 2016). Reproduced with permission of Elsevier.*

The Washburn's regime is the part of the profile that is used when doing further calculations. In the Washburn zone the fluid progression through the capillaries is due to the natural attraction between the liquid and solid phases of the bed. The forces of adhesion to the solid are dominant in moving the liquid through the bed. The forces of gravity are negligible in this zone and the movement of liquid is from capillarity. Based on this the Washburn equation was developed to describe the rate of flow of fluid through a capillary tube.

The rate of flow of a liquid through a capillary is described using the Hagen-Poiseuille equation (Siebold et al., 1997), which is:

$$\upsilon = \frac{r^2 \Delta P}{8\eta h} \qquad (1)$$

Where: υ – fluid velocity; r – average capillary diameter; η – fluid viscosity; h – height of the fluid in the capillary tube and ΔP – pressure drop across the fluid surface

The pressure drop across the fluid surface can be calculated as follows (Alghuniam et al., 2016):

$$\Delta P = P_c - P_H = \frac{2\gamma_L cos(\theta)}{r} - \rho g h \qquad (2)$$

Where: P_c – Capillary pressure; P_H – Hydrostatic pressure; r – average capillary diameter; γ_L – fluid surface tension; ρ – density of fluid; h – height of the fluid in the capillary tube and g – gravitational constant ($9.81 m.s^{-2}$)

The Washburn equation is applied in the region of the profile where the effects of gravity are small and the capillary pressure is high to allow spontaneous permeation of fluid. In doing so the P_H term of equation (2) can be negated.

Substituting equation (2) into equation (1) and where υ = dh/dt, the following formula is yielded (Alghuniam et al., 2016; Siebold et al., 1997) :

$$\frac{dh}{dt} = \frac{r^2}{8\eta h} \cdot \frac{2\gamma_L cos(\theta)}{r} \qquad (3)$$

Setting the boundary condition such that at time (t=0) the height is (h=0) and at time (t=t) the height is (h=h), equation 3 can be integrated to yield the Washburn equation (Alghuniam et al., 2016; Siebold et al., 1997):

$$h^2 = \frac{r_{eff}\gamma_L cos(\theta)}{2\eta} t \qquad (4)$$

Equation 4 is used when the height of the fluid front is measured as it progresses through the packed bed of particles. The limitation with this equation/form of data collection is that only the height of the liquid front at the visible surface of the packed bed is measured. The progression of the liquid may not necessarily be uniform across the visible surface of the packed bed or even within the bulk of the packed bed.

To have a more concise and accurate measurement for the progression of fluid, the increase of weight over time can also be collected. This is the form of data collection used for the work in this thesis. To transform equation (4) into a weight based equation, the height of

fluid in a packed bed of particles can be related to weight using the formula (Siebold et al., 1997):

$$w = \epsilon.\rho.\pi.r_{eff}^2.h \qquad (5)$$

Where: ε – Porosity of packed powder bed; r – effective capillary tube radius; ρ – density of fluid; h – height of the fluid in the capillary tube

Substituting equation (5) into equation (4) yields:

$$w^2 = \left(\epsilon.\pi^2.r_{eff}^4\right)\frac{\rho^2\gamma_L\cos(\theta)}{2\eta}t = \frac{C\rho^2\gamma_L\cos(\theta)}{\eta}t \qquad (6)$$

The 'C' factor in equation 6 refers to a packing factor that needs to be determined. The geometric factor is an all-encompassing value that aims to quantify the total available space in a packed bed. The reason for this is based on the structure of the voids once the particles are packed in a receptacle. In a porous medium the cross-section of a capillary tube, whose walls are comprised of solid particles, would not be uniform. As the fluid progresses through the capillary tube it would be subject to local expansions and contractions as it made its way through (see Figure 5.8). (Siebold et al., 1997).

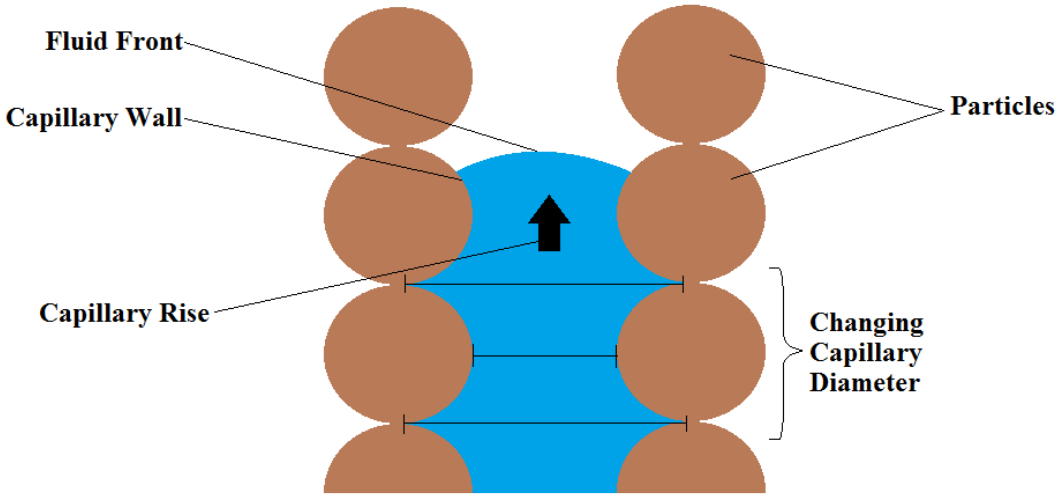

Figure 5.8 – Structure of Capillary Tubes in packed beds. *In a packed bed of particles the diameter of the tube is not a uniform structure. Because the walls of the tube are made from particles as the fluid progresses through, the liquid encounters a changing in diameter as it progresses up the tube. (Siebold et al., 1997)*

The equations developed to model the capillary flow through the tube rely on the use of uniform cross-section tubes through which the fluid flows. However, in a packed bed of particles the shapes of pores are more complicated in structures than simple cylindrical capillaries. In addition, the pore network is more inter-connected than assuming a simple bundle of parallel capillaries. (Siebold et al., 1997)

For this reason, the calculations use an 'r_{eff}' value, which is an effective radius. Studies conducted by (Siebold et al., 1997) show that an average value for radius across the pore length suffice for the calculation in contact angle. Beyond that the calculation of a packing factor allows for the classification of the entire pore space between particles. This is a value that can be determined experimentally.

The packing factor value ‘C’ for the packed bed is calculated using a reference liquid (Alghuniam et al., 2016). This is akin to a calibration run. A fluid that is considered to be completely wetting (i.e. $\cos(\theta) = 1$) is used. In the case of capillary wicking experiments the reference liquid used is typically octane (Alghuniam et al., 2016). Octane is typically used due its low surface tension, moderate viscosity and low vapor pressure. The reference liquid used should have predictable complete/near complete wetting of the solid that it is in contact with. This allows for the calculation of ‘C’ in equation as all the other factors are known.

Once this has been done, a fluid whose contact angle with the solid is unknown can be used and from which the contact angle can be calculated. The idea behind the capillary wicking experiments is that the preparation of the packed beds needs to be done systematically and be done the same way each time the experiment is run. This is to ensure that the geometric factor calculated using octane is the same when other fluids are used (Siebold et al., 1997). By ensuring the reproducibility in the preparation differences in the rate of uptake (and ultimately) contact angle can be more concisely attributed to the differences in the fluid properties being used.

5.2.4 Capillary Wicking for Ore Material

The surfactants act at the surface of the fluid and in the previous chapter the interaction at the air water interface was calculated. With the capillary wicking experiments the aim is to see if the surfactants affect the liquid-solid interface. As mentioned in the initial section of this chapter the measurement of a contact angle for this work is important to understand where the surfactants have an effect within a heap leach system. The degree to which the surfactants

affect a change will be measured by the change in contact angle as calculated by the Washburn equation. Essentially, the presence of surfactant should affect the adhesive properties between the solid and the liquid and affect the rate of uptake through the packed bed. The capillary wicking experiments should also provide a more representative value of contact angle as the leaching fluid will be in contact with all the phases of the ore as it ingresses through the packed bed.

5.3 Experimental Preparations

The following sections detail the various preparation stages for the different parts of the experiment prior to running the actual experiments

5.3.1 Ore/Solid Phase Preparation

5.3.1.1 Ore Sizing

For the capillary wicking experiments the particle size distribution employed for all the experiments played a major role in the data collection process. To calculate the contact angle for the liquid-solid contact, the slope from the graph of the weight^2 vs. time needs to be obtained. For the accurate calculation of the contact angle the slope needs to be linear. This indicates the progression of the fluid is in Washburn's regime and Washburn's equation can indeed be used.

According to (Alghuniam et al., 2016) in a thorough review of capillary wicking experiments the best particle size range for the packed beds should be less than 150 μm. The best results obtained are when a mixture of particle sizes are used up to a maximum of 150 μm.

However, beyond this, for the ingress of the fluid, the weight^2 vs. time deviates from linearity. Using non-linear values in the Washburn's equation reduces the accuracy of the obtained contact angle value.

For the work performed in this thesis the maximum particle size chosen for the packed beds was -140 mesh (-106 μm) in size. This maximum particle size for the experiment was chosen based on prior trials. The ore used for these experiments was the same ore used in the column leach experiments. The ore was sent to Bureau Veritas for grinding. Approximately 2.8 kg was sent for processing.

The ore was returned as a wet grind product and was then dried. The grinding water was decanted from the ground solid. The wet solid was laid out in trays and allowed to dry at ambient room temperature. The solids were rotated regularly to ensure complete evaporation of the moisture. The drying was performed at room temperature as per ASTM c702 standard for the splitting of aggregate sample (ASTM, 2011). Prior to running each experiment the bulk sample needed to be split (highlighted in the next section). One of the requirements for the use of a mechanical splitting procedure, according to the ASTM standard, is that samples being split need to be dried at the temperature no higher than the temperatures at which the test work will be performed at. In addition to this the use of high temperature drying ovens was avoided due to the possible oxidation or transformation of the mineral species. The problem is exacerbated with fine materials due to the increased surface area.

As the material was drying the wet particles had a tendency to stick together forming agglomerated chunks. These had to be regularly separated by hand to ensure that trapped moisture between particles was fully eliminated. Once dried the ground ore was mixed and the bulk mixture needed to be verified for size.

5.3.1.2 Size Verification

The size verification was performed in multiple stages. One of the key components of the experiment was ensuring that the size of the particles was consistent. The first stage of screening involved the use of a 100 mesh screen. This was a rough screening stage to eliminate any small agglomerates from the bulk mixture that could not be separated by hand. The removal of these types of particles is important because of these types of particles tend to have their own network of pores. Particles with an intra-porous network can cause the ingress profile to deviate from linearity as the particles swell with moisture (Alghuniam et al., 2016). This also changes the overall structure of the pore network of the packed bed rendering the Washburn analyses inaccurate.

Once separated from the bulk, the second stage of screening involved a more refined verification stage to eliminate oversize particles. The second round of size verification involved using a Ro-Tap machine. A Ro-Tap machine allows for sizing of particles using mechanical vibration. Sieves with screens attached to them are used for this purpose. Sieves in descending order (screens with larger openings are placed at the top and screens with the smallest opening are placed at the bottom) are stacked. Material is fed into the top most screen. The premise of the Ro-Tap is that solid particles smaller than the screen opening fall

through, while larger particles remain constrained above the screen. When the mechanical vibration is activated the particles are forced into motion. This ensures that larger particles are not blocking openings through which the smaller particles can pass through due to gravity. Sieves are typically numbered according to the size of the screen openings that they have. The purpose descending screen openings is for particles to continue passing through sieves until they hit a screen for which the openings are too small for them to pass through. At this point the particle is sized as being smaller than the preceding screen but larger than the one they sit on. A collection pan is usually set at the bottom of the stack to catch material that passes through the smallest screen.

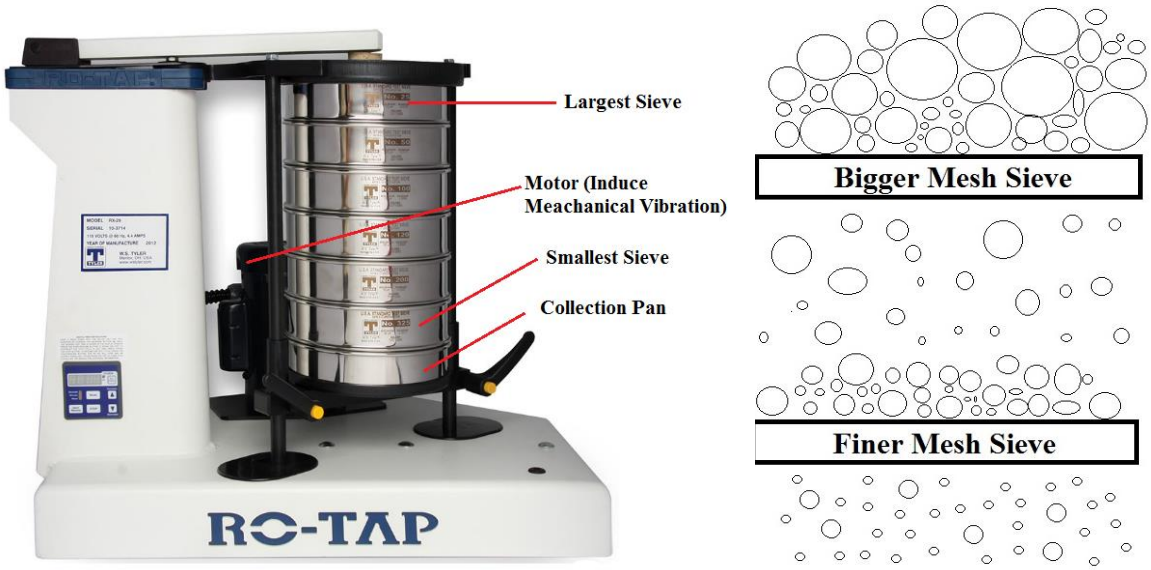

Figure 5.9 – Ro-Tap Functionality. Ro-Tap Machine (Left) *(W.S. Tyler, 2017)***. Sieve Functionality (Right).** *The ro-tap machine works by stacking sieves in descending order of size. Material is fed into the top screen. Vibration and gravity allow particles to pass through the screens until they hit a screen they too big to pass through. Particles are typically size as being smaller than the mesh opening of the previous screen but larger than the mesh opening of the screen they are sitting on.*

In the size verification for this stage of the sample preparation, the Ro-Tap machine was set-up with a 140 mesh screen and a collection pan as a stack. Some of the bulk mixture was fed into the top of the 140 mesh screen and the whole stack was placed into a Ro-Tap machine. The machine set about vibrating and shaking the screen stack. Any particles smaller than 140 mesh in size would pass through the screen openings.

2 concurrent Ro-Taps were set-up and the bulk mixture was run through to remove the oversize particles. All undersize material was then stored in a separate container. The oversize material collected in the first round and second round of screening had to be ground down to ensure they met the correct size requirements for the experimental work. The oversize material was fed into ring mill pulverizer. The ring mill was run for a minute and the ore material was removed for re-screening. Anything above 140 mesh in size was fed back into the ring mill and re-ground. The process was repeated till everything was smaller than 140 mesh in size.

5.3.1.3 Sample Splitting

Once the size verification was complete, the re-processed oversize ore material was mixed with the undersize material. Using a tarp all the bulk was laid out and mixed together by lifting the edges of the tarp and allowing all the material to roll over itself.

The bulk aggregate still needed to be split into usable sizes for the test work. To provide a consistent splitting method a mechanical riffle splitter was used. The finely ground ore material had a variety of particles of different size up to 106 μm in size. Simply scooping the

required masses for the test charges would not have guaranteed that the particle size distribution in each test charge was representative of the larger bulk sample.

To split the sample using a mechanical riffle the procedures highlighted in the ASTM c702 "Standard Practice for Reducing Samples of Aggregate to Testing Size" was used. The standard was designed for the reduction of large aggregate samples to appropriate sizes for testing purposes. The procedures are designed such that variations in the characteristics between split test samples and the larger bulk are minimized. (ASTM, 2011).

Figure 5.10 – Mechanical Riffle Splitter. *The riffle splitter provides an easy and convenient way to split a bulk sample of aggregate in half. Bulk sample is fed via the use of a hopper at the top. The sample is split in half as the aggregate flowing through it flows into receptacles on either side of the riffle. The standard developed by ASTM for splitting samples provides a convenient way to produce test size samples of an aggregate material that have the characteristics of the larger bulk it was split from.*

According to the ASTM standard there were certain conditions that needed to be met in order to use the mechanical riffler for splitting. For fine samples (defined as material smaller than 3/8" according to (ASTM, 2011)), the following was required:

- Dried aggregate material in temperatures no higher than those in which the test work will be performed.
- A splitter with no less than 12 chutes which discharge material to alternative sides from where the material is loaded into the splitter.
- Chute widths must be between ½" to ¾" (12.5 mm – 20 mm) for effective splitting.

For the work in this experiment the riffling conditions used were:

- Samples were dried at room temperatures (as highlighted in the previous section)
- A splitter with 12 chutes was employed (as seen in Figure 5.10)
- The average chute width for the splitter was 15 mm.

For the splitting of the sample the procedure used was as follows:

- The bulk aggregate was placed on a flat pan and leveled out.
- The flat pan spanned the breadth of the chutes in the area that the material was fed to.
- The material was fed in gently to avoid spills and to ensure unobstructed flow through the chutes.
- The weight of the bulk material was weighed before the splitting was done.
- The weight of the individual receptacles was recorded after the splitting was done.
- The mass difference between the 2 buckets was calculated as a percentage of the total fed into the riffler. If the mass difference was more than 1-2% the material in the buckets was re-combined and the split re-performed.

The total mass of material bulk fine aggregate material was approximately 2.8 kg. Using the splitting technique mentioned above the bulk sample was split into 16 individual samples of test charges of approximately 180 g. The individual test charges had to be further prepared for the capillary wicking experiments.

5.3.2 Packed Bed Preparations

5.3.2.1 Receptacle/Containment Unit Preparation

For each experiment a packed bed of particles needed to be prepared. Each test charge was loaded into an acrylic tube, the dimensions and specs of which are shown in Figure 5.11.

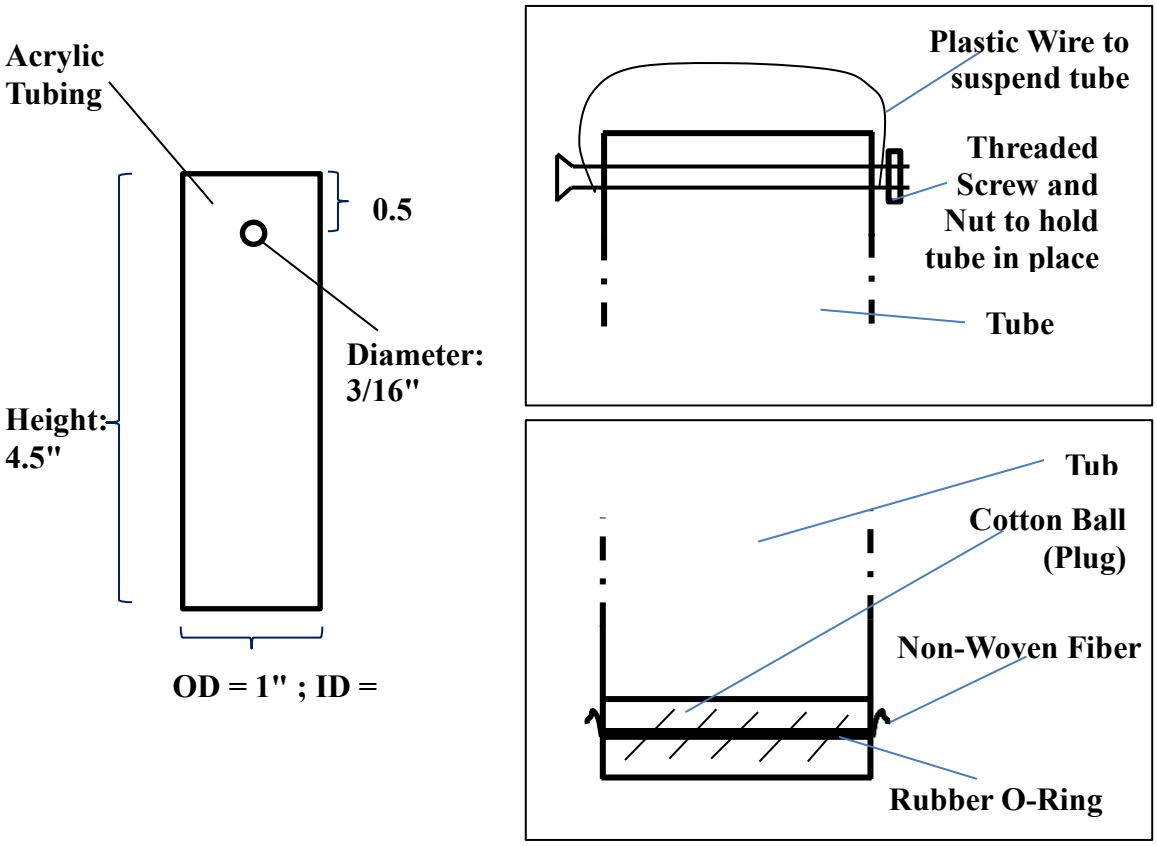

Figure 5.11 – Dimensions of Holding Receptacle. *The bed of particles through which fluid ingress was to be measured had to be packed in holding receptacles. For the work in this thesis the bed of particles were packed in acrylic tubes with the dimensions and specs as shown.*

For the acrylic tubes a hole was drilled just about 0.5” from the top of the tube. This allowed for a screw to be threaded through. This allowed for a wire/string to be hooked on either end of the screw and the entire tube could then be suspended from a load cell. The experiment needed to weigh the mass gained over the time the experiment is running. As the fluid is introduced to the packed the tube gets heavier as the fluid permeates through. This results in the overall mass of the tube increasing. By suspending the tube from a load measuring device, the heavier the tube gets the greater the force exerted. The act of suspension provides an accurate way to measure the weight gained.

The bottom of the tube was loaded with supporting materials to hold the packed bed of particles in place. This was necessary as the particles needed to remain still for the duration of the experiment. To hold the particles in place and support the weight of the bed, a cotton plug was used at the bottom of the tube. Cotton was chosen for this purpose due to its sturdy nature and ability to hold weight in this instance. Additionally, cotton as a material is hydrophilic and does not prevent/hinder the movement of fluid through it (Alghuniam et al., 2016). This is important as the fluid needs to permeate through the support before it permeates through the packed bed of particles. To prevent the movement of ore particles into the cotton supports, a filter paper was placed in between. On the outside of the tube, but still at the bottom, a piece of non-woven fiber was placed and secured by a rubber O-ring. This served 2 functions: (a) it ensured that during the packing procedure the contents of the tube did not fall out of the bottom of the tube, and (b) ensured that while the experiment was running the increasing mass of the packed bed did not cause it to fall out of tube.

For each experiment the preparation of each bed followed the same regiment:

- Clean each tube and rinse with DI water to remove contaminants
- Prepare the supporting structure at each tube base
- Pack each tube with ore particles
- Thread and suspend each tube on the load cells for the experiments

5.3.2.2 Packed Bed Preparation

Each round of experiments was structured in such a way that the surfactant concentrations tested in the previous chapter were also used for testing in these experiments. For each experiment 4 packed beds were run simultaneously. For this a procedure was developed to split the test charges into individual charges to be loaded into each tube.

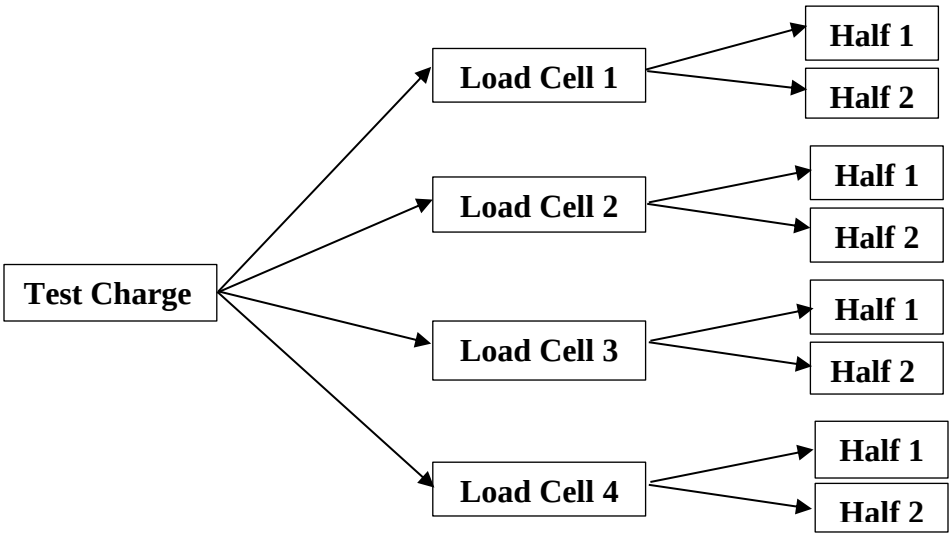

Figure 5.12 – Splitting procedure for test charge into individual charges for packed bed preparation. *Each of the test charges produced in the sample splitting section (section 5.3.1.3) needed to be further split into individual test charges which could be packed into the acrylic tubes. Each individual test charge (approximately 180g) was riffled down to 4 sub-charges (approximately 45g). These sub-charges were used to produce packed particle beds.*

For each surfactant concentration being tested 4 packed beds needed to be prepared. The nature of the ore was such that, even in the individual test charges, there were a variety of different particles at different sizes and with many different phases. To ensure complete randomization of the samples, the individual test charges needed to be split using a riffle splitter into 4 separate samples, which could be loaded into the acrylic tubes. To separate the samples for testing using capillary wicking a micro-riffler was used, as depicted in (Figure 5.13).

Figure 5.13 – Micro-Riffler for Sample Splitting. *A micro-riffler was used to split the test charges down to sub-charges for the packed beds. A riffle split was used because in each test charge there were particles of different sizes and phases present in the mixture. The riffle splitter provided and easy way to split and randomize the produced samples. Samples fed into the hopper had an equal probability of flowing out of either discharge chute. This ensured randomization of the split samples.*

The procedure used to split and pack the samples was as follows (see flow chart in Figure 5.12):

- The 16 samples produced from the splitting of the main bulk aggregate were individually stored and marked. Each sample that was produced was assigned to a particular surfactant concentration for testing.
- For the preparation of the packed beds the individual test charges were split in the micro-riffler in the following sequence of steps:
    I. The test charge was placed in a feeding pan and gently fed through the riffle to allow the material to flow freely and evenly through the riffle chutes.
    II. The individual test charge was split into two. The two charges were once again split into a further two charges, for a total of four sub-samples.
    III. Each sub-sample once again split into two halves.
    IV. One half of the sample was loaded into an acrylic tube (with a base support structure in place) with the aid of a funnel.
    V. The height of the particles in the tube was measured from the base of the tube.
    VI. The particles were then packed in place by "tapping" the tube.
        - The tubes were tapped by raising them off the lab bench by a small height and releasing it.
        - The effect of the tube impacting the lab bench causes the particles to re-arrange themselves such that smaller particles can move into the spaces between larger particles
    VII. The tubes were tapped in increments of 10 and the height was measured after each set of incremental taps.

VIII. Once the height of the bed of particles stopped changing, the second half of the split sub-charge from step III., was loaded into the tube.

IX. Steps IV. To VII were repeated until the height of the bed of particles stopped changing.

X. The fully prepared packed beds were mounted onto the load cells.

The procedure had to be repeated for each packed bed of particles for each surfactant being tested. By following the same packing procedure the contact angle derived from Washburn's equation becomes more accurate. Since the preparation and testing conditions remain the same, changes in the observed values can be more definitively attributed to the change in the fluid constitution. Additionally particles are packed till the height of the bed stops changing as this typically means that the maximum packing density has been reached (Alghuniam et al., 2016).

5.3.3 Solvent/Solution Preparation

The measurements for this work sought to determine the change in contact angle for a leach solution in contact with ore, in the presence of a surfactant. For this experiment the solutions used were 1% sulfuric acid with increasing concentrations of surfactant. The same concentrations used during the interfacial tension experiments were also used for testing in this experiment.

	MC1000	DP-HS-1002
0 ppm	✓	✓
25 ppm		✓
50 ppm	✓	✓
100 ppm	✓	✓
200 ppm	✓	✓
500 ppm	✓	✓
1000 ppm	✓	✓

Table 5.1 - The concentrations of surfactant solutions used for contact angle testing. *All surfactant solutions were prepared by dissolving the surfactant in a matrix solution of 1% sulfuric acid (10g/L H_2SO_4).*

Just as in the previous chapter, the solutions were all prepared by dissolving the surfactants in a matrix of 10g/L sulfuric acid (1% H_2SO_4) corrected for purity. The sulfuric acid was prepared by diluting concentrated sulfuric acid (manufactured by BDH chemicals) in DI water.

The surfactant solutions in Table 5.1 were prepared in the following manner:

- A bulk solution of surfactant was prepared by initially dissolving 1g of the respective surfactant in 1L of 1% sulfuric acid to create a 1g/L surfactant solution. The acid solution and surfactants were placed in a volumetric flask and shaken thoroughly to ensure complete dissolution.
- The density of 1% sulfuric acid at room temperature (~20°C) is 1.0049 g/cm^3 according to CRC's Handbook of Chemistry and Physics (Lide, 2008). Because of the close proximity of the density of 1% sulfuric acid to that of water, it was assumed that the density of sulfuric was 1g/L. This meant that to create a 1000ppm surfactant solution, 1g for every 1L of 1% sulfuric acid was needed. (In reality, assuming the density of 1% sulfuric acid to be 1.0049g/cm^3, to create a 1000ppm surfactant

solution, 1.0049g of surfactant solution would have been needed. This was very close to the original amount used).

- For each experiment 200mL of surfactant loaded solution was prepared. This was distributed amongst the 4 packed beds. For each run the 4 packed beds used the same solution. An average of the slope data gathered from each packed bed was obtained. The average was used as the contact angle for that particular surfactant concentration on the ore.
- Based on the required surfactant concentration for testing, the 1000ppm solution was diluted by the factors shown in Table 5.2. To prepare the solutions the needed amount of 1000ppm solution was measured out. The solution was placed in a 200mL volumetric flask. The rest of the volume was topped with 1% sulfuric acid.

	0 ppm	25 ppm	50 ppm	100 ppm	200 ppm	500 ppm	1000 ppm
Dilution Factor	-	40	20	10	5	2	1
Bulk Solution Per 200mL	-	5mL	10mL	20mL	40mL	100mL	200mL

Table 5.2 - Dilution factors and final concentrations for solution testing. *The final solutions for testing were prepared by diluting a bulk sample of 1 g/L (1000 ppm) surfactant solution down to the final concentrations as shown in the table above. The needed amounts of the bulk solutions were measured out using an auto-pipette and placed in a 10mL volumetric flask. The rest of the volume was filled with 1% sulfuric acid solution.*

5.3.4 Data Collection Set-Up

The method of monitoring the fluid progression through was through the measurement of the weight of packed bed over time. As the fluid ingresses through the packed bed the weight of the structure would naturally increase over time. As mentioned in section 5.2.3 the monitoring the weight of the structure over time provides a more concise reading of the rate

of uptake. Regardless of the shape or size of the pores and capillaries the weight gives an accurate value of the exact amount of water that has permeated at a given time, t.

To measure the weight of the packed beds, load cells were used. For the work in this thesis, the load cells used were LFS 270 Miniature S-Beam Load Cells as manufactured by Cooper Instruments. The load cells provided an easy and accurate way to measure weight. A load cell is able to convert the load acting on them into measurable electrical signals. The load cells primarily function through the use of a series of inter-connected strain gauges housed in a containment unit. As depicted in Figure 5.14 the load cells used were tension based. When the load cell is in tension the resistance across the strain gauges changes. The degree to which it does is a direct function of the load applied. The resistance can be measured by the application of a voltage across the load cell.

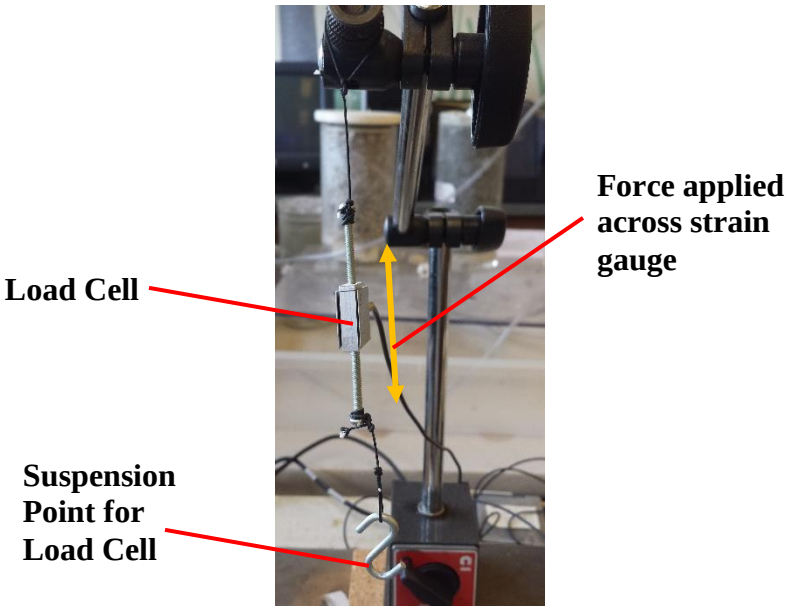

Figure 5.14 – LFS 270 S-Beam Miniature Load Cells. *When a load is applied across the load cells the unit is in tension. The increase in mass results in a resistance across the strain gauges in the load cell unit. The change in resistance is a function of the change in mass applied across the load cell. This means that the mass applied can be measured by the change in electrical signal across the strain gauges in the load cell.*

The load cells were controlled using a computer but connected to a National Instruments NI9219 Universal Analogue Input and a NI USB-9162 C-Series USB Module Carrier. These devices served as an interface between the load cells and the computer through which the data was collected. The devices sent a voltage signal to the load cells and collected the signals received by the load cells. The signals were then sent to a computer. The computer software was used to control the load cells overall was LabVIEW instrument control as designed and manufactured by National Instruments. The software allowed for the creation of a virtual interface that could control the rate at which data was gathered from external instruments. The software collected the data signals from the external data cards and collated everything into readable spreadsheets.

For the experiments in this thesis the weight of the load cell was measured every 0.5 s. This meant that for the final analysis of the weight against time there were more data points against which a slope could be calculated using linear regression. This provided a more accurate value of slope and in turn a more concise value for contact angle.

5.4 Final Experimental Set-Up

The final experimental set-up is depicted in Figure 5.15 and Figure 5.16. In order to begin the process of data gathering from the packed bed the following procedures were used:

- The acrylic tubes prepared and packed as highlighted in section 5.3.2, were hung on the suspended load cells.
- The solutions prepared in section 5.3.3 was poured into beakers. Approximately 50ml was dispensed into each beaker. The beakers were placed on raisable platforms. At

the time the experiments were being prepared, each beaker was placed under a suspended acrylic tube, but a good distance away from the bottom from the tube. This was to ensure no accidental or premature ingress of fluid into the packed bed.

- When the experiment had been fully prepped, the load cells were activated to collect data. This was to ensure a baseline value for the weight of the tube was obtained prior to any fluid ingress occurring.
- After approximately 30s, the beaker was raised up gently. The level of the fluid lifted to meet the bottom of the packed tube. A raisable platform was used as it allowed for a steady and controlled contact of the fluid to the tube surface. It was imperative that the particles in the tube remain undisturbed so as to ensure the packing factor was constant.
- The fluid ingress was allowed to run.
- The experiment was terminated when the fluid reached the top of the packed bed indicating full saturation of the structure. As this point the beaker was lowered away from the base of the tube.
- When all four beakers had been separated from their respective tubes the load cells were de-activated.
- The weights recorded by the load cells were compiled into a readable CSV file which was extracted from the computer and taken for further analysis.

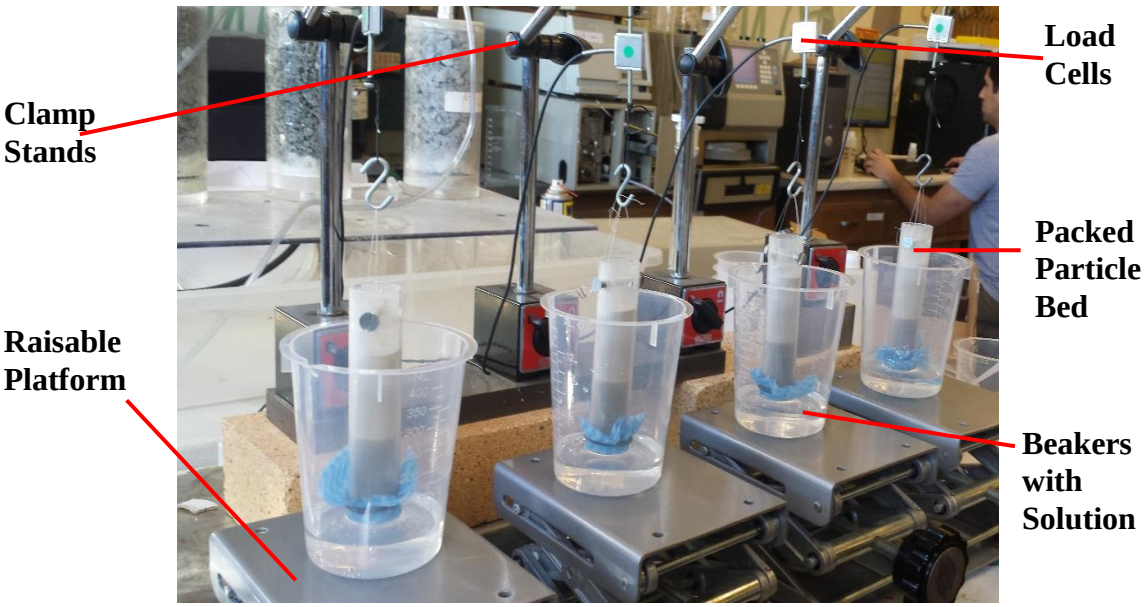

Figure 5.15 – Final experiment set-up for capillary wicking.

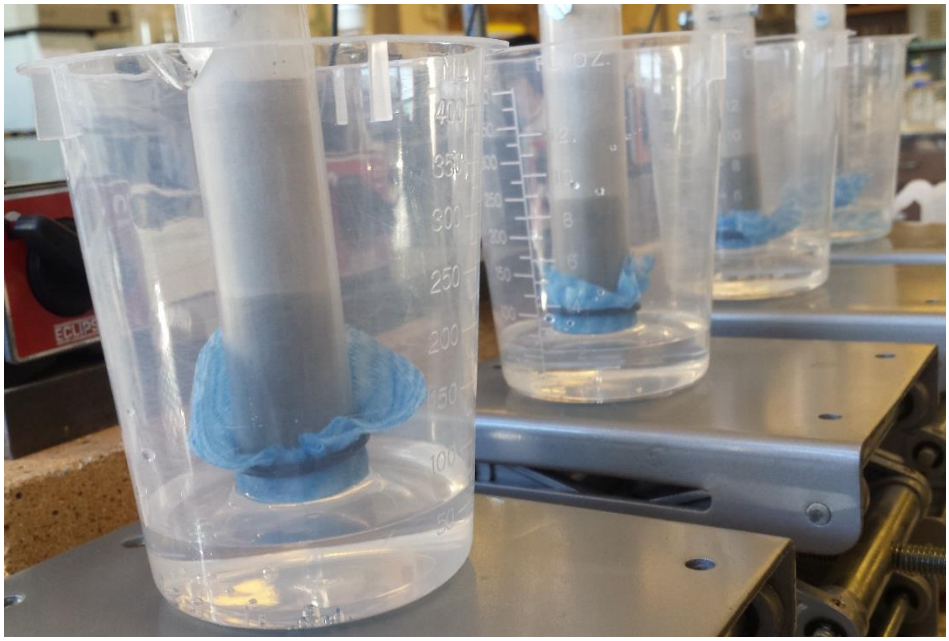

Figure 5.16 – Fluid permeation through packed bed. *The permeation of fluid through the packed bed of particles was clearly displayed by the moving fluid front.*

5.5 Results and Discussion

This section highlights the results from the capillary wicking experiments run to determine the contact angle of the leach solution on ore material.

5.5.1 Octane Results & Geometric Packing Factor

The profiles of weight^2 vs. time for the octane runs is shown in Figure 5.17. The octane used for the packed beds was n-Octane as manufactured by Acros Organics which had a purity of 97%. The profiles shown in Figure 5.17 are of the square value of the change in weight over time. When the experiment was running the load cell captured the weight of the entire structure (acrylic tube + support structure + particles in bed + suspension structure) with time. The weight of the structure did change over time with the ingress of fluid, however only the rate of uptake of fluid was needed for the application of Washburn's equation. For this reason the values of weight recorded by the load cells were subtracted by the baseline weight reading just before the fluid was introduced to the tube. This allowed for the normalization of the curves and as a result each gave a progression profile consisting solely of the rate of rise of fluid through the structure.

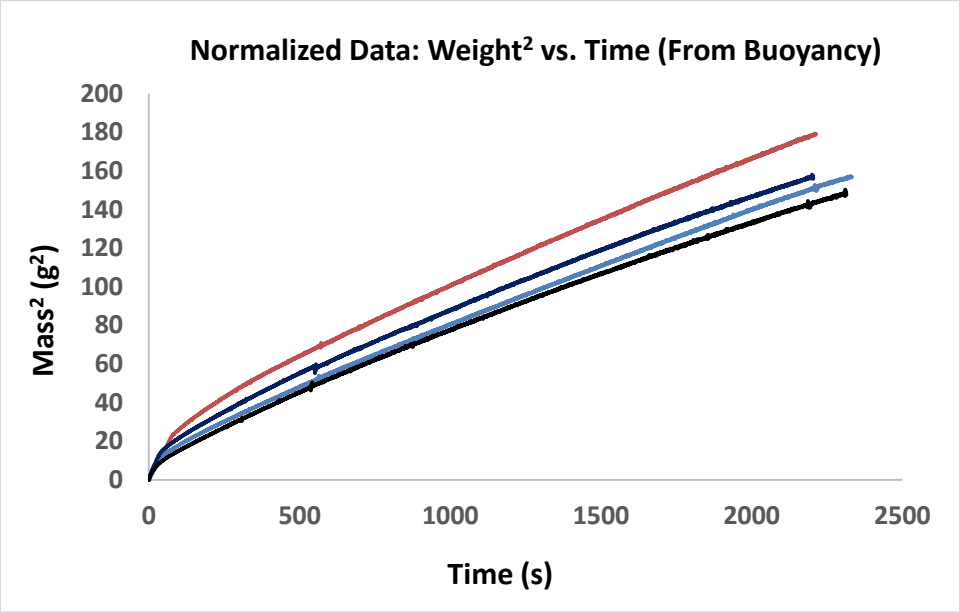

Figure 5.17 – Weight^2 vs. time for packed beds exposed to octane.

Each profile produced was analyzed by fitting a slope to each one. A regression analysis was also used to confirm the linearity of the slope value derived for each profile. It is important to note that for each profile, the slope values obtained were done so from approximately one-third of the way through the experiment to the point of completion. In the case of octane the experiment ran for approximately 2400s, so the slopes were calculated by fitting a line from 800 s onward. The initial part of the slopes were ignored as the fluid needed to diffuse through the cloth and cotton and filter paper at the bottom of the tube before reaching the particle bed. The latter two-thirds of the profile represented the rise of fluid through the particle bed. The values obtained were more representative of liquid in contact with the solid ore phases.

As discussed in section 5.2.3 from equation (6) the Washburn's equation is:

$$w^2 = \left(\epsilon.\pi^2.r_{eff}^4\right)\frac{\rho^2\gamma_L\cos(\theta)}{2\eta}t = \frac{C\rho^2\gamma_L\cos(\theta)}{\eta}t \qquad (6)$$

And where the slope value calculation is:

$$Slope = \frac{C\rho^2\gamma_L\cos(\theta)}{\eta} \qquad (7)$$

Where: C – packing factor; ρ – fluid density; η – fluid viscosity; γ – surface tension of fluid and cos(θ) – contact angle

For octane the fluid properties are:

Density (ρ) [g.cm^{-3}]	**Viscosity (η) [Pa.S]**	**Surface Tension (γ) [mN.m^{-1}]**	**Contact Angle (°)**
0.703	0.00054	0.0587	0

Table 5.3 – Fluid Properties of Octane. *Contact angle for octane is assumed to be 0 as it is considered completely wetting fluid. Values obtained from (Alghuniam et al., 2016).*

The slope value for each profile is summarized in Table 5.4. Based on equation (7) and the fluid properties for octane in Table 5.3, an associated packing factor was calculated for each slope. The average of these packing factors was determined and used for the calculations of contact angle for the other solutions.

	Load Cell 1	***Load Cell 2***	***Load Cell 3***	***Load Cell 4***	***Average***
Slope Values (g^2.s)	*0.06579*	*0.05876*	*0.0587*	*0.05496*	***0.03028***
Packing Factor (m^5)	*3.297E-15*	*2.944E-15*	*2.942E-15*	*2.754E-15*	***2.985E-15***

Table 5.4 – Determination of Packing Factor from Octane run.

5.5.2 Contact Angle Determination for Surfactant Solutions

5.5.2.1 Slope Determination

For the contact angle measurements the same procedure for gathering slope data as in the octane run was applied for the other solutions tested. The profiles of the weight^2 vs. time for all the other solutions generated needed to be normalized so that only the progression of the fluid was obtained. A sample of the fluid ingress profiles are shown below.

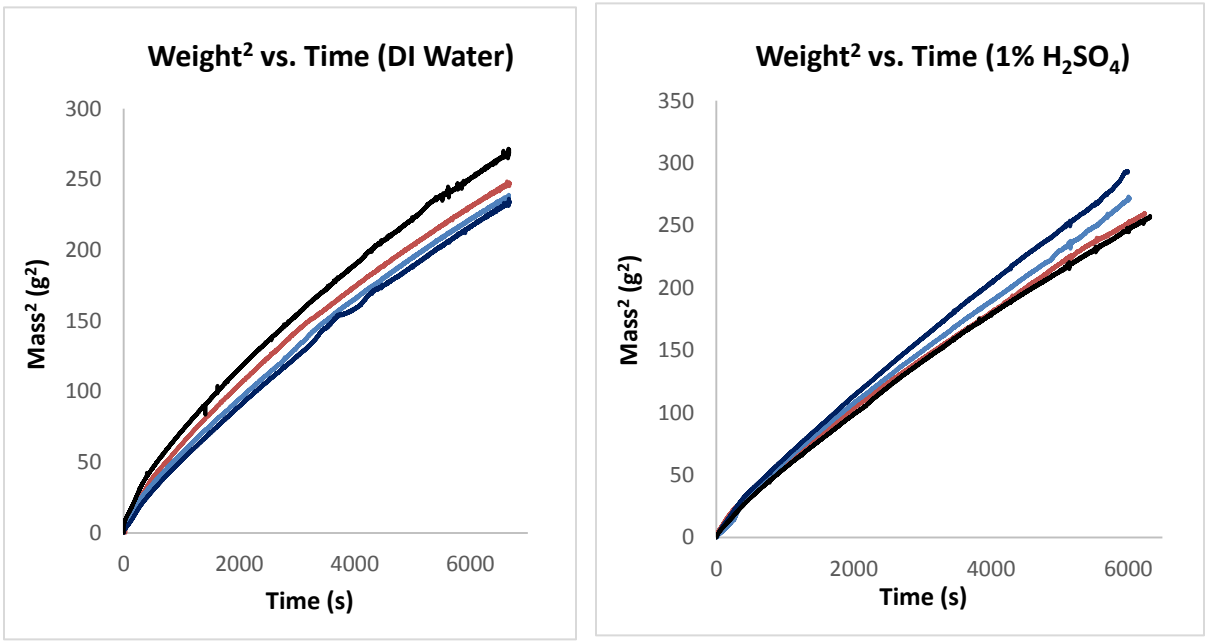

Figure 5.18 - Weight^2 vs. time for packed beds exposed to DI water and 1% H_2SO_4

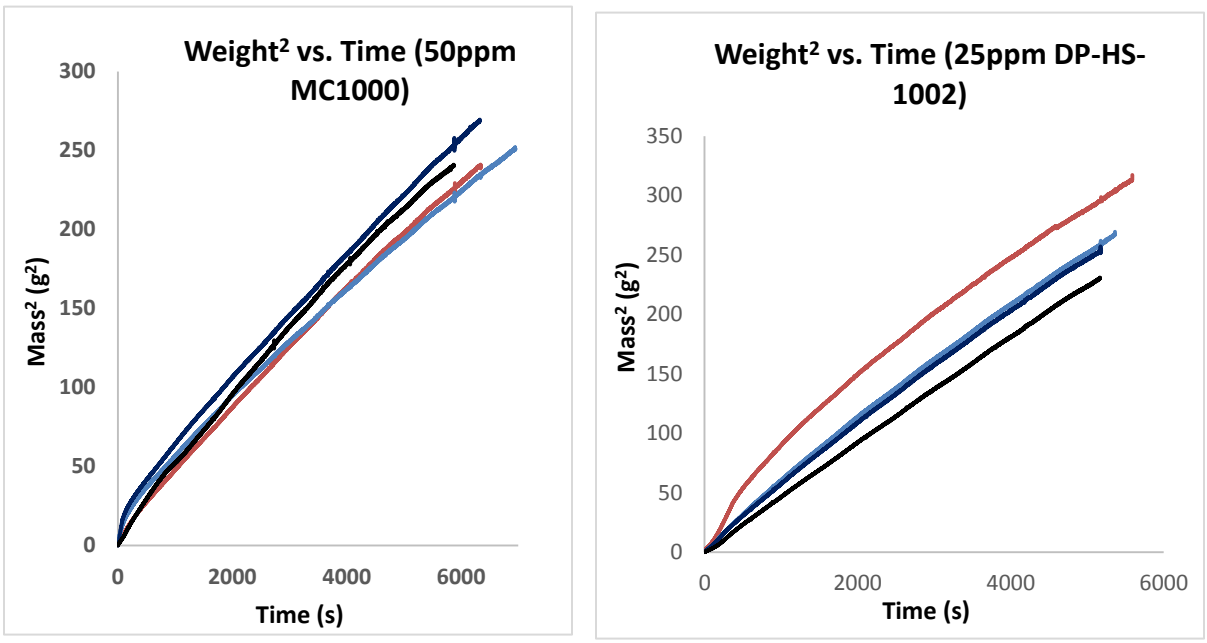

Figure 5.19 - Weight^2 vs. time for packed beds exposed to MC1000 at 50ppm and DP-HS-1002 at 25ppm

The values of weight^2 vs. time profiles for all the solutions tested are summarized in Figure 5.20 and Figure 5.21. In these graphs the data points represent an average slope value gleaned from the four individual weight^2 vs. time profiles for each respective solution. Each surfactant solution was tested on 4 individual packed beds that generated their own ingress profiles. An average profile for each solution was calculated. The error bars for each point represent the standard deviation associated with each data point. As with the octane run, the slope values calculated from each profile, for each surfactant solution, did not include data points from the initial one-third of the experiment.

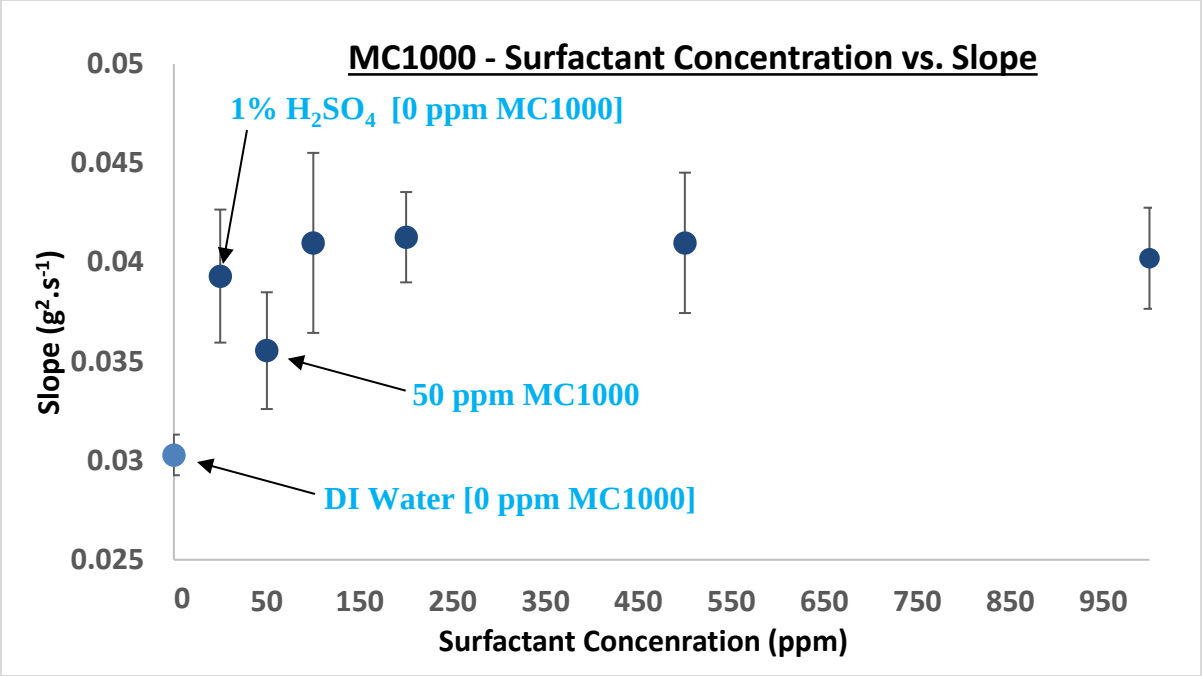

Figure 5.20 – Slope values vs. surfactant concentration for MC1000. *Each data point is average slope value from weight^2 vs. time profiles from the 4 individual runs performed for each solution. The error bars represent standard deviation associated with each average value calculated.*

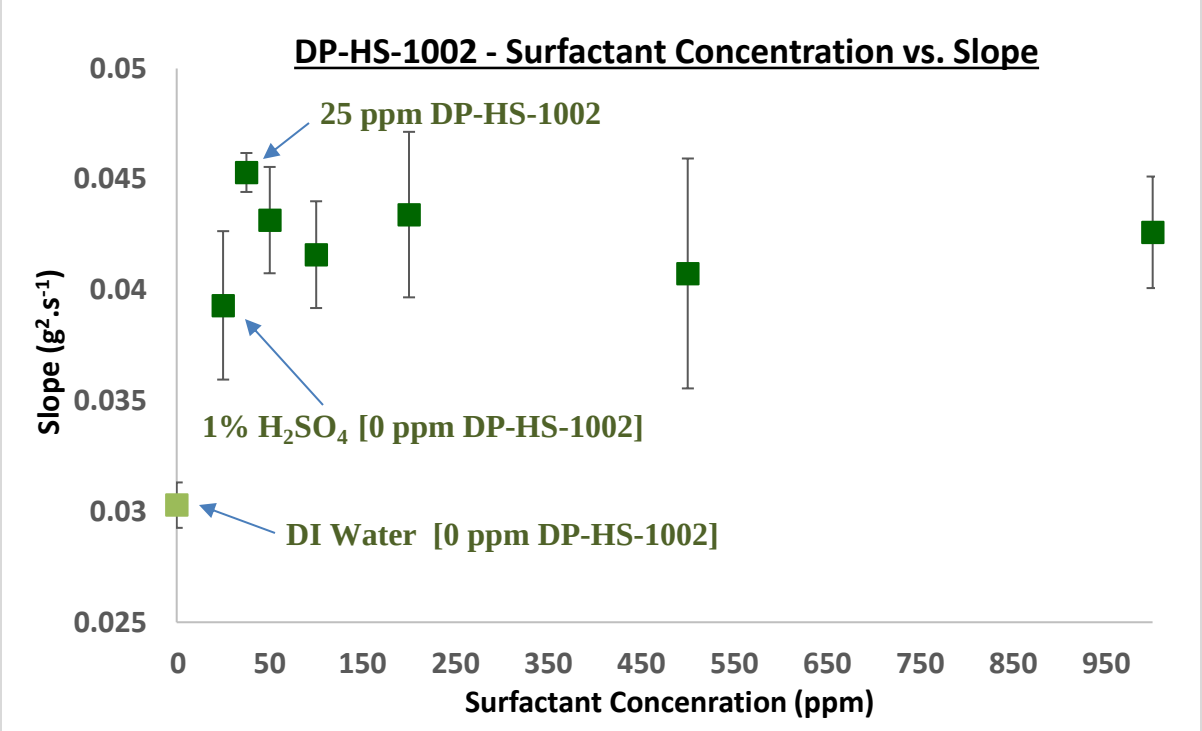

Figure 5.21 –Slope values vs. surfactant concentration for DP-HS-1002. *Each data point is average slope value from weight^2 vs. time profiles from the 4 individual runs performed for each solution. The error bars represent standard deviation associated with each average value calculated.*

The graph for MC1000 (Figure 5.20) the average slope value with just DI water is approximately 0.03 $g^2.s^{-1}$. The addition of sulfuric acid to DI water to create a 1% sulfuric acid solution increases the average slope value to approximately 0.039 $g^2.s^{-1}$. The first surfactant concentration tested in these experiments for MC1000 was the same working concentration as tested in the column leach experiments. At 50 ppm MC1000 in 1% sulfuric acid solution the average slope value drops from 0.039 $g^2.s^{-1}$ to about 0.035 $g^2.s^{-1}$. As the surfactant concentration is steadily increased to 100 ppm the average slope value rises again to approximately 0.041 $g^2.s^{-1}$. All subsequent additions of surfactant to the 1% sulfuric acid solution (i.e. MC1000 at 100ppm, 200ppm and 500ppm), have slope values that average at values close to 0.041 $g^2.s^{-1}$. The slope value for MC1000 at 1000 ppm is very close to the steady value coming in at just 0.04 $g^2.s^{-1}$.

For the graph of DP-HS-1002 (Figure 5.21) the initial average slope value with just DI water the same as with MC1000 at approximately 0.03 $g^2.s^{-1}$. Again, as with MC1000 the addition of sulfuric acid to DI water to create a 1% sulfuric acid solution increases the slope value to approximately 0.039 $g^2.s^{-1}$. The first surfactant concentration tested in these experiments for DP-HS-1002 was the same working concentration as tested in the column leach experiments. At 25 ppm DP-HS-1002 in 1% sulfuric acid solution, the average slope value rises once again from 0.039 $g^2.s^{-1}$ to about 0.045 $g^2.s^{-1}$. As the surfactant concentration is increased to 50 ppm and then to 100 ppm the average slope value steadily declines to approximately 0.042 $g^2.s^{-1}$. All subsequent additions of surfactant to the 1% sulfuric acid solution (i.e. DP-HS-1002 at 100ppm, 200ppm, 500ppm and 1000ppm), have slope values that hover about

this value. Unlike with MC1000 at the same concentrations, the values for DP-HS-1002 deviate to some degree about this value.

Overall, both MC1000 and DP-HS-1002 have effect on the rate of fluid ingress into the particle beds. The effect can be noted at the lowest concentrations tested. Additionally, for both surfactants, the rate of ingress is impacted beyond the minimum working concentrations. For both surfactants the rate of ingress is affected up to a concentration of 100ppm beyond which the extra addition of surfactant has no added benefit. Each data point on the graphs in Figure 5.20 and Figure 5.21 had its own variance. The effect of the variance associated with each data point and its impact on the results collected is further discussed in section 5.5.4. The change in uptake rate was not enough to completely classify the effect of surfactant. For this the contact angle needed to be calculated.

5.5.2.2 Contact Angle Calculations

From the compiled values of the slope for each surfactant concentration the contact angle could be calculated. Just as with the calculations in the octane section, equation (7) was used. The properties for fluid surface tension, viscosity, and density for the different solutions at the surfactant concentrations are shown in Table 5.5.

		Density [σ] ($g.cm^{-3}$)	*Viscosity [μ] ($N.s.m^{-2}$)*	*Surface Tension [γ_L] ($Pa.s = mN.m^{-1}$)*	*Packing Factor 'C' (m^5)*
DI Water (H_2O)		1	0.00089	72.5	2.985×10^{-15}
1% H_2SO_4		1.005	0.001019	71.35	
MC1000 diluted in 1% H_2SO_4	**50ppm**	1.005	0.00109	70.21	
	100ppm			69.42	
	200ppm			67.42	
	500ppm			63.31	
	1000ppm			57.55	
DP-HS-1002 diluted in 1% H_2SO_4	**25ppm**	1.005	0.001019	70.50	
	50ppm			69.31	
	100ppm			69.75	
	200ppm			69.00	
	500ppm			67.39	
	1000ppm			66.32	

Table 5.5 – Physical properties for the various solutions tested

The values of surface tension were the ones determined through the use of the interfacial tension measurements as highlighted in the previous chapter. The viscosity and density values for the solutions containing surfactant were considered to be the same as that of 1% sulfuric acid solution. The reason for this is because the volume fraction of the surfactant was very low in comparison to the acid solution matrix it was held in. The value of the packing factor as calculated in the previous section was assumed to be the same for all the capillary wicking experiments. The solids preparation method was the same of all the experiments as per the requirement for the Washburn equation to apply.

The calculation for the contact angle required the use of equation (7). Since all other variables in the equation were identifiable quantities, the equation was re-arranged to solve

for, θ. The method to obtain the contact angle for each surfactant concentration was as follows:

- For each solution type tested, the weight^2 vs. time profiles were compiled into a single graph.
- The slope values for each of the four profiles was identified.
- The contact angle relating to each slope was calculated.
- The average of the four newly calculated angles was determined for each solution type. This average was then considered the contact angle for that particular solution with the ore.

The values of the slopes for each solution and their related contact angles are summarized in Table 5.6. The values show the average values for the slope vs. surfactant concentration as well as their related contact angles. The table also summarizes the standard deviation for each one.

		Slope Values		*Contact Angle Values*	
		Average Slope Value ($g^2.s^{-1}$)	**Std. Deviation ($g^2.s^{-1}$)**	**Average Contact Angle Value (°)**	**Std. Deviation (°)**
DI Water (H_2O)		0.03029	0.001025	82.84	0.2435
1% H_2SO_4		0.03930	0.003354	79.27	0.9272
MC1000 diluted in 1% H_2SO_4	**0ppm**	0.03555	0.002945	80.15	0.8240
	100ppm	0.04098	0.004537	78.49	1.291
	200ppm	0.04127	0.002279	78.06	0.6686
	500ppm	0.04098	0.003540	77.36	1.108
	1000ppm	0.04021	0.002551	76.34	0.8835
DP-HS-1002 diluted in 1% H_2SO_4	**25ppm**	0.04531	0.0008804	77.45	0.2477
	50ppm	0.04316	0.002404	77.85	0.6865
	100ppm	0.04160	0.002410	78.37	0.6830
	200ppm	0.04340	0.003737	77.72	1.075
	500ppm	0.04075	0.005192	78.20	1.525
	1000ppm	0.0426	0.002518	77.46	0.7530

Table 5.6 – Contact Angle measurements for each solution type tested.

The contact angle as function of solution type and increasing surfactant concentrations for both MC1000 and DP-HS-1002 are depicted in Figure 5.22 and Figure 5.23, respectively.

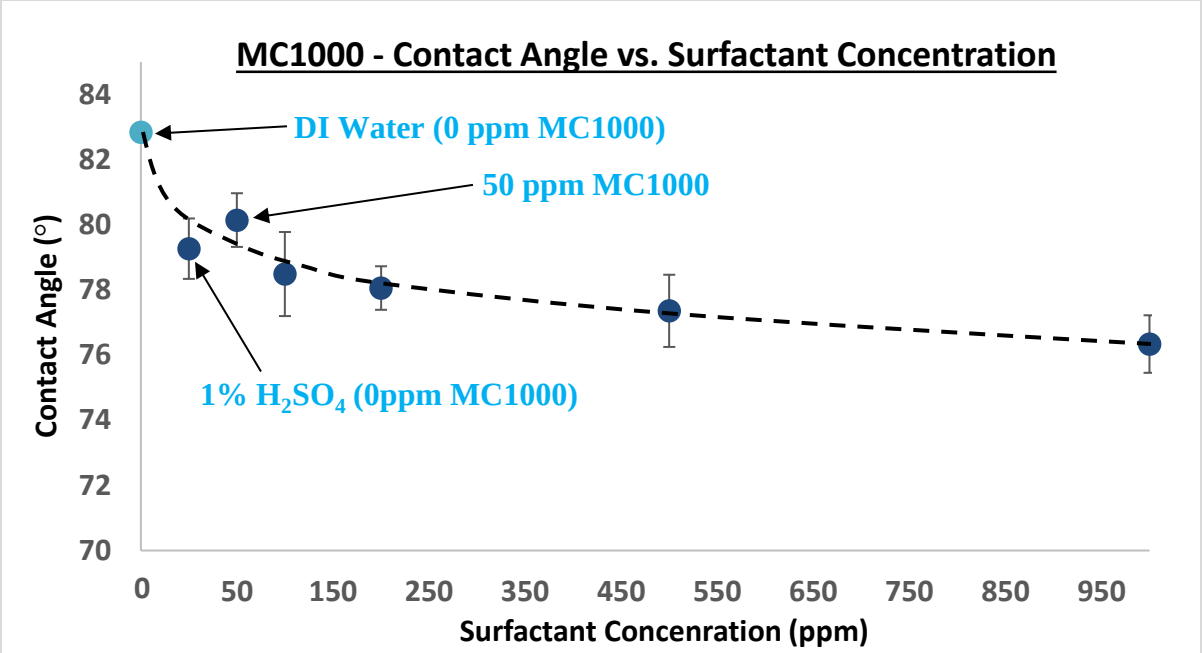

Figure 5.22 - Contact angle vs. surfactant concentration for MC1000. *Each data point is an average contact angle value. For each surfactant concentration, a contact angle was calculated for each of the 4 slopes obtained from each experimental run. The average was then calculated from this.*

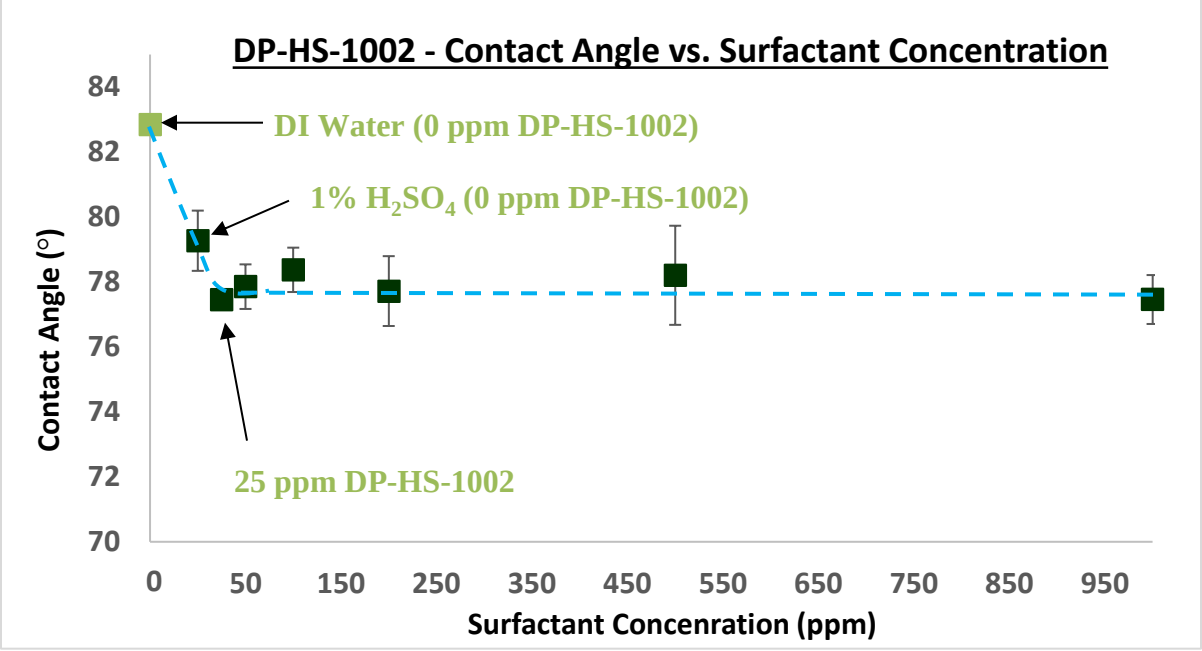

Figure 5.23 –.Contact angle vs. surfactant concentration for DP-HS-1002. *Each data point is an average contact angle value. For each surfactant concentration, a contact angle was calculated for each of the 4 slopes obtained from each experimental run. The average was then calculated from this*

For MC1000, Figure 5.22 shows the final calculated contact angles as a function of surfactant the concentration. With just DI water, the contact angle is approximately 83°. With the addition of sulfuric acid to DI water to create a 1% sulfuric acid solution, the contact angle drops to roughly 79°. From 0 ppm surfactant concentration to 50 ppm MC1000 in 1% sulfuric acid solution, the contact angle rises slightly from 79° to about 80°. This drop in contact angle value correlates with Figure 5.20, as the value of the slope dropped in this same concentration range. However, as the surfactant concentration is steadily increased beyond 50 ppm, from 100 ppm to 1000 ppm the contact continues to subsequently decrease each time. In Figure 5.20 the slope value remains constant in this range of concentration. The decreasing trend stems from the decrease in surface tension as noted in the previous chapter (see Figure 4.13 [page 87]). The solutions loaded with increasing concentrations of MC1000 decrease more drastically (as compared to DP-HS-1002). With all factors being equal the drop in contact angle seems to be due to the drop in surface tension.

For DP-HS-1002, the contact angle as function of surfactant concentration is depicted in Figure 5.23. The overall trend obtained differs from that of MC1000. Starting with just DI water the contact value obtained was 83°. The addition of sulfuric acid to DI water to create a 1% sulfuric acid solution, results in the contact angle dropping to roughly 79°. At 25 ppm DP-HS-1002 in 1% sulfuric acid solution, the contact angle drops further to approximately 77.5°. As with MC1000, this trend correlates to the slope values seen in Figure 5.21 as the slope increases in these concentration ranges. Beyond this, the subsequent additions of DP-HS-1002 into the sulfuric acid solution, from 50 ppm to 1000 ppm, show no increase or decrease in contact angle. The values obtained for these particular concentrations hover at

just around 77.5°. The reason for this seems to be due to the relatively small changes observed in solution surface tension from 25ppm onwards (see Figure 4.14 [page 87]), as well as the average slope values shown in Figure 5.21. Essentially beyond 25 ppm the fluid properties at all the higher concentrations are virtually the same. This indicates that the biggest change in contact angle is observable at 25 ppm and greater surfactant concentrations yield no further reductions in contact angle.

5.5.3 Solid Phase Analysis

The contact angle measurements were derived from the rate at which a solution ingressed through a bed of particles. The bed of particles was composed from the same type of ore as used in the column leaching experiments in chapter 2. The rate of permeation of the solutions depends on several factors including the degree of attraction between the mobile liquid and the particles in the bed. The rate of rise of the fluid allows for the degree of attraction to be calculated via the contact angle.

The aim of the capillary wicking experiments was to gain a more substantive value for the contact angle, by maximizing the contact between the leach liquid with the different phases inherently present in the ore. Because of this an analysis of the particles in the packed beds was undertaken to gain a better understanding of the composition of the solid phases. The contact angles calculated in the previous section provided overarching values that corresponded to sulfuric acid solution(s) on ore as a whole. The aim of the solid phase analysis was to more concisely ascribe the contact angles, as a whole, to the specific components that constituted the ore that the liquid phase was tested on.

5.5.3.1 Particle Size Verification

The particle size verification was performed as means to determine the particle size distribution in the packed beds. Section 5.3.1.3 detailed the procedure used to reduce the sample from the bulk aggregate down to smaller test charges. Section 5.3.2.2 detailed the procedure used to further reduce the test charges to mass sizes that would allow the particles to be packed in the tubes. While the splitting of the samples was performed in a way to be representative of the larger bulk from which it was derived, confirming that this was the case could be achieved with a size analysis.

For size verification a Ro-Tap machine was used. As highlighted in section 5.3.1.2 the Ro-Tap machine works by inducing vibratory mechanical action on a set of screens in which resides the material being segregated. A set of screens in descending order of size is used and material is sized according to the width of the mesh of screen which it is not able to pass through within the stack.

For the size verification used in this section of the work 2 samples from the bulk material split in section 5.3.1.3. The original bulk aggregate sample was about 2.8kg and this was systematically reduced in size to 16 individual samples of approximately 180g each. Of the 16 samples, 14 were used in the capillary wicking test work. The remaining 2 samples were run through a Ro-Tap machine to compare the particle size distribution in each one.

The screens used for the sizing of the samples were:

Screen Size	*Mesh Opening*	Sample 1	Sample 2
140 Mesh	106µm	✓	✓
200 Mesh	75µm	✓	✓
270 Mesh	53µm	✓	✓
325 Mesh	45µm	✓	✓
400 Mesh	38µm		✓
450 Mesh	32µm	✓	
500 Mesh	25µm	✓	✓

Table 5.7 – Screen used for sample sizing.

The following procedure was employed and used for the Ro-Tap and size segregation of the sample:

- The required screen were gathered for each sample. The screens were cleaned prior to use. The sieves were stacked in descending order of size (screens with biggest mesh openings at the top and smallest at the bottom).
- The separation of the sample was performed as follows:
  - I. The test charge was weighed prior to being fed into the stack. Once the weight was recorded the material was fed into the top-most stack.
  - II. The stack was placed in the Ro-Tap and machine was set to run for 15 minutes.
  - III. After 3 runs at 15 minutes each time, the machine was stopped and separated masses extracted.

- Once completed, the collection of the samples went as follows:
  - I. Each sieve was carefully extracted from the stack.

II. On a large sheet, the sieve was turned upside down. The sieve was tapped around the edges and a brush was run on the underside of the sieve to loosen stuck particles from the mesh openings.

III. The extracted mass from each sieve was weighed and recorded.

The results from the separation of the sample in the Ro-Tap are as follows:

Sample 1

Mesh Size (Tyler Number)	*Equivalent Mesh Size (µm)*	*Mass Retained (g)*	*Percent Retained (%)*	*Cumulative Percent Passing (%)*
(+)140	+ 106µm	3.48	1.97%	98.03%
-140,+200	-106µm + 75µm	41.83	23.68%	74.35%
-200,+270	-75µm + 53µm	31.25	17.69%	56.66%
-270,+325	-53µm + 45µm	15.78	8.93%	47.73%
-325,+450	-45µm + 32µm	74.8	42.34%	5.39%
-450,+500	-32µm + 25µm	7.29	4.13%	1.26%
-500	-25µm	2.23	1.26%	0.00%
	Total Mass :	176.66		

Table 5.8 – Particle Size Distribution from first sample analyzed.

Sample 2

Mesh Size (Tyler Number)	*Equivalent Mesh Size (µm)*	*Mass Retained (g)*	*Percent Retained (%)*	*Cumulative Percent Passing (%)*
(+)140	+ 106µm	5.38	2.952%	97.048%
-140,+200	-106µm + 75µm	43.45	23.841%	73.207%
-200,+270	-75µm + 53µm	33.69	18.486%	54.722%
-270,+325	-53µm + 45µm	16.77	9.202%	45.520%
-325,+400	-45µm + 38µm	22.47	12.329%	33.191%
-400,+500	-38µm + 25µm	57.43	31.512%	1.679%
-500	-25µm	3.06	1.679%	0.000%
	Total Mass :	182.25		

Table 5.9 - Particle Size Distribution from second sample analyzed.

Particles are sized according to the mesh openings on the screen they cannot pass through. For example, any particles unable to pass through the 140 mesh screen are considered larger than 106µm. Particles that pass through the 140 mesh screen but cannot pass through the 200 mesh screen, are considered to be smaller than 106 µm but larger than 75 µm. This sizing is applied for all the particles as they go down the stacks. The finest material collected in the bottom collection pan is simply considered smaller than the mesh opening of the finest screen.

The particle size distribution as well as the cumulative size distribution is shown in Figure 5.24 and Figure 5.25. This allowed for a comparison of the particle sizes in each fraction.

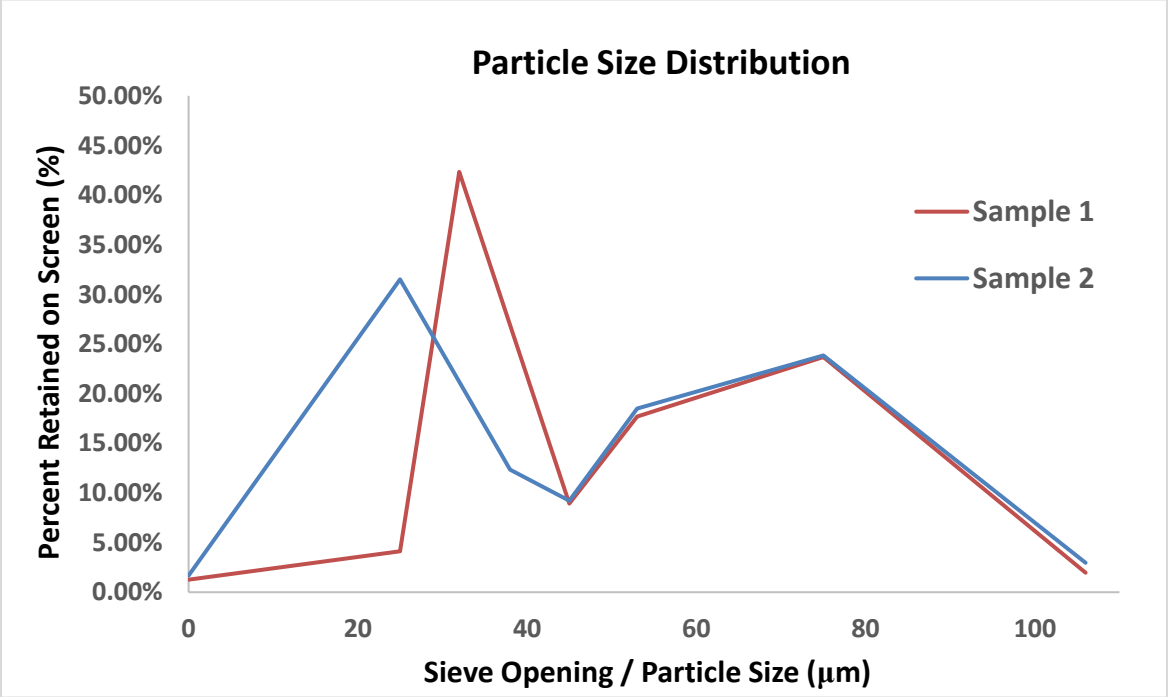

Figure 5.24 - Particle size distribution for samples run through Ro-Tap. *The particle size distribution was determined for the 2 samples. The distribution was determined by dividing the mass retained in each sieve by the overall mass fed into the stack. This gave a value of percent retained.*

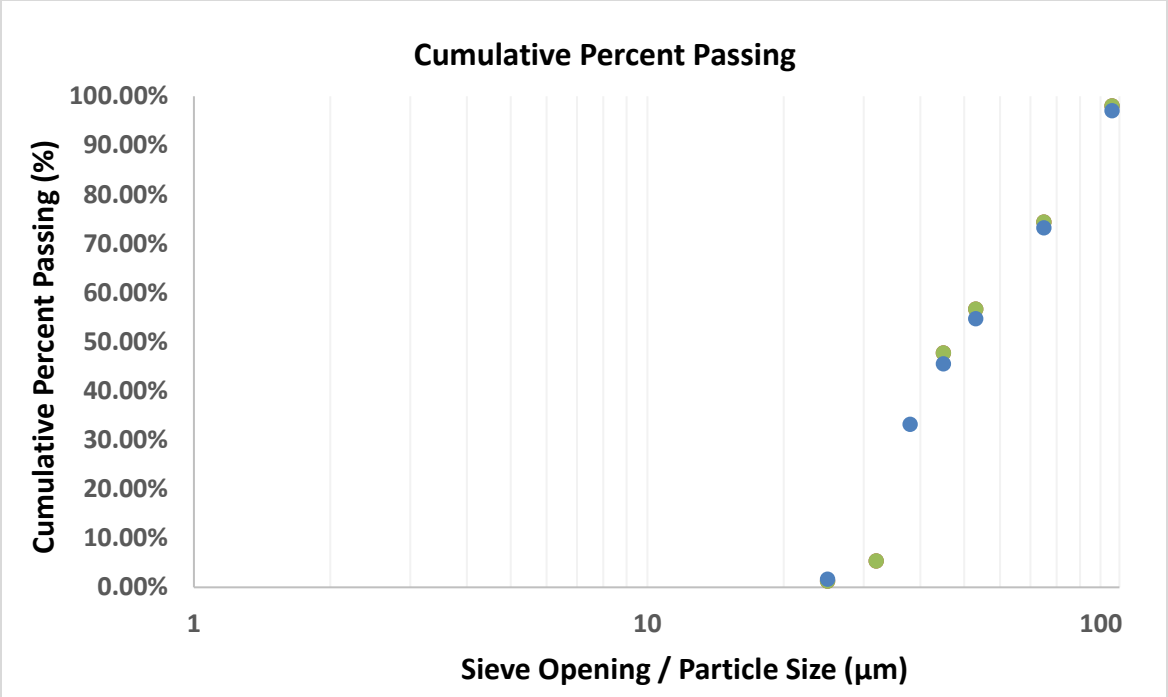

Figure 5.25 – Cumulative particle size distribution for samples run through Ro-Tap. *The cumulative particle size distribution was determined for the 2 samples. For this the percent retained is cumulatively totaled for the screens going from smallest to largest.*

From Figure 5.24 and Figure 5.25 it can be seen that the 2 samples have a slightly varied particle size distribution. The graph in Figure 5.24 shows the distribution of the particles in terms of the amount retained in each sieve as a percentage of the mass fed into the stack. For both samples the particle size shows a bi-modal distribution. The general trend noted in Figure 5.24 was that at the higher particle sizes (roughly greater than 45µm), the two samples had the same distribution. In this region for the, for both samples, the peak occurs at 75µm. Where the samples differed in particle size distribution was in the region of very material (in the area below 45µm). For the first sample its peak in this region occurred at roughly 32µm. For the second sample, its peak occurred at roughly 25µm.

The cumulative size distribution curve Figure 5.25 had been calculated for the 2 samples as well. This was determined by sequentially summing the percent retained values for each sieve. In this graph the cumulative percent passing was plotted as a function of sieve size. This meant that a given sieve size (for example 45 μm), the data point represented the total mass smaller than that (i.e. the mass retained on the 25 μm and 32/38 μm sieves). This was done sequentially for all the sieves. From this data it can be seen that for both the sample sets the P_{80} for the sample was approximately 80μm. The P_{80} (passing 80% value) values essentially shows that 80% of the particles were smaller than this value. This finding indicated that the overall particle size distribution was within an acceptable range for the capillary wicking experiments.

The variance in the particle size distribution for the 2 samples indicates that the dissemination of the fines in the bulk aggregate was not the same. For example, at 25μm the percent retained in the sieve for sample 1 was 4% of the total mass, whereas for sample 2 in the same sieve the mass retained was 31.5% of the total. Examining the next sieve in the series, for sample 1 the mass retained at 32μm the mass retained 42.3% of the total mass, where for sample 2 it was 12.3% of the total.

The procedure used to split the sample was the ASTM standard which was designed to create sub-samples which were representative of the bulk aggregate sample. In a bulk aggregate sample the distribution of these particles cannot be predicted, and as such during a riffle the possibility of having a concentrate of certain particles is possible. (ASTM, 2011). While the difference in particle size distribution is not vastly different, the existence of a difference and

its implications are discussed in further detail in the ‘Discussion’ section of this chapter (section 5.5.4).

5.5.3.2 Phase Analysis

The phase analysis sought to identify the mineral phases present in the packed beds. The phase identification and verification was performed by the, Electron Microbeam & X-Ray Diffraction Facility at the University of British Columbia’s department for Earth, Ocean and Atmospheric Sciences.

Sample Preparation

In order to identify the samples in the packed powder bed experiments samples needed to be prepared for analysis. For this 5 samples were prepared based on the particle size distribution as highlighted in the previous section.

For both samples passed through the Ro-Tap machine in the previous section, each separated sample was stored separately. For the phase identification the separated ore from the second sample, mentioned in the previous section, was the one used.

Due to the large number of phases in each size fraction, the separated samples were riffled down to appropriate sizes for testing. This ensured the samples sent in were randomized. Based on this the samples were apportioned as follows:

Mesh Size (Tyler Number)	Equivalent Mesh Size (µm)	Original Mass Retained (g)	Post Riffle Mass (g)		Final Sample Masses (g)
(+)140	+ 106µm	5.38	1.6	} ⇨	4.9
-140,+200	-106µm + 75µm	43.45	3.3		
-200,+270	-75µm + 53µm	33.69	4.4	*{Fractions Combined}*	4.4
-270,+325	-53µm + 45µm	16.77	4.3		4.3
-325,+400	-45µm + 38µm	22.47	5.6		5.6
-400,+500	-38µm + 25µm	57.43	3.7	} ⇨	5.3
-500	-25µm	3.06	1.6		

Table 5.10 – Sample preparation metrics of phase analysis by XRD. *Samples separated in the size verification step of the previous samples were stored separately. The samples were subsequently split using a micro-riffle down to the final masses shown in the table. These samples were sent for analysis.*

The +140 mesh and -500 mesh samples were very small compared to the rest of the sample at hand. For this reason they were combined with the (-140,+200) mesh and (-400, +500) mesh samples respectively. The individual samples were riffled (and recombined where necessary) until they were approximately 5 g in mass.

Analysis Method

The analysis method for analyzing the samples was provided by the facility who performed the analysis (Raudsepp, Pani, Czech, & Lai, 2017). The method for analyzing the samples was as follows:

- The samples were reduced into fine powder (<10µm). This the optimum grain-size range for X-ray analysis.
- Grinding was done under ethanol in a vibratory McCrone Micronising Mill for 10 minutes.

- Analysis machine used was a Bruker D8 Advance Bragg-Brentano diffractometer equipped with an Fe monochromator foil, 0.6 mm (0.3°) divergence slit, incident- and diffracted-beam Soller slits and a LynxEye-XE detector.
- Step-scan X-ray powder-diffraction data was collected over a range of 3-80°2θ with CoKa radiation.
- The long fine-focus Co X-ray tube was operated at 35 kV and 40 mA, using a take-off angle of 6°.

- The X-ray diffractograms were analyzed using the International Centre for Diffraction Database PDF-4 and Search-Match software by Bruker.
- X-ray powder-diffraction data of the samples were refined with Rietveld program Topas 4.2 (Bruker AXS).

Phases Detected

The results from the diffractometry and Reitveld analysis are as follows:

Mineral	***Ideal Formula***	***+200 mesh***	***-200, +270 mesh***	***-270, +325 mesh***	***-325, +400 mesh***	***-400 mesh***
Actinolite	$Ca_2(Mg,Fe^{2+})_5Si_8O_{22}(OH)_2$	6.9	8.6	10.2	10.0	8.7
Albite low	$NaAlSi_3O_8$	39.5	36.3	34.9	34.2	35.3
Biotite 1M	$K(Mg,Fe)_3AlSi_3O_{10}(OH)_2$	1.4	1.8	2.2	2.3	1.8
Clinochlore	$(Mg,Fe^{2+})_5Al(Si_3Al)O_{10}(OH)_8$	3.6	5.1	5.8	6.7	8.0
Illite/Muscovite 1M	$K_{0.65}Al_{2.0}Al_{0.65}Si_{3.35}O_{10}(OH)_2$	2.6	2.4	2.4	2.9	3.1
Illite/Muscovite 2M1	$K_{0.65}Al_{2.0}Al_{0.65}Si_{3.35}O_{10}(OH)_2$	3.2	3.4	4.0	4.7	5.0
Microcline intermediate	$KAlSi_3O_8$	11.1	10.7	10.7	10.3	10.0
Orthoclase	$KAlSi_3O_8$	13.7	13.0	12.5	12.4	12.5
Quartz	SiO_2	18.1	18.6	17.3	16.5	15.5
Siderite	$FeCO_3$					0.2
	Total:	***100.0***	***100.0***	***100.0***	***100.0***	***100.0***

Table 5.11 – Phases identified in test charges used for capillary wicking experiments

The results of the XRD and Reitveld analyses applied show that in the 5 size fractions of ore that constitute the material for the packed beds, the phases shown in Table 5.11 were present in all of them except siderite which was only present in low concentrations at the smallest size fraction.

From the results there is also a general trend noted. Minerals, such as quartz or albite, which can be considered hard minerals occur in higher concentrations in the size fractions with the larger particles. As the size fraction decreases the occurrence of these minerals also reduces. On the other hand softer clay like minerals, such as illite or clinocore, are at lower concentrations at the larger particle sizes and at higher concentrations within the lower particle sizes.

The reason for this could be attributed to the relative hardness of the minerals and their amenability to grinding. Harder minerals would typically longer attrition times and/or greater force to reduce the size drastically. This would mean that they would mean they exist at higher concentrations in larger particle sizes as they are more resistant to size reduction. Conversely, softer clay like minerals would likely be more present at lower concentrations. Their amenability to grinding means less effort is required for overall size reduction.

5.5.4 Discussion

From the contact angle profiles in Figure 5.22 and Figure 5.23, it can be seen that the presence of surfactant had an impact on the overall interaction between the acidic medium and the solid phases of the ore. The contact angle vs. concentration graphs for the two surfactants showed different profile shapes, indicating that the surfactants altered the interaction with the solid and liquid in different ways. For MC1000, from no surfactant to 50 ppm in solution, there was an increase in the contact angle, from 79° to 80°. Subsequent increases in surfactant concentrations responded with decreases in contact angle. For DP-HS-1002, from no surfactant to 25 ppm in solution, there was a decrease in the contact angle

from 79° to 77.5°. Beyond that subsequent increases in the surfactant concentrations did not yield further decreases in the contact angle. This is corresponded with data in experiments performed by BASF, wherein DP-HS-1002 was tested at both 25 ppm and 50 ppm in heap leach columns. 50 ppm solution was not tested further as no benefits were seen in copper extractions at concentrations greater than 25ppm. This results yielded significant findings as it showed that the presence of surfactants affected the interaction between the solid and the solid liquid.

A limitation encountered in this experiment was the variability in the experimental data collected. Each calculated data point in Figure 5.22 and Figure 5.23 was an average of 4 packed beds being run concurrently. For each solution type the rate of ingress for each packed bed needed to be determined (the results of which are in Figure 5.20 and Figure 5.21) and from which the final contact value could be measured. The variability for each data point can be attributed to the particle make-up used in each packed bed.

This is best exemplified by Figure 5.24. The particle size distribution for 2 unused test charges showed that the particle size distribution in each varied. For all the experiments run in this chapter the source of all the material came from a bulk aggregate mixture. To split the sample an ASTM procedure was adopted to ensure that samples separated from the bulk aggregate had minimal characteristic variations from the bulk. The same splitting procedure was used all the way down to samples being prepared for the individual packed beds. However, Figure 5.24 shows that the there was still a variation in the particle size distribution. It is important to note that the samples analyzed in Figure 5.24 were test charges

which would have otherwise been split into a further four samples for individual packed beds. It serves to illustrate that the samples used for the packed beds likely had some variation with respect to the particle size distribution. This variation was also likely present when the samples were split for the individual packed beds.

This variation meant that the each packed bed likely had a slightly different particle make-up and hence the geometric factor in each bed was slightly different. This would have affected the rate of fluid uptake as the particles directly affect the space which fluid can occupy as well as the shape of the channels through which it flows. For example, a bed with a higher occurrence of fine particles may have a reduced volume which fluid can occupy. This in turn could have meant that the effective radius of the capillaries was smaller and therefore the overall uptake was perceived to be faster. The opposite would be the case in a bed with the occurrence of particles was on the larger side. For this reason, multiple beds with the same fluid was used and an average determined. In Figure 5.22 and Figure 5.23 each contact angle was an average value calculated from the four packed beds of each experiment. The error bars on each data point represented the associated standard deviation for each solution condition.

However, even within the same surfactant, no two data points had the same standard deviation. Each standard deviation was unique to the solution concentration that was being tested. One reason for this, as discussed, was the variation of the in the particle size distribution. However, in addition to this the shape of the particles in the packed beds could have an impact on the geometric factor.

In addition to a large number of particle sizes being used in the experiments, a large number of phases were also present in the mixture as determined by XRD and Rietveld analyses in Table 5.11. In order to better understand how the shape factor could affect the packed beds, the powdered grains were examined under an SEM. (See Figure 5.26, Figure 5.27, and Figure 5.28).

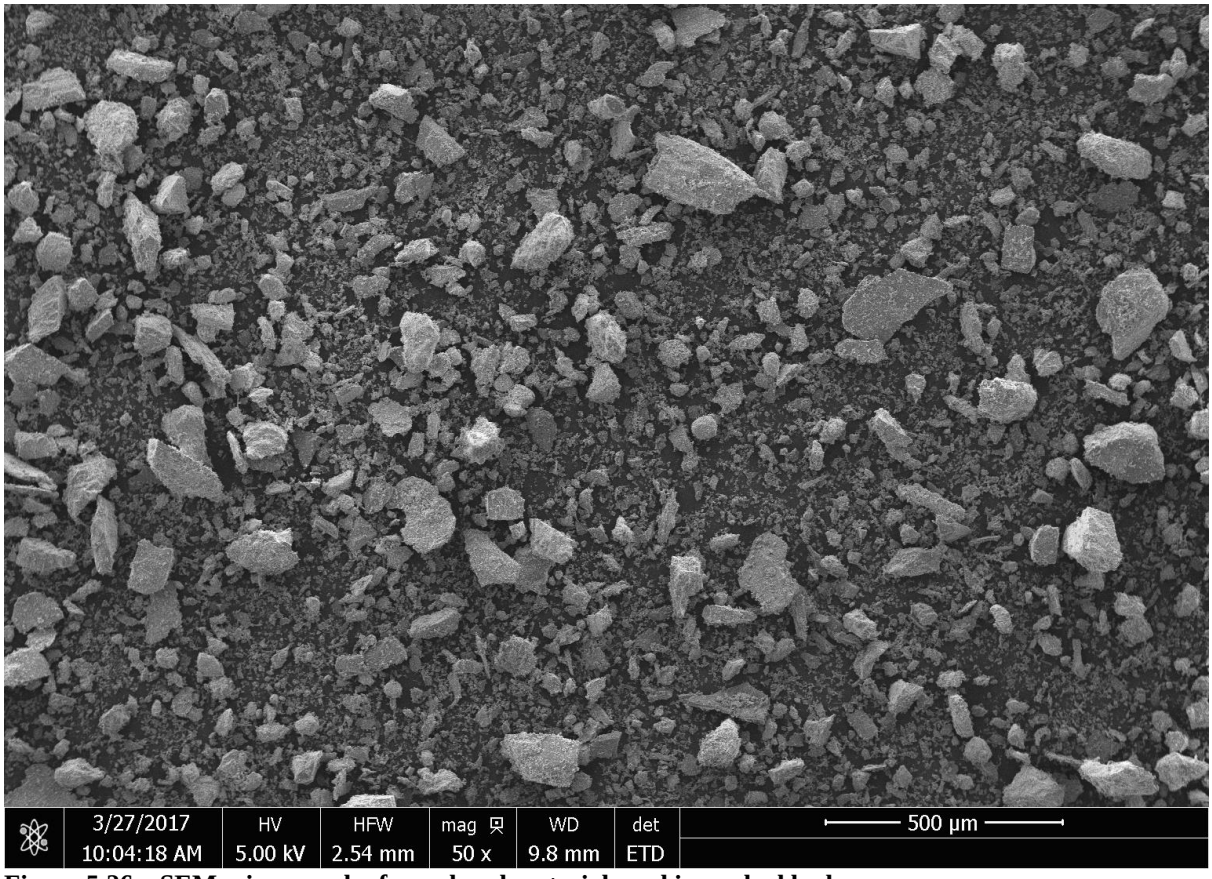

Figure 5.26 – SEM micrograph of powdered material used in packed beds.

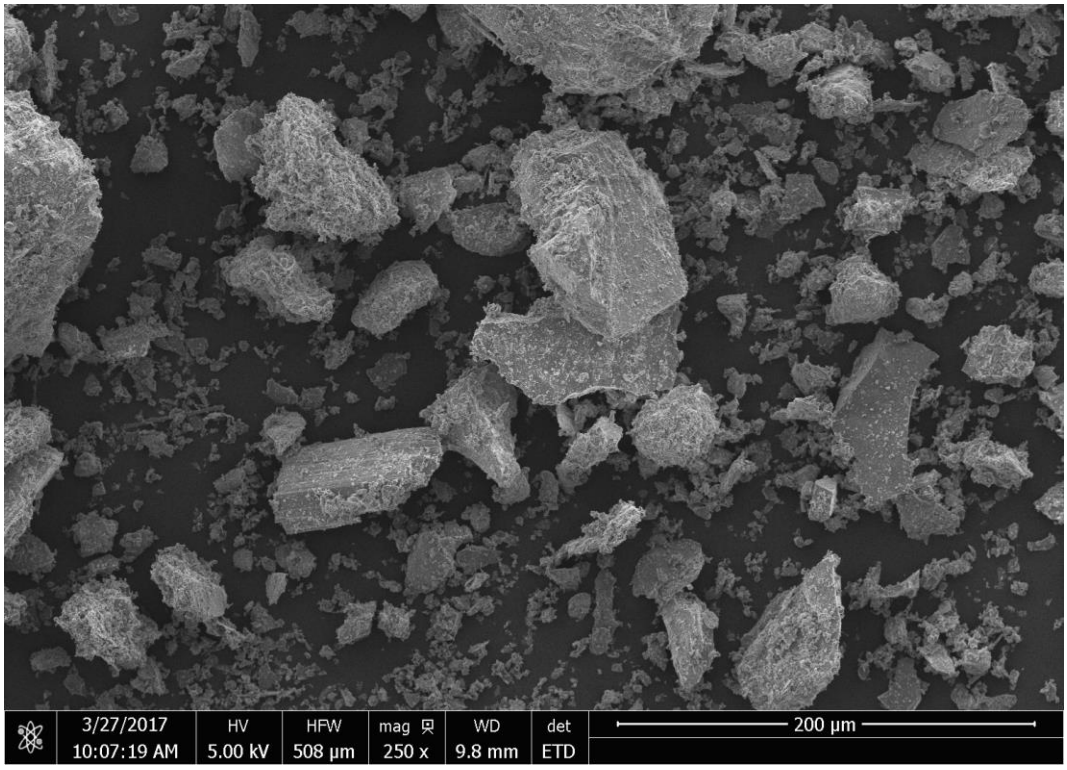

Figure 5.27 - SEM micrograph of powdered material used in packed beds.

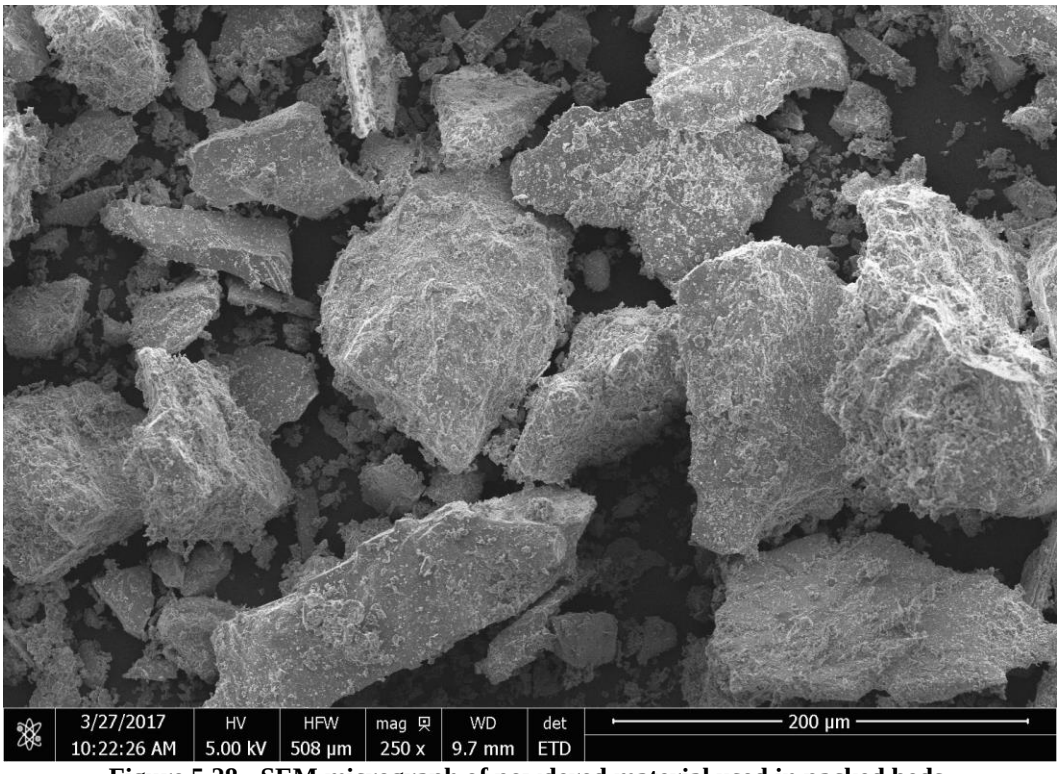

Figure 5.28 - SEM micrograph of powdered material used in packed beds.

The ore used in these experiments was ground down to a fine size range. This allowed for the liberation of the various mineral grains in the ore. When packed into the bed the mobile fluid can more freely contact these particles. However, as seen in Figure 5.26, Figure 5.27, and Figure 5.28, the minerals in ground form all have different shapes. Mineral particles inherently have different shapes as part of their physical structure. This relates to their crystal lattice structure, which affects their physical shape. This can change the overall geometry of the available space in a bed when the particles are packed together. This also has an effect on the effective radius of the capillaries through which the fluid rises.

This is a limitation encountered when attempting to perform this type of experimental work when using ores as the solid phase. A possible method to overcome this is to use particles of the same size but this doesn't entirely eliminate the variation encountered. When sizing particles a Ro-Tap is used and as a measure to control size, the particles on only one sieve can be used. The issue with this is that the particles will still rarely be one size. They will be in a size range where they are smaller than the preceding sieve but larger than the one they sit on. Added to that is the fact that the particles will also have different shapes. This still means that the size of the geometric factor will have a variation from packed bed to packed bed.

Overall performing contact angle measurements using capillary wicking can provide a useful way to measure the affinity between the liquid and solid phases. This is especially so for ores whose mineralogical make-up can include many different phases. Capillary wicking provides a useful method of obtaining a representative value by ensuring complete contact between the fluid and all the phases available. However, the limitation is that there will be a variance

in the data collected. This means there is a trade-off between precision and representativity. While precision is desired to demonstrate repeatability – there is a strong dependence on the geometric factor to be as uniform as possible. Despite the same preparation method there is no guarantee of the same geometric factor each time the experiment is performed. The best, and possibly only way to overcome this, is to run several experiments under the same conditions and reduce statistical error.

Chapter 6: Conclusion

6.1 Experimental Findings

The focus of this thesis was to explore the use of surfactants in heap leaching systems and better understand their role and functionality within the system. Heap leaching systems tend to suffer from long leach times and variable recoveries owing to the nature of they are operated. Decreased leaching periods and/or improved recoveries are much desired to increase the profitability of such operations. Surfactants have been considered a viable option through which the leachability of ore can be increased. They operate by altering the surface tension of a fluid that is contact with a secondary phase. Surfactants have been explored as agents to improve wetting in heaps and increase the yield of copper overall. However their function in heaps is not well understood and their use is not applied commercially. The work in this thesis was based on work performed by BASF on increasing leachability of ores using surfactants (Bender et al., 2016). The surfactants used in this thesis were also developed by BASF whose very purpose is for use in the heap leaching industry. The surfactants used were: MC1000 and DP-HS-1002.

The first set of experiments to understand the role of surfactants in the heap leach process was to run simulated heap leaches at a lab scale. This entailed loading ore into a column and pumping acidic media through it. Two columns used acid solution with surfactant loaded into it and one column was a control in which no surfactant was added. The columns run in this experiment were performed as flooded vats wherein all particles in the column were submerged in leach fluid. A limitation commonly encountered in heap leaches (in both

industrial heaps and column simulations) is limited wetting. While heaps are optimized for ensuring near complete permeation of leaching fluid, various factors prevent this from being fully achieved. This has an effect of limiting the mass transport of aqueous species to and from the ore particles and prevents complete leaching from occurring. The aim of completely immersing the ore particles in the acidic solution, was to ensure no complications from limited wetting occurred and to more completely and confidently attribute changes in extraction solely to the presence of surfactants in solution. The surfactant concentrations tested were MC1000 at 50 ppm and DP-HS-1002 at 25 ppm. The overall result from the columns was that the ones with surfactant overall achieved greater leaching than the one without. The ones with surfactant attained 91-92% copper extraction whereas the one without any was at 88-89% extraction.

The next stage involved studying how the surfactants behaved with respect to the fluid they were being hosted in. The surfactants were introduced into the system by dissolution into the leaching fluid. Surfactants are designed to alter the surface tension of a hosting fluid when in contact with a secondary phase. As such the next stage of study involved the observing the changes the surfactants imparted on the hosting fluid by way of studying the surface tension. Surfactants are amphipathic molecules that have two structures on the same monomer. They have a lyophilic group with an affinity for the hosting solvent and a lyophobic group with little affinity for the host fluid. The surfactant monomers adsorb at the surfaces of fluids where the lyophilic groups adsorb at the liquid boundary and the lyophobic group points away from the group. These lyophobic groups create a “new surface” on the fluid which is now in contact with the secondary phase and alters the surface tension overall. For the

measurement of interfacial tension hanging droplet experiments were performed. In a droplet the molecules in the fluid have a tendency to stick together. By suspending the droplet the effects of gravity become apparent and the drop is distorted. The interfacial tension is a measure of the work the fluid does to hold itself together against external forces acting on it. The effect of surfactant in the fluid means that the change in surface tension can be measured directly. The surface tension value is also representative of the air-liquid interface as the droplets in this case were suspended in air. The surfactant concentrations tested were from 0ppm to 1000ppm for both of them. For MC1000 the change in surface tension was found to be 71-57 mN/m. For DP-HS-1002 the change was found to be 71-66 mN/m. Also at the concentrations tested in the columns, MC1000 at 50 ppm and DP-HS-1002 at 25 ppm, the tension values were found to be 69 mN/m and 70.4 mN/m. This entailed that the surfactants had little effect at the liquid-air boundary as surface tension of the fluid did not change very much.

The final study undertaken in this thesis was determining the contact angle of the solid on liquid. This was achieved through the use of packed beds of powdered ore material. The ore material had many different mineral species and so a representative value of contact angle was necessary to achieve. Using a packed bed of powdered material, capillarity and Washburn's equation could be used. By immersing a packed bed of particles in the fluid capillarity would result in the movement of fluid through the bed of particles. The rate at which the fluid permeated the bed could be analyzed using Washburn's equation and the contact angle of the liquid on the solid could be calculated. The Washburn's equation calculates relates the rate of movement to the adhesion the liquid has for the solid. For these

experiments the same concentrations of surfactant solution used in the surface tension measurements was used in these experiments too. For 1% sulfuric acid solution the contact angle on the ore was found to be approximately 79°. It was found that overall for MC1000 the initial presence of the surfactant at 50ppm increased the contact angle slightly to 80°. But then subsequent increases in the surfactant concentration was found to reduce the contact angle, driven mainly by the larger reduction in surface tension. For DP-HS-1002 the presence of surfactant at 25ppm reduced the contact angle to 77.5°. Testing at higher surfactant concentrations yielded no further change in surfactant concentration.

6.2 Implications and Discussion

The capillary wicking experiments provided a method of characterizing the solid-liquid interaction and how that interaction was affected with the presence of surfactant. The rate of rise through the capillaries in the packed bed is direct function of the affinity of the liquid and solid phases. And because the packed bed was comprised of a number of different phases, the final contact angle(s) determined was representative of the whole ore in general. Additionally the capillary wicking experiments provide a more concessive method to determine the change brought on by the presence of surfactants in the leach fluid.

In the heap leach process, transport effects and interaction of the various phases govern the success of the operation. Aeration results in the movement of oxygen and/or air (referred to as the gas phase) up through the heap. Irrigation results in the movement of the acidic solution down through the heap. In the midst of all this transportation through the bed of

particles, the different phases inherently present in the operation (solid, liquid and gas) interact with each other.

The points of contact between the different phases, and the degree to which they balance and interact with each other are important considerations when aiming to optimize a heap leach. As mentioned in the previous section one of the aims of running a successful heap requires the adequate/near complete wetting of the particles in the porous matrix. This serves as a transport path for species to and from the particles. This needs to be balanced by the distribution of gaseous phases that may be required for temperature control or to deliver oxygen necessary for dissolution (e.g. the dissolution of primary sulfide minerals (Schlesinger et al., 2011a))

However, a key consideration for the heap leach process is the ingress of the acidic leach solution into the ore particles themselves. This is because the sought after copper minerals are largely hosted within a larger bulk matrix of other gangue minerals. This remains the case after crushing and sizing the ore prior to placing them on the heap. The success of the leach depends on how well the acidic media is able to penetrate the ore particles to reach the disseminated copper minerals within. As highlighted in the previous section, despite efforts to do so, maintaining a completely homogenous mixture of liquid to solid is not always possible. This means that not all particles in a heap are wet to the same degree or at all in some cases. To compensate for this, where the liquid contact with the ore is more than adequate, the ingress and leaching should be more exhaustive.

The presence of surfactants in leach solution seems to achieve this as test work has shown an impact on the overall yield and rate of extraction of copper from test columns. The lyophobic groups of the surfactants increase the affinity between the acidic media and the ore surfaces. This allows it to better reach the minerals located within the sub-surface regions of the particles and thereby increase the leachability of the ores.

Finally, the capillary wicking experiment also provides a convenient method through which the effect of surfactant on ore can be measured. Heap leaching operations are conducted with different types of ores and leaching solutions. If surfactants are to be introduced into an established heap, the degree to which they will have an effect would be a desired quantity. The capillary wicking experiment provides a useful method by which the effect of surfactant can be measured. The experiment uses finely ground material and can therefore integrate the full composition of the ore to ensure more representative results. The experiment can also be adjusted to accommodate the different leach solutions. All-in-all, the experiment can be easily set-up to measure the effect of a surfactant when the composition at the points of contact (solid-liquid interface) change in any way.

6.3 Future Work and Recommendations

1) **Contact angle measurements with different ores**

   The contact angle measurements performed in this work were done on one type of ore with a fixed composition. To determine the response of ores to varying solid compositions the contact angle should be measured using different ore types.

2) **Capillary Head**

The test work performed in this thesis focused on determining the effect of the surfactant at the solid-liquid interface. The contact angle measurements were performed using ore but whose phases were separated using grinding. The movement of the fluid within the ore should be studied in greater detail. As the fluid ingresses through the cracks and pores of the ore pieces, the movement of the fluid is affected by interactions with solid phases as well as the displacement of air within the pores. The movement of the fluid head in these spaces should be better understood so as to have better predictability of the effect of surfactant when introduced into the same conditions.

3) **Surfactant Consumption**

The consumption of a surfactant should be better understood within a heap leach system. In this thesis the consumption of the surfactant in the heap was not studied. Within the heap it should be determined if the surfactant is susceptible to consumption from chemical or biological compounds. The rate of consumption should be well understood as the purchasing of surfactant would be a direct reagent cost to the operator of the heap.

4) **Heap Component Behaviors**

In heap leaching operations a variety of ionic species are present. These are for example, $Cu2^{+}$, $Fe2^{+}$, Fe^{3+}, SO_4^{2-}, etc… The behavior of the surfactant with respect to the various ionic species should be further explored with both short term and long term exposure. Additionally changes to the surfactants chemistry, if any, should be better understood.

This would allow for better optimization and economical reagent in commercial operations.

Bibliography

1)Alghuniam, A., Kirdponpattara, S., & Newby, B. Z. (2016). Techniques for determining contact angle and wettability of powders. *Powder Technology, 287*, 201-215.

2)ASTM. (2011). C702/C702M-11 - standard practice for reducing samples of aggregate to testing size. *ASTM volume 04.02 - concretes and aggregates* (2016th ed., pp. 1-5) ASTM International.

3)Bartlett, R. W. (1997). Metal extraction from ores by heap leaching. *Metallurgical and Materials Transaction B, 28*(4), 529-545.

4)Bender, J., Hight, L., Emmerich, N., & Brewer, R. (2016). Leaching aids for dump and heap leach; SX compatibilty, biocompatibility, and recycle of lixiviant. Paper presented at the *Copper 2016*, Kobe, Japan. pp. 1523-1533.

5)Bouffard, C. (2008). Agglomeration for heap leaching: Equipment design, agglomerate quality control, and impact on heap leach process. *Minerals Engineering, 21*(15), 1115-1125.

6)Brierley, C. (2001). Bacterial succession in bioheap leaching. *Hydrometallurgy, 59*(2-3), 249-255.

7)Bureau Veritas. (2017). *Mixed acid digest and ICP*. Retrieved April, 20, 2017, from http://www.bureauveritas.com/services+sheet/metals-minerals/mixed-acid-digest-icp .

8)Captaine, S., & Carlson, C. (2017). *Agglomeration drums in heap leach process.* Retrieved 5/17, 2017, from http://feeco.com/agglomeration-drums-in-the-heap-leaching-process/ .

9)Connelly, D., & West, J. (2009). Trips and traps for copper heap leaching. *ALTA Copper 2009*, Melbourne: ALTA Metallurgical Services.

10)Data Physics Instruments GmbH. (2017). *Pendant drop method - optical determination of the surface/interfacial tension.* Retrieved 4/27, 2017, from http://www.dataphysics.de/2/start/understanding-interfaces/drop-shape-analysis/pendant-drop-method/ .

11)Dhawan, N., Safarzadeh, M., Miller, J., Moats, M., & Rajamani, M. (2013). Crushed ore agglomeration and its control for heap leach operations. *Minerals Engineering, 41*, 53-70.

12)Dixon, D., & Petersen, J. (2007). [Chapter 8] - modeling and optimization of heap bioleach processes. In D. Rawlings, & D. Johnson (Eds.), *Biomining* (pp. 153-176) Springer Berlin Heidelberg.

13)Dreisinger, D. (2006). Copper leaching from primary sulfides: Options for biological and chemical extraction of copper. *Hydrometallurgy, 83*(1-4), 10-20.

14)Eastoe, J., & Dalton, J. (2000). Dynamic surface tension and adsorption mechanism of surfactants at the air-water interface. *Advances in Colloid and Interface Science, 85*(2-3), 103-144.

15)Ghorbani, Y. (2012). On the progression of leaching from large particles in heaps. (Degree of Philosophy, University of Cape Town).

16)Lide, D. (2008). Concentrative properties of aqueous solutions: Density, refractive index, freezing point depression, and viscosity. *CRC handbook of chemistry and physics* (88th ed., pp. 8-52-8-79) CRC LLC.

17)Liu, W., Pawlik, M., & Holuszko, M. (2015). The role of colloidal precipitates in the interfacial behavior of alkyl amines at gas–liquid and gas–liquid–solid interfaces. *Minerals Engineering, 72*, 47-56.

18)Lupo, J. (2006). *Design and operation of heap leach pads* Golder Associates.

19)Majdi, A., Amini, M., & Chermahini, A. (2009). An investigation on mechanism of acid drain in heap leaching structures. *Journal of Hazardous Materials, 165*(1-3), 1098-1108.

20)Marsden, J., & House, C. (2006a). Leaching. *The chemistry of gold extraction* (Second ed., pp. 233-295) Society for Mining, Metallurgy, and Exploration, Inc.

21)Marsden, J., & House, C. (2006b). Prinicipals of gold hydrometallurgy. *The chemistry of gold extraction* (Second ed., pp. 111-145) Society for Mining, Metallurgy, and Exploration, Inc.

22)Moskalyk, R., & Alfantazi, A. (2003). Review of copper pyrometallurgical practice: Today and tomorrow. *Minerals Engineering, 16*(10), 893-919.

23)Padilla, G., Cisternas, L., & Cueto, J. (2008). On the optimization of heap leaching. *Minerals Engineering, 21*, 673-678.

24)Rakovan, J. (2003). A word to the wise: Hypogene and supergene. *Rocks and Minerals, 78*(6), 419.

25)Raudsepp, M., Pani, E., Czech, E., & Lai, J. (2017). In Personal Communication (Ed.), *Quantitatve phase analysis of 5 powder samples using the rietveld method and X-ray powder diffraction method*. Vancouver: Department of Earth and Ocean Sciences, UBC.

26)Rosen, M. J. (2004a). [Chapter 1] characteristic features of surfactants. *Surfactants and interfacial phenomena* (Third ed., pp. 1-33) John Wiley & Sons Inc.

27)Rosen, M. J. (2004b). [Chapter 5] reduction of surface and interfacial tension by surfactants. *Surfactants and interfacial phenomena* (Third ed., pp. 208-242) John Wiley & Sons Inc.

28)Scheffel, R. (2002). Copper heap leach design and practice. In A. Mular, D. Halbe & D. Barratt (Eds.), *Mineral processing plant design, practice, and control, vol 2.* (pp. 1571-1605) Society for Mining, Metallurgy, and Exploration, Inc.

29)Schlesinger, M., King, M., Sole, K., & Davenport, W. (2011a). [Chapter 15] hydrometallurgical copper extraction: Introduction and leaching. *Extractive metallurgy of copper* (Fifth ed., pp. 281-322) Elsevier Ltd.

30)Schlesinger, M., King, M., Sole, K., & Davenport, W. (2011b). [Chapter 16] solvent extraction. *Extractive metallurgy of copper* (Fifth ed., pp. 323-347) Elsevier Ltd.

31)Schlesinger, M., King, M., Sole, K., & Davenport, W. (2011c). [Chapter 2] production and use. *Extractive metallurgy of copper* (Fifth ed., pp. 13-30) Elsevier Ltd.

32)Sherrit, R., Pavlides, A., & Weekes, B. (2005). Design and commissioning of the sepon copper pressure oxidation circuit. *1st Extractive Metallurgy Operators' Conference,* Victoria: Australasian Institute of Mining and Metallurgy. pp. 21-27.

33)Siebold, A., Walliser, A., Nardin, M., Oppliger, M., & Schultz, J. (1997). Capillary rise for thermodynamic characterization of solid particle surface. *Journal of Colloid and Interface Science, 186*(1), 60-70.

34)Underwood, T. (2000). In Golden West Industries (Ed.), *Method for improved percolation through ore heaps by agglomerating ore with a surfactant and polymer mixture* (75/772; 23/313 R; 423/27; 423/29; 423/DIG. 17 ed.). United States: C22B 1/244; C22B 1/14; C22B 11/00.

35)United States Geological Survey. (2016). *Surface tension and water.* Retrieved 4/24, 2017, from https://water.usgs.gov/edu/surface-tension.html .

36)Vest, M., Lüzerath, A., Freidrich, B., & Seelmann-Eggebert, H. (2009). Improvements in copper heap leaching by use of wetting agents. *Emc 2009,* .

37)W.S. Tyler. (2017). *Ro-tap sieve shaker.* Retrieved 5/10, 2017, from http://wstyler.com/product/ro-tap-sieve-shakers/ .

38)Watling, H. (2006). The bioleaching of sulphide minerals with emphasis on copper sulfides - A review. *Hydrometallurgy, 84*(1-2), 81-108.

39)Wikimedia Commons. (2010). *Contact angle.* Retrieved 5/4, 2017, from https://commons.wikimedia.org/wiki/File:Contact_angle.svg .

40)Wikimedia Commons. (2012). *Water molecules in droplets.* Retrieved 4/25, 2017, from https://commons.wikimedia.org/wiki/File:Wassermolek%C3%BCleInTr%C3%B6pfchen.svg .

41)Woods, R. (2010). *Extracting metals from sulfide ores.* Retrieved 11/5, 2017, from http://knowledge.electrochem.org/encycl/art-m02-metals.htm .

42)Woodward, R. (2000). *Surface tension measurments using the drop shape method*.